Dissipation-Induced Collective Effects in Two-Level Systems

Dissertation
zur Erlangung des Doktorgrades des Fachbereichs Physik der Universität Hamburg

vorgelegt von
Till Vorrath
aus Essen

Hamburg
2003

Gutachter der Dissertation:	Prof. Dr. B. Kramer PD Dr. T. Brandes
Gutachter der Disputation:	Prof. Dr. B. Kramer Prof. Dr. U. Eckern
Datum der Disputation:	21.10.2003
Vorsitzender des Prüfungsausschusses:	PD Dr. S. Kettemann
Vorsitzender des Promotionsausschusses:	Prof. Dr. R. Wiesendanger
Dekan des Fachbereichs Physik:	Prof. Dr. G. Huber

Zusammenfassung

Thema dieser Arbeit sind kollektive Effekte in Zwei-Niveau-Systemen, die allein durch die Ankopplung aller Systeme an dieselbe dissipative Umgebung hervorgerufen werden. Wir untersuchen zunächst das Modell eines dissipativen großen Spins. Dieses Modell dient sowohl zur Beschreibung eines physikalischen Spins unter Einfluß seiner Umgebung, als auch zur Beschreibung kollektiver Effekte in einem Ensemble von Zwei-Niveau-Systemen. In diesem Fall läßt sich von der Dynamik eines großen Pseudo-Spins auf die Polarisierung des Ensembles schließen. Formal ist das Modell des dissipativen großen Spins die Verallgemeinerung des Spin-Boson-Modells auf beliebig große Spins. Zudem enthält das Modell auch das Dicke-Modell, das kollektive Effekte in Zwei-Niveau-Atomen beschreibt. Das Modell eines dissipativen großen Spins erlaubt so, das Zusammenwirken von kohärenten Oszillationen und kollektiven Effekten zu studieren.

Zur Beschreibung des großen Spins verwenden wir eine Master-Gleichung, die in der Born-Markov-Näherung hergeleitet wird. Bei der Berechnung der Raten der Umgebung nehmen wir eine ohmsche Dissipation an. Wir untersuchen das Modell in zwei Bereichen, zuerst im Grenzfall schwacher Wechselwirkung zwischen dem Spin und seiner Umgebung und dann im umgekehrten Fall starker Wechselwirkung. In beiden Bereichen finden wir gute Übereinstimmung der Master-Gleichung mit den Ergebnissen des Spin-Boson-Modells. Im Grenzfall schwacher Wechselwirkung zeigt der große Spin ein superradianzartiges Verhalten, das charakteristisch für das Dicke-Modell ist. Für einen kleinen oder verschwindenden Energieunterschied zwischen den beiden Zuständen der Zwei-Niveau-Systeme zeigt sich der Einfluß der nichtresonanten Moden der Umgebung in Schwebungen der kohärenten Oszillationen des großen Spins. Ein völlig unterschiedliches Verhalten ergibt sich im Bereich starker Wechselwirkung. Je nach Anfangszustand relaxiert der Spin in diesem Fall zu einem der beiden polarisierten Zustände. Die Relaxation verläuft näherungsweise logarithmisch in der Zeit.

Zur experimentellen Untersuchung derartiger kollektiver Effekte schlagen wir ein System von zwei gekoppelten Quantenpunkten vor. Bei der Berechnung des Tunnelstroms durch die Quantenpunkte zeigt sich, dass kollektive Effekte tatsächlich den Tunnelstrom beeinflussen. So führt das Auftreten der Superradianz in den doppelten Quantenpunkten zu einem Anstieg des Tunnelstroms. Durch entsprechende Veränderung der Parameter läßt sich auch der umgekehrte Effekt, die Subradianz, beobachten. Diese führt zu einer Abnahme des Tunnelstroms.

Abstract

The subject of this thesis are collective effects of two-state systems which are solely caused by the coupling of all systems to the same dissipative environment. First, we investigate the model of a dissipative large spin. This model applies to an intrinsic large spin under the influence of its environment as well as to collective effects in an ensemble of two-state systems. In that case, the polarization of the ensemble follows from a large pseudo-spin. Formally, the model is the generalization of the spin-boson model to spins of arbitrary size. It also includes the Dicke model which describes collective effects of two-level atoms. Thus, the model of a dissipative large spin allows to study the combination of coherent oscillations and collective effects.

The large spin is described by a master equation. We employ the Born-Markov approximation for the derivation of the master equation. The rates of the environment are calculated for an ohmic dissipation. We study the model in two regimes. First in the limit of weak interactions between the spin and the environment and then in the opposite regime of strong interactions. In both regimes we have found good agreement of the master equation with the results of the spin-boson model. In the weak-coupling regime, the spin shows a superradiance-like behavior which is characteristic for the Dicke model. For a small or zero bias the influence of the nonresonant modes of the environment becomes visible in beats of the coherent oscillations of the large spin. A different dynamics is observed in the strong-coupling regime. There, the spin relaxes towards one of the polarized states depending on its initial value. The relaxation is approximately logarithmic in time.

We propose an array of double quantum dots for the experimental realization of these collective effects. For the case of two double quantum dots, we calculate the tunnel current and find that it is modified by collective effects. The effect of superradiance in the two double dots leads to an increase of the tunnel current. For different parameters, also the opposite effect, the subradiance, occurs. This results in a decrease of the tunnel current.

Contents

Chapter 1

Introduction

Quantum mechanics exhibits phenomena which cannot be understood from a classical point of view. One of these effects is the tunneling which allows a particle to cross a classically forbidden region. Tunneling is also an important feature in one of the simplest, if not the simplest, quantum mechanical system: the two-level system. A tunnel coupling leads to coherent oscillations in the system which means that the particle tunnels with a constant frequency between the two states. An example for such oscillations is found in the ammonia molecule NH_3 in which the nitrogen atom can have two equivalent positions. Oscillations between these states, the inversion resonance, have already been observed in the early days of quantum mechanics [1, 2]. Another example is given by an electron in a double quantum dot [3, 4, 5]. Under appropriate conditions, this system is described by the two states in which the electron is localized in either of the quantum dots. Coherent oscillations of the electron between the two dots have only been observed this year by Hayashi and co-workers [6].

These two-state systems just like any other real system are never entirely isolated but interacting with their environment. This may be an electromagnetic field, lattice vibrations, or other external forces. The influence of a macroscopic environment on a quantum system leads to dissipation and decoherence [7, 8]. Dissipation is the loss of energy which allows a system to relax to its equilibrium. Decoherence on the other hand means the disappearance of superpositions and hence of quantum interferences.

The investigation of a two-state system under the influence of a dissipative environment is the subject of the *spin-boson model* [9, 10]. This model has been studied extensively by a great number of scientists during the last two decades. It turns out that the coherent oscillations of the two-state system are damped or even completely suppressed as a result of interaction with the environment. Still, a closed solution for all parameters is not known. Depending on the coupling strength and the temperature, the model shows a rich variety of dynamics as damped oscillations,

exponential relaxation, or localization.

The spin-boson model describes the physics of a single two-state system. It does not include any collective effects. These are effects in an ensemble of many particles that cannot be explained by the behavior of independent particles. Physics offers numerous examples for collective effects such as phase transitions, magnetism, superconductivity, and superfluidity to name but a few [11]. The appearance of collective effects requires that the particles are interacting with each other. A particular kind of interaction arises if all particles are coupled to the same dissipative environment. Superconductivity is a spectacular example for such an indirect, environment-induced interaction. The coupling of electrons in a superconductor to the phonons can lead to an attractive interaction between the electrons and thus to the formation of a new ground state – the superconducting state.

Collective effects also appear in an ensemble of two-state systems that are independent of each other apart from the coupling to the common environment which introduces an indirect interaction between the systems. The most prominent effect is probably the *superradiance* which was already predicted half a century ago by Dicke [12]. Superradiance is the collective spontaneous emission of an ensemble of initially excited two-level atoms interacting with the radiation field – the so-called *Dicke model* [13, 14]. The collective decay happens much faster than that of an independent atom. The duration of the superradiant decay is roughly inverse proportional to the number of atoms in the ensemble. It is accompanied by the emission of a short and intense radiation pulse.

With regard to the two-state systems, the Dicke model is not as general as the spin-boson model. Coherent tunneling, an essential part of the spin-boson model, is not included in the Dicke model. In many applications, for instance in quantum optics, the restriction of the Dicke model is of no importance. There are, however, indications that collective effects also occur in two-level systems which show distinct coherent oscillations. Recently, Ahn and Mohanty suggested that collective effects of tunneling systems in crystalline micromechanical resonators are responsible for an unexpected high dissipation observed in these systems [15]. Moreover, we expect that the technological progress will soon facilitate the experimental realization of two-state systems that combine coherent tunneling and collective effects. One may think of several double quantum dots close to each other. Coherent tunneling of an electron in the double dot as well as the coupling of the dots to the phonons have been demonstrated experimentally [6, 16]. What are the consequences of possible collective effects for instance on the tunnel current? Furthermore, the interplay of coherent tunneling and collective effects is an exciting question from a theoretical point of view. Neither the spin-boson model nor the Dicke model contains a combination of both effects.

In this thesis, we study collective effects of identical two-state systems which include coherent oscillations. We employ the model of a dissipative large spin.

Formally, this is the generalization of the spin-boson model to spins greater than one half. The connection between the large spin and the ensemble of two-state systems lies in the fact that the large spin yields the polarization of the ensemble.

At the same time, the model describes an intrinsic large spin in contact with a dissipative environment. In fact, there are a number of examples for spins greater than one half. The elements gallium and arsenic used in the majority of modern solid state experiments have a nuclear spin of 3/2. Another example is given by molecular magnets. These are molecules of a few metallic atoms. Because of the magnetic coupling of the atoms, the molecule obtains a large magnetic moment. The most prominent examples, Mn_{12} and Fe_8, are believed to have a total spin of ten [17, 18].

The following questions are of particular interest in the investigation of a dissipative large spin. How does the interplay of coherent oscillations and collective effects affect the physics of an ensemble of identical two-state systems? Does the effect of superradiance also appear in this generalized model? How does the behavior of the spin-boson model change if the spin size is increased? To our knowledge, these problems have not been addressed yet.

Since two complex models, the spin-boson model and the Dicke model, are contained in the problem of a dissipative large spin we cannot hope to find a closed solution for the whole parameter space. Instead, we concentrate on two limits, first the regime of weak coupling between the spin and the environment and second the opposite limit of strong interactions. In the theoretical investigation of the spin-boson system, the functional integral method proved to be a useful tool [10]. Another approach to open quantum systems, a master equation, is often preferred in the field of quantum optics [19]. In this work, we employ a master equation for the description of the large spin. The master equation is derived within the Born-Markov approximation which is perturbative in the spin-environment interaction. The validity of the Born-Markov approximation seems sometimes controversial in literature. Our aim is to demonstrate that a careful derivation in the exact eigenstate basis of the coherent system indeed yields reliable results down to zero temperature for all parameter values, as long as the dissipative coupling is small. The dissipation is assumed to be ohmic throughout this work.

Chapter 2 gives a survey of some spin and two-state systems as well as theoretical models. We present in more detail the systems mentioned above, double quantum dots, tunneling systems in glasses, and molecular magnets. Then, we discuss the spin-boson model and the Dicke model. We also introduce the Bloch equations for the description of a dissipative spin. Finally, we consider the connection between a large spin and an ensemble of identical two-state systems.

In chapter 3, we investigate the model of a dissipative large spin in the regime of weak interactions with the environment. In the limit of spin one half where the model reduces to the spin-boson model, the master equation is transformed into a

set of Bloch equations. Comparing the solution of the Bloch equations with that of the spin-boson model in literature confirms that the master equation gives a reliable description for all temperatures in the limit of weak dissipation. For a finite bias i.e. an energy difference between the states of the two-level systems we find a superradiance-like decay of the ensemble. The influence of the nonresonant modes of the environment becomes visible in beats in the coherent oscillations of the large spin.

The opposite regime of a strong coupling between the spin and the environment is considered in chapter 4. We employ a combination of a polaron transformation and the Born-Markov approximation for the derivation of the master equation. This allows a perturbative treatment of the tunneling. It is well-known that this approach fails to describe the spin-boson model for intermediate coupling strengths at low temperatures. For strong couplings, however, we can reproduce the results of the spin-boson model. Altogether, we have found an entirely different behavior of the large spin as compared to the weak-coupling regime. The large spin approaches one of the polarized states for long times. Which of the two depends on its initial value. For an ohmic dissipation, the relaxation is approximately logarithmic in the time.

In chapter 5, we return to an ensemble of several double quantum dots. We address the question of how far the results of the dissipative large spin are applicable to this system. We calculate the tunnel current through two double quantum dots with indirect interactions due to the coupling to the same phonons. The system is not completely identical to an ensemble of two-state systems. On the one hand, we have to consider leads to enable transport. Thus, apart from the two states describing an electron in one or the other dot a third state exists when the electron has left the double dot. On the other hand we allow different parameters in the two double dots. Despite these differences to the previous chapters, we have found clear evidence for collective effects in the tunnel current. The appearance of superradiance in the dots results in an increase of the tunnel current. By an appropriate choice of parameters, it is also possible to realize the opposite effect, the *subradiance*. This leads to a decrease of the tunnel current through the double quantum dots.

Chapter 2

Dissipative Systems

Before turning to the investigation of collective effects in ensembles of two-level systems, we familiarize ourselves with dissipative systems and possible theoretical descriptions in this chapter. Examples for two-state systems and spins from the field of solid state physics are presented in the first section. We introduce electrons tunneling between two quantum dots, tunneling systems in glasses, and molecular magnets. Inherent to these solid state systems are interactions with lattice vibrations. They are considered as a dissipative environment for the systems. In the second part of this chapter, we will briefly present theoretical models which illuminate different aspects of dissipation. These models are the Bloch equations, the Dicke model and the spin-boson model. We shall return to these models at certain points of this thesis. Finally, the representation of an ensemble of two-level systems by a large spin is introduced.

2.1 Spins and Two-Level Systems

Let us begin with considering some dissipative systems. Examples can be found in practically every field of physics, but we will concentrate here on solid state physics. Two of our examples, *electrons in double quantum dots* and *two-level systems in glasses* are described under appropriate conditions as two-state systems or equivalently as a ficticious spin one half. *Molecular magnets* constitute an example for a greater spin. In principle, dissipation induced collective effects are conceivable in all three systems. We take these examples as a motivation for the general investigation of such effects.

2.1.1 Double Quantum Dots

Quantum dots belong undoubtedly to the most fascinating topics in modern solid state physics. We shall briefly recall some of their features in this section and make a connection to dissipative two-level systems. A quantum dot is a system of a few to a few hundred electrons spatially confined to a region of typically some hundred nanometers [20]. One possible realization is based upon a two-dimensional electron gas (2DEG) arising at the interface of a semiconductor heterostructure. An additional lateral confinement in the remaining two spatial directions is achieved by the application of small metallic gates on the surface of the sample. The gates create an approximately harmonic potential in which the electrons are trapped. The physics of the electrons in the quantum dot is governed by the interplay between their mutual Coulomb repulsion and the confining potential.

At low temperatures, these systems have to be regarded as quantum mechanical systems. In particular, the electrons in the dot have a partly discrete spectrum as is known from atoms. For that reason, quantum dots are also refered to as artificial atoms [21, 22]. In contrast to real atoms, however, their parameters like the number of electrons and their effective mutual interaction can be adjusted experimentally. These features make quantum dots very attractive for the investigation of quantum many-body effects. The Kondo effect, for instance, was detected in quantum dots a few years ago [23, 24]. Moreover, quantum dots constitute one candidate for a qubit – the basic element of a future quantum computer [25].

A useful tool for the experimental investigation of quantum dots is the transport spectroscopy [26]. There, the dot is connected to two leads via tunnel contacts. The application of a voltage between the leads results in a current as electrons tunnel from one lead to the dot and then from the dot to the other lead. The tunnel current as a function of the voltage gives information about the quantum dot such as the number of electrons in the dot and the spectrum.

Just as real atoms can be combined to form molecules one can also form an artificial molecule by connecting two quantum dots via a tunnel coupling [4, 27]. For a weak coupling and a sufficiently strong Coulomb repulsion within each dot, only one additional electron can tunnel between the two dots while all other electrons of each dot are restricted to that dot. Then, the double quantum dot can be understood as a two-level system. The two states correspond to the localized states of the additional electron in one or the other dot. Due to the tunnel coupling, the localized states are no eigenstates of the system and one expects coherent oscillations of the additional electron between the dots [28]. Such oscillations have indeed been observed in a recent experiment by Hayashi and co-workers [6].

Like any other real system, a quantum dot is not free from influences of the environment. The main sources of dissipation in quantum dots are interactions with photons and phonons. Since electrons are charged particles, they interact with the

electromagnetic field. Thus, excitations or tunnel processes in quantum dots can be stimulated by irradiation with light. One of the resulting effects is the so-called photon assisted tunneling [29, 30]. On the other hand, quantum dots can be used to construct semiconductor lasers [31]. Moreover, lattice vibrations, i.e. phonons, are always present in any solid state sample. The coupling of the electrons in quantum dots to the phonons was demonstrated by Fujisawa in L. Kouwenhoven's group in Delft [16, 32]. They measured the tunnel current through a double quantum dot while a small voltage was applied between the two dots. Then, conservation of energy requires that a phonon is emitted if an electron tunnels from one dot to the other. The emission becomes visible in the tunnel current [33]. It is possible to modify the inelastic current by the design of the sample in which the quantum dots are realized. Changes of the geometry of the sample alter the phonon spectrum and the electron-phonon coupling in the quantum dots [34, 35].

We conclude that a double quantum dot coupled to the phonons of the sample can be regarded as a dissipative two-level system. According to the considerations of the introduction, we might ask whether the behavior changes if two or more double dots are placed close to each other. The coupling to the same dissipative environment, the phonons, could lead to some collective effects. We shall come back to this question in chapter 5 of this thesis. There, we investigate a realistic model for two double quantum dots with leads and coupling to bulk acoustic phonons. It will turn out that an important collective effect, the Dicke effect, is indeed observable in the tunnel current as a function of the voltage applied between the dots.

2.1.2 Tunneling Systems in Crystals and Amorphous Solids

Other examples of dissipative two-level systems are found in crystals and glasses. The low temperature properties of these systems are determined by tunneling of atoms, molecules or groups of atoms [36, 37]. Tunneling of atoms has been discussed from the very beginning of quantum mechanics. It was first observed in ammonia molecules, NH_3, in 1929. Because of the symmetry of the molecule, the nitrogen atom tunnels between two equivalent positions in the molecule with a characteristic frequency. Later, it was shown that tunneling of atoms similarly takes place in crystalline solids where an impurity atom can tunnel between several positions in the host lattice. It was rather unexpected when thermal anomalies in the low temperature behavior of glasses implied that tunneling systems also exist in amorphous solids. The microscopic nature of these tunneling systems is still not fully understood.

Let us first consider impurities in crystalline solids. A typical example is a Lithium atom in a potassium chlorid crystal (KCl). Due to the different size, the impurity atom does not fit into the KCl lattice. Instead, the host crystal offers several equivalent positions to the impurity, typically 6, 8, or 12, depending on the

symmetry of the crystal. A tunnel coupling lifts the degeneracy of these states and at low temperatures it is sufficient to consider only the two lowest states. Moreover, the impurity atom causes a dipole moment. If the concentration of the impurities is high enough, and consequently their average distance is sufficiently small, dipole interaction between the impurities becomes effective. This interaction leads to decoherence of the two-level systems.

In amorphous solids, on the other hand, the situation is not that clear. The difficulty arises since systems of quite different microscopic structure show similar phenomena at low temperatures, e.g. in the thermal and acoustic behavior. A microscopic explanation of these observations is still not available. Many properties of amorphous solids, however, can be derived from the so-called *tunneling model*, independently suggested by Phillips [38] and Anderson, Halperin, and Varma [39] in 1972. These authors predict the existence of two-level systems in amorphous solids. It seems that groups of atoms rather than single atoms or molecules are tunneling between potential minima. The tunneling systems are coupled to phonons leading to dissipation. Dissipation of the two-level systems is an important part of the tunneling model affecting, for instance, the sound velocity and the sound attenuation. Direct interactions between the tunneling systems are believed to be of minor importance.

Altogether, we find another example for dissipative two-level systems in certain crystalline and amorphous solids. The question whether these systems exhibit collective effects has been addressed recently by Ahn and Mohanty who consider micromechanical resonators [15]. The quality of such resonators is limited due to dissipation of the two-level systems in the crystal. The authors suggest that a superradiant decay of the two-level systems leads to an increased dissipation of the micromechanical resonators. We won't discuss the details and particularities of tunneling systems in glasses and crystals further. We take these systems as a motivation for the general study of dissipation-induced collective effects.

2.1.3 Molecular Magnets

Another system of interest in this context is given by molecular magnets [17, 18, 40, 41]. These mesoscopic magnets constitute an example for a real spin in contrast to the description of two-level systems by means of a pseudo-spin. The most prominent examples for molecular magnets, Mn_{12} and Fe_8, behave like a spin of size $J = 10$. These systems have attracted much interest both from experimental and from theoretical side in the last decade. Possible applications include quantum computing and data storage.

Molecular magnets are clusters of a small number of metallic ions. These clusters form with regular spacings in certain organic materials. Mn_{12}, for instance, consists of eight Mn^{3+} ions and four Mn^{4+} ions. Oxygen atoms link the manganese ions. The

structure is accomplished by acetic acids and water molecules [42]. The peculiarities of these clusters are caused by the magnetic coupling of the metallic ions. As a consequence, the clusters behave at low temperatures like nanomagnets with a large spin, e.g. $J = 10$ for Mn_{12}. The different magnetic molecules in the crystal do not interact magnetically since the distance between neighboring molecules is too large. Thus, each molecule can be considered as independent. The magnetic properties become visible in the magnetization which shows a hysteresis as a function of the external magnetic field. Such behavior is known from ferromagnetic materials, yet, the origin is different for molecular magnets. Here, the hysteresis is caused by exponentially long relaxation times at low temperatures [17].

One property which seems to be common to all molecular magnets is a high anisotropy. This is accounted for by a quadratic term of one or more spin components in the Hamiltonian, for instance J_z^2. One should remark, though, that the Hamiltonian used for the description of molecular magnets is not microscopically derived from first principles but rather a phenomenological description. Due to the anisotropy, the ground states of Mn_{12} and Fe_8 are given by the polarized states, $\langle J_z \rangle = \pm 10$. The proposal for the implementation of Grover's algorithm in molecular magnets is actually based on this anisotropy [43].

Naturally, molecular magnets also interact with the environment. The influence of phonons becomes visible in thermally activated tunneling between different spin states. The coupling to the phonons is discussed in [44]. Similarly, molecular magnets interact with the electromagnetic field. The wavelength of the resonant radiation can be much longer than the distance between adjacent nanomagnets in the crystal. Then, an identical coupling of many molecular magnets is expected. This is the typical situation where coherent effects arise. In fact, superradiant transitions in molecular magnets have recently been predicted by Chudnovsky and Garanin [45].

Molecular magnets constitute another example for dissipative large spins which are studied in this thesis. The model, that we shall investigate in the following, however, does not include an anisotropy and we do not expect that the results of this model are immediately applicable to molecular magnets.

2.2 Theoretical Models

We will now turn to theoretical models describing various aspects of dissipative spins. The first model to be presented, the *Bloch equations*, originally applied to nuclear magnetic moments in an oscillating magnetic field. Collective effects in an ensemble of spins with indirect interaction due to the coupling to the same reservoir are studied in the *Dicke model*. A comprehensive treatment of the influence of a dissipative environment on the behavior of a spin one half is given within the *spin-boson model*.

2.2.1 Bloch Equations

From a classical point of view, a spin or an angular momentum is a vector which is completely described by its three spatial components. This view is reflected by the Bloch equations that give the time evolution of the three spin components. The Bloch equations are closely related to experiments on the nuclear magnetic resonance (NMR) [46]. There, the spin describes the magnetization of a sample caused by its nuclear moments. A static magnetic field is applied to the sample in NMR experiments. In addition, a small oscillating field acts in the plane orthogonal to the static field. The absorbed energy exhibits a pronounced maximum if the frequency of the external field is in resonance with the Larmor frequency of the nuclear spins. Nowadays, NMR is used for the investigation of complex molecules in chemistry and as a diagnostic tool in medicine.

If the z-axis is chosen parallel to the static magnetic field, the Bloch equations for the magnetization $\boldsymbol{M}$ in an external magnetic field $\boldsymbol{B}$ read

$$\begin{aligned} \dot{M}_{x,y} &= \gamma \left(\boldsymbol{M} \times \boldsymbol{B}\right)_{x,y} - \frac{1}{T_2} M_{x,y} \,, \\ \dot{M}_{z} &= \gamma \left(\boldsymbol{M} \times \boldsymbol{B}\right)_{z} - \frac{1}{T_1} \left(M_z - M_0\right). \end{aligned} \tag{2.1}$$

The equilibrium value of the magnetization in z-direction is given by M_0 and γ is the gyromagnetic ratio. The influence of the dissipation becomes visible in the relaxation times T_1 and T_2. These times describe the relaxation parallel, T_1, and orthogonal, T_2, to the static magnetic field. In general, they are not equal since the symmetry is broken by the applied field.

The Bloch equations (2.1) can be derived classically. This approach was chosen by Bloch in his original work [47]. The equations follow if the magnetization is considered as an angular momentum on which a torque acts caused by the magnetic field. Dissipation is taken into account phenomenologically by adding the relaxation times T_1 and T_2. Later, Bloch gave a microscopic derivation of these equations [48, 49]. For that, it is sufficient to regard the spin of a single nucleus in contact with a heat reservoir in thermal equilibrium. Microscopic expressions for the relaxation times follow from this approach. The derivation is perturbative in the spin-reservoir coupling and thus the equations are limited to weak dissipation. A similar derivation of the Bloch equations was given at the same time by Redfield [50]. Therefore, equations of this type are sometimes refered to as Bloch-Redfield equations.

Similar equations are also used in other fields of physics. The *optical Bloch equations* describe a two-level atom in a monochromatic laser field [51]. The two-level atom is equivalently represented by a fictitious spin one half [28]. The probability of finding the atom in either of the two levels follows from the z-component of that spin. The coupling to the electromagnetic field leads to dissipation, in particular to

spontaneous emission. Then, the equations for the time evolution of the spin components are formally identical to the Bloch equations (2.1). The difference between the energy of the photons and the excitation energy of the atom is identified with the static magnetic field in (2.1). The Rabi frequency, a measure for the coupling strength between the atom and the laser field, corresponds to the amplitude of the oscillating magnetic field. The relaxation times can be expressed by the spontaneous emission rate Γ as

$$T_1 = \frac{1}{\Gamma}\,, \qquad T_2 = \frac{2}{\Gamma} = 2T_1. \tag{2.2}$$

The Bloch equations give a clear description of a spin in a time dependent field in the limit of weak dissipation. They determine the time evolution of the three spin components. The Bloch equations are independent of the spin size. For a spin one half, the density matrix of the spin has three independent entries. They follow from the knowledge of the three spin components. For larger spins, however, the dimension of the density matrix increases which is not reflected by the Bloch equations. In fact, the microscopic derivation of the Bloch equations is strictly valid only for spin one half, as discussed already by Bloch [48]. For greater spins the equations are restricted to higher temperatures. A generalization of the Bloch equations to greater spins was recently given by Apel and Bychkov [52]. However, the set of equations derived by these authors contains more than three equations and lacks the clarity of the Bloch equations. In chapter 3 of this thesis we shall derive a set of Bloch equations for the spin-boson model and show that they give a good description in the regime of weak coupling to the environment. We shall see in detail why these equations cannot be generalized to greater spins.

2.2.2 The Dicke Model

In this section, we consider a collective effect of two-level systems that was predicted almost half a century ago by Dicke [12]. The two-level systems in the Dicke model are supposed to be independent of each other apart from the coupling to the common environment. This leads to a collective spontaneous emission, the so-called *superradiance* [13, 14]. The effect becomes already visible for only two systems, for instance two two-level atoms interacting with the radiation field. The Hamiltonian for a single two-level atom with excitation energy ω_0 ($\hbar$ is set to one) reads [53]

$$H = \frac{\omega_0}{2}\,\sigma_z + \sum_{\boldsymbol{q}} \omega_{\boldsymbol{q}}\, a^\dagger_{\boldsymbol{q}} a_{\boldsymbol{q}} + \frac{1}{2}\,\sigma_x \sum_{\boldsymbol{q}} (\gamma_{\boldsymbol{q}}\, e^{i\boldsymbol{q}\boldsymbol{r}} a^\dagger_{\boldsymbol{q}} + \gamma^*_{\boldsymbol{q}}\, e^{-i\boldsymbol{q}\boldsymbol{r}} a_{\boldsymbol{q}}). \tag{2.3}$$

The two-level atom is described as fictitious spin one half by the Pauli spin matrices,

$$\sigma_x = \begin{pmatrix} 0 & 1 \\ 1 & 0 \end{pmatrix}, \qquad \sigma_y = \begin{pmatrix} 0 & -i \\ i & 0 \end{pmatrix}, \qquad \sigma_z = \begin{pmatrix} 1 & 0 \\ 0 & -1 \end{pmatrix}. \tag{2.4}$$

Spin up corresponds to the excited state and spin down to the ground state of the atom. The electromagnetic field is represented by a continuum of harmonic oscillators with creation operator $a_{\boldsymbol{q}}^{\dagger}$ for a photon with energy $\omega_{\boldsymbol{q}}$ in mode $\boldsymbol{q}$. The last term in the Hamiltonian describes the dipole interaction between the atom and the field with amplitude $\gamma_{\boldsymbol{q}}$. The rate Γ for spontaneous emission can be derived with Fermi's Golden Rule. It turns out that Γ can be written as a sum of rates $\Gamma_{\boldsymbol{q}}$ for spontaneous emission of a photon in mode $\boldsymbol{q}$, $\Gamma = \sum_{\boldsymbol{q}} \Gamma_{\boldsymbol{q}}$.

The extension to two atoms is straightforward. The Dicke effect is most clearly seen by using singlet and triplet states as a basis for the two pseudo-spins. The upper triplet state, $|T_+\rangle = |\uparrow\uparrow\rangle$, corresponds to two excited atoms whereas the lower triplet state, $|T_-\rangle = |\downarrow\downarrow\rangle$, corresponds to both atoms in the ground state. The remaining triplet state, $|T_0\rangle = (|\uparrow\downarrow\rangle + |\downarrow\uparrow\rangle)/\sqrt{2}$, is the symmetric, the singlet state $|S_0\rangle = (|\uparrow\downarrow\rangle - |\downarrow\uparrow\rangle)/\sqrt{2}$, is the antisymmetric combination of one excited atom and one atom in the ground state. Thus, the decay of two initially excited atoms to their ground state is equivalent to the transition from $|T_+\rangle$ to $|T_-\rangle$. This can happen in two different ways, either via $|T_0\rangle$ or via $|S_0\rangle$, as indicated in Fig. 2.1. Again, we employ Fermi's Golden Rule and find for the rates of spontaneous emission,

$$\Gamma_{\boldsymbol{q}}^{\pm} = \frac{\Gamma_{\boldsymbol{q}}}{2} \left| 1 \pm e^{i\boldsymbol{q}(\boldsymbol{r}_1 - \boldsymbol{r}_2)} \right|^2. \tag{2.5}$$

Here, $\Gamma_{\boldsymbol{q}}$ is the spontaneous emission rate of an independent atom. $\Gamma_{\boldsymbol{q}}^{+}$ is the rate for transitions in the symmetric channel, $|T_+\rangle \to |T_0\rangle \to |T_-\rangle$, and $\Gamma_{\boldsymbol{q}}^{-}$ for the antisymmetric channel, $|T_+\rangle \to |S_0\rangle \to |T_-\rangle$. This splitting of the decay into two different channels with different rates is the Dicke effect. If the distance $|\boldsymbol{r}_1 - \boldsymbol{r}_2|$ between the atoms is much smaller than the emitted wavelength, the rate $\Gamma_{\boldsymbol{q}}^{+}$ becomes greater than $\Gamma_{\boldsymbol{q}}^{-}$. Thus, the decay via the symmetric state $|T_0\rangle$ is faster than via the antisymmetric state $|S_0\rangle$. The fast decay is called *superradiant* and the slow one *subradiant*. This phenomenon becomes most spectacular in the limit when both atoms take the same position, yielding $\Gamma_{\boldsymbol{q}}^{+} = 2\Gamma_{\boldsymbol{q}}$ and $\Gamma_{\boldsymbol{q}}^{-} = 0$. Then, the subradiant decay is completely suppressed and the two atoms decay in a superradiant fashion. We conclude that the spontaneous emission of two atoms differs from that of an independent atom as a result of the Dicke effect. The origin of this effect is the indirect interaction between the atoms as caused by the coupling of both atoms to the same radiation field, i.e. the same environment. This emission characteristics was verified experimentally by DeVoe and Brewer a few years ago [54]. They measured the spontaneous emission of two trapped Ba_{138}^{+} ions for varying distances between the ions.

The Dicke effect becomes even more pronounced if the number of atoms is increased. Let us consider N identical two-level atoms which are assumed to couple identically to the radiation field. This is justified if the distance between the atoms is much smaller than the wavelength of the resonant photons. The Hamiltonian of

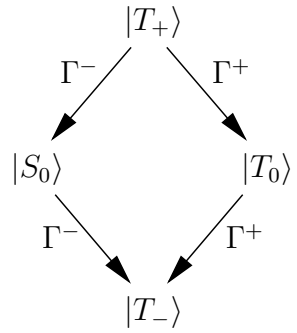

Figure 2.1: Different decay channels for two excited atoms

this system follows from that of a single atom (2.3),

$$H = \frac{\omega_0}{2} \sum_{i=1}^{N} \sigma_z^i + \sum_q \omega_q \, a_q^\dagger a_q + \frac{1}{2} \sum_{i=1}^{N} \sigma_x^i \sum_q \gamma_q \, (a_q^\dagger + a_{-q}). \tag{2.6}$$

We will neglect the vector character of the mode $\boldsymbol{q}$ in our notation from now on and assume that the coupling fulfills $\gamma_q^* = \gamma_{-q}$. The atoms are located at the origin. Since only sums of the Pauli spin matrices appear, it seems reasonable to define the new quantity

$$\boldsymbol{J} = \frac{1}{2} \sum_{i=1}^{N} \boldsymbol{\sigma}^i. \tag{2.7}$$

It follows immediately that $\boldsymbol{J}$ obeys the angular momentum algebra and hence can be considered as a large spin. With that, the Hamiltonian (2.6) reads

$$H = \omega_0 \, J_z + \sum_q \omega_q \, a_q^\dagger a_q + J_x \sum_q \gamma_q \, (a_q^\dagger + a_{-q}). \tag{2.8}$$

The Hamiltonian appears simplified due to the introduction of the large spin. However, this is only of advantage if we can relate the behavior of the large spin to the physics of the two-level atoms. This is indeed the case. The z-component of the large spin yields the polarization of the ensemble, namely the difference between the number of excited atoms and the number of atoms in the ground state. We cannot deduce the state of one individual atom from the knowledge of J_z. Yet, the collective emission of the ensemble is sufficiently described by the large spin. A differential equation for the time evolution of the large spin can be derived from the Hamiltonian (2.8), see [55]. We only mention the important steps in the calculation as they will be discussed in detail in the subsequent chapters. First, a master equation for the density matrix of the spin is derived within the Born-Markov approximation. This approach is perturbative in the coupling of the spin to the environment and

thus restricted to weak interactions. Moreover, the so-called secular approximation is applied and the influence of the nonresonant photons is neglected. An equation of motion for J_z follows from the master equation in the classical limit of a large spin, when the variance of J_z is believed to be negligible,

$$\frac{d}{dt}\langle J_z\rangle = -\Gamma\left(J+\langle J_z\rangle\right)\left(J-\langle J_z\rangle+1\right). \tag{2.9}$$

The rate Γ follows from the spectral function $\rho(\omega)$ of the environment (2.14) to be defined in the next section,

$$\Gamma = \frac{\pi}{2}\,\rho(\omega_0). \tag{2.10}$$

Obviously, this equation for J_z is not included in the Bloch equations (2.1). A quadratic term, $\langle J_z\rangle^2$, appears in (2.9) due to the collective character of the large spin, whereas the Bloch equations are linear in the spin components. We choose an initially polarized ensemble, which means that all atoms are in the excited state at $t=0$. This corresponds to the maximum spin value J,

$$\langle J_z\rangle_0 = J = \frac{N}{2}. \tag{2.11}$$

Then, the solution of the differential equation (2.9) reads

$$\langle J_z\rangle_t = \frac{2J(J+1) - J\,e^{\Gamma(2J+1)t}}{2J + e^{\Gamma(2J+1)t}}\,. \tag{2.12}$$

This function describes the collective decay of an initially excited ensemble to the final state, $\langle J_z\rangle_\infty = -J$, where all atoms occupy the ground state. In spite of all approximations made in its derivation, this solution grasps the essential properties of the Dicke effect. The most striking feature is the dependence on the number of atoms, N. The decay becomes faster as the number of atoms in the ensemble increases. The solution (2.12) predicts that the time of the decay is inverse proportional to the number of atoms. During the decay, the excitation energy of the atoms is transferred to the radiation field. Thus, the intensity of the radiation is peaked as a function of the time and the width of the peak is also inverse proportional to the number of atoms. Due to the conservation of energy, the maximum of the intensity, $I_{\max}$, increases with the square number of atoms, $I_{\max} \propto N^2$. For a large number of atoms, we expect a fast relaxation to the ground state under the emission of a short and strong radiation pulse, which accounts for the term superradiance. This behavior has been found experimentally by Greiner and co-workers [56]. They use a laser pulse to excite Tm^{3+} ions embedded in a thin slab. The measured radiation intensity clearly shows a superradiant peak.

The Dicke model does not only include the superradiance effect but also exhibits other phenomena. Often, the Dicke model is studied in a modified form where the

large spin couples to a single bosonic mode instead of a continuum. This model shows a phase transition in the thermodynamic limit of an infinite large spin with a renormalized interaction strength, as first pointed out by Hepp and Lieb [57, 58]. For a finite spin, numerical diagonalization shows the transition from Poisson to Wigner level statistics indicating quantum chaos [59, 60].

We conclude that the collective behavior is inherent to a dissipative large spin. One cannot distinguish, whether the Hamiltonian (2.8) describes a single large spin or an ensemble of two-level systems. The interesting property of the Dicke model is that the collective behavior is exclusively caused by the coupling of all systems to the same environment. No direct interaction between the atoms is considered. We shall study such dissipation induced collective effects in more detail in this thesis.

2.2.3 The Spin-Boson Model

Subject of the spin-boson model is the physics of a two-state system, a spin one half, under the influence of a dissipative environment. The latter is modeled by a bath of harmonic oscillators, that is bosons. While the applications of the Bloch equations and the Dicke model, for instance in quantum optics, often justify a perturbative treatment of the dissipation, it is the intention of the investigation of the spin-boson model to predict the behavior for all parameters, including intermediate and strong couplings [9]. A comprehensive summary of the dissipative two-state system was given by Weiss [10].

The original motivation of the spin-boson model was the investigation of macroscopic quantum tunneling in an rf SQUID [61]. The question was whether the quantum phenomenon of coherent tunneling between two separated states can appear on a macroscopic scale and how dissipation destroys the coherence. A magnetic flux trapped in an rf SQUID can be described for appropriate parameters as a particle in a double well potential. The two minima of this potential correspond to macroscopically different situations where the supercurrent in the rf SQUID has an opposite sense of rotation [10]. Further applications of the spin-boson model can be found in almost every field of physics. Apart from the systems already presented in Sec. 2.1, we mention the inversion resonance in NH_3, the motion of a muon in metals, and electron transfer in chemical reactions.

The Hamiltonian of the spin-boson model reads

$$H = \frac{\varepsilon}{2}\,\sigma_z - \frac{\Delta_s}{2}\,\sigma_x - \frac{1}{2}\,\sigma_z \sum_q \gamma_q (a_q + a_q^\dagger) + \sum_q \omega_q\, a_q^\dagger a_q. \tag{2.13}$$

The first two terms describe the unperturbed two-state system. The description by the Pauli spin matrices apply to intrinsic spins as well as any other system with a two-dimensional Hilbert space. The z-component, σ_z, typically corresponds to

the experimentally accessible quantity of the system. The energies of the eigenstates of σ_z, the so-called localized states, differ by a bias ε. However, these states are no eigenstates of the Hamiltonian (2.13) due to the tunneling with the matrix element Δ_s yielding coherent oscillations between the two eigenstates of σ_z. The dissipative environment is modeled by a bath of harmonic oscillators with creation operators $a_q^\dagger$ for a boson in mode q with eigenenergy ω_q. As the environment couples to the z-component of the spin, the interaction depends on the state of the system and thus acts as a kind of measurement. This is expected to destroy the phase coherence of the wavefunction. Hence, the physics of the dissipative two-state system is governed by the interplay between coherent tunneling and localization. The system shows qualitatively different types of behavior such as damped oscillations, exponential relaxation, and localization. The influence of the environment is completely described by the spectral function

$$\rho(\omega) = \sum_q |\gamma_q|^2 \, \delta(\omega - \omega_q), \tag{2.14}$$

where γ_q is the interaction strength of the mode q. For the so-called ohmic dissipation, the spectral function is assumed to be linear with an exponential cutoff at high frequencies. A great deal of the numerous publications on the spin-boson model apply to the ohmic dissipation since this leads to all sorts of dynamics as a function of the temperature and the coupling strength. We shall discuss the solutions in two regimes of parameters in detail in the following chapters. Although a two-state system is the smallest non-trivial quantum mechanical system, no exact solution is known for the dissipative two-state system for all regimes of parameters. The most suitable method for the theoretical description of the system seems to be the functional integral approach, on which most of the known results rely.

The Hamiltonian of the spin-boson model (2.13) resembles the Dicke model of a single atom (2.3). However, the spin-boson model is more general as the Dicke model does not include tunneling in the unperturbed system. The coupling is different in these models. We shall come back to the similarities of the two systems and the physical implications in the subsequent chapters.

Some generalizations of the spin-boson model have been investigated. The driven two-state system [62] allows for time-dependent parameters, in particular the bias $\varepsilon(t)$ and the tunnel matrix element $\Delta_s(t)$. The extension to higher dimensions is studied in the dissipative multi-state system, a tight binding model with constant tunnel rates between neighboring states and coupling to a dissipative environment [63, 64, 65]. Another approach is to consider excited states in a double well potential [66]. In chapters 3 and 4 of this thesis we shall discuss another generalization of the spin-boson model where the spin one half is replaced by a greater spin.

2.3 The Large Spin and Two-State Systems

A large spin was introduced in the Dicke model to describe the collective behavior of many two-level atoms, Sec. 2.2.2. We shall have a closer look at the relationship between the large spin and an ensemble of identical two-state systems in this section. Then, we will determine the equilibrium value of a large spin in contact with a heat bath.

Let us first consider a single two-level system. We refer to the two states as the ground state and the excited state in the following. The two-level system is equivalently described as a spin one half. Usually, one identifies the two states with the eigenstates $|\uparrow\rangle$ and $|\downarrow\rangle$ of the z-component of the spin,

$$\sigma_z |\uparrow\rangle = |\uparrow\rangle , \qquad \sigma_z |\downarrow\rangle = -|\downarrow\rangle , \tag{2.15}$$

where σ_z is the Pauli spin matrix (2.4). Thus, spin up corresponds to the excited state and spin down to the ground state. The expectation value of σ_z tells in which of the two states the system is found.

Consider now an ensemble of several two-state systems. The Hilbert space of the ensemble is the product space of the two-dimensional Hilbert spaces of all systems. For an ensemble of N systems, its dimension is 2^N. A possible basis for the product space is given by the states

$$\psi_\alpha = |m_1\rangle \otimes \ldots \otimes |m_N\rangle , \qquad \text{with } m_i \in \{\uparrow, \downarrow\}. \tag{2.16}$$

Here, α labels the 2^N basis states ψ_α. Important for the investigation of collective effects is the polarization P, defined as the difference of the number of excited systems, $N_\uparrow$, and the number of systems in the ground state, $N_\downarrow$,

$$P = N_\uparrow - N_\downarrow. \tag{2.17}$$

We do not take into account the normalization in this definition which can easily be included by an additional factor $1/N$. For a product state in the form of (2.16), the polarization follows immediately as the sum over the z-components of the spins,

$$P = \sum_{i=1}^{N} \langle \sigma_z^i \rangle . \tag{2.18}$$

In the Dicke model (2.6), the two-level atoms are assumed to be identical. Then, the sum over the Pauli spin matrices in the Hamiltonian can be replaced by the new quantity, cf. (2.7),

$$\boldsymbol{J} = \frac{1}{2} \sum_{i=1}^{N} \boldsymbol{\sigma}^i. \tag{2.19}$$

The new operator $\boldsymbol{J}$ obeys the angular momentum algebra and thus is again a spin, however, greater than one half. What makes the new operator so useful is the fact that its z-component describes the polarization of the ensemble, as follows from (2.18) and (2.19),

$$\langle J_z \rangle = \frac{1}{2} P. \tag{2.20}$$

An expectation value of $N/2$ hence corresponds to an ensemble of exclusively excited systems while an expectation value of $-N/2$ corresponds to an ensemble where all systems are in the ground state. If the number of excited systems equals the number of systems in the ground state, the expectation value becomes zero.

It is readily verified that the square of the new spin, $\boldsymbol{J}^2$, commutes with the Dicke-Hamiltonian (2.8) and with the Hamiltonian of the large-spin model (3.1) to be studied in the following. In that case, $\boldsymbol{J}^2$ is a constant of the motion. The states ψ_α (2.16), however, are no eigenstates of $\boldsymbol{J}^2$. Thus, it is preferable to choose another basis $|J, M\rangle$ of simultaneous eigenstates of $\boldsymbol{J}^2$ and J_z,

$$\boldsymbol{J}^2 |J, M\rangle = J(J+1) |J, M\rangle , \qquad J_z |J, M\rangle = M |J, M\rangle . \tag{2.21}$$

Then, the quantum number J is conserved while the quantum number M yields the polarization of the ensemble (2.20).

From quantum mechanics [67], we know that the maximum possible value of the quantum number J is given by half the number of systems, $J = N/2$. In the further discussion, we shall restrict ourselves to the $N+1$ states with maximum J. These states span a $N+1$ dimensional subspace of the 2^N dimensional Hilbert space of the ensemble. In order to justify this restriction, we note that the entirely polarized states lie in that subspace. The state $|J, M\rangle$ with $M = J$ describes an ensemble of excited two-state systems while the state with $M = -J$ corresponds to all systems in the ground state. Thus, if the initial state of the ensemble is a polarized state, the ensemble will always stay in the subspace spanned by the states $|J, M\rangle$ with $J = N/2$ since J is conserved. These states with maximum J are the symmetrized wavefunctions of $J+M$ excited systems and $J-M$ systems in the ground state [55]. They follow for instance by the successive application of the ladder operator $J_\pm$ (3.4) to the polarized state

$$|J, M\rangle = \sqrt{\frac{(J+M)!}{(2J)!\,(J-M)!}}\; J_-^{(J-M)} \; |J, M = J\rangle . \tag{2.22}$$

In the section on the Dicke model, Sec. 2.2.2, we employed triplet and singlet states for the discussion of two two-level atoms. It turned out that the decay of the two atoms occurs only in the subspace of the triplet states if the coupling of the atoms to the radiation field is identical. In fact, the states $|J, M\rangle$ with maximum J are exactly the triplet states for $N = 2$.

We conclude that an ensemble of N identical two-state systems without direct interaction can be described by a large spin of size $J=N/2$. The polarization of the ensemble follows directly from this large spin.

2.3.1 Thermodynamic Equilibrium of a Large Spin

We shall now determine the thermodynamic equilibrium of a spin of size J which is described by the Hamiltonian

$$H = \varepsilon\, J_z + 2T_c\, J_x, \tag{2.23}$$

with bias ε and the tunnel matrix element $2T_c$. The Hamiltonian will be discussed in more detail in the next chapter. It is assumed that the spin is in contact with a heat bath with inverse temperature $\beta=1/k_BT$. The density matrix ρ follows as

$$\rho = \frac{1}{Z}\, e^{-\beta H}, \qquad \text{with } Z = \mathrm{Tr}\{e^{-\beta H}\}. \tag{2.24}$$

For the Hamiltonian (2.23), the partition function Z becomes

$$Z = \frac{\sinh\big(\beta\Delta(J+1/2)\big)}{\sinh(\beta\Delta/2)}, \tag{2.25}$$

where $\Delta=\sqrt{\varepsilon^2+4T_c^2}$ is the level spacing of the Hamiltonian (2.23). Due to the symmetry of the Hamiltonian, the expectation value $\langle J_y\rangle$ vanishes in thermal equilibrium. The expectation values of the other spin components follow as derivatives of the partition function. Alternatively, they can be calculated from the density matrix, $\langle J_{x,y}\rangle=\mathrm{Tr}\{\rho J_{x,y}\}$, yielding

$$\langle J_x\rangle = -\frac{2T_c}{\Delta}\, J\, B_J(\beta\Delta), \qquad \langle J_z\rangle = -\frac{\varepsilon}{\Delta}\, J\, B_J(\beta\Delta). \tag{2.26}$$

We used the definition of the Brillouin function $B_J(x)$ [68],

$$B_J(x) = \left(1+\frac{1}{2J}\right)\coth\!\left(x\left(J+\frac{1}{2}\right)\right) - \frac{1}{2J}\coth\!\left(\frac{x}{2}\right). \tag{2.27}$$

These expressions simplify for a spin one half, $J=1/2$,

$$\langle J_x\rangle = -\frac{T_c}{\Delta}\tanh\!\left(\frac{\beta\Delta}{2}\right), \qquad \langle J_z\rangle = -\frac{\varepsilon}{2\Delta}\tanh\!\left(\frac{\beta\Delta}{2}\right), \tag{2.28}$$

We will compare these expressions with the results of the large spin model in chapter 3.

2.4 Conclusion

In this chapter, we have presented dissipative two-state systems and spins as well as corresponding theoretical approaches. While a two-state system is equivalently represented by a ficticious spin one half, a large spin is employed to describe the collective behavior in an ensemble of two-level systems with identical coupling to the environment. This description is used, for instance, in the Dicke model. On the other hand, this means that an intrinsic large spin with dissipation shows identical effects as an ensemble of two-level systems. We conclude that the model of a dissipative large spin which we will study in the following applies both to ensembles of two-level systems and to intrinsic large spins.

Chapter 3

The Large-Spin Model with Weak Dissipation

In this chapter, we turn to the investigation of the large-spin model. This model is a generalization of the spin-boson model to spins larger than one half. The model applies both on intrinsic large spins and on dissipation induced collective effects. Such effects occur in ensembles of two-level systems whose sole interaction is caused by the coupling of each system to the common dissipative environment. The collective behavior can then be described by a large spin.

The large-spin model contains the spin-boson model and the Dicke model as different special cases. This indicates how rich and comprehensive the physical properties of this model are. In this thesis, we concentrate on the investigation of the model in two limits. This chapter is devoted to weak interactions between the spin and its environment. The limit of strong interactions is considered in the subsequent chapter. Both chapters focus on an ohmic dissipation.

We employ a master equation to describe the large spin. This allows to take into account the influence of the dissipative environment on the spin without the necessity of solving the environmental degrees of freedom in presence of the large spin. The master equation is derived in Born-Markov approximation which is perturbative in the system-environment coupling. The dynamics of the spin follows from the numerical solution of the master equation.

For spin one half, the master equation can be transformed into a set of Bloch equations for the spin components. The numerical solution of which is in excellent agreement with the solution of the spin-boson model for weak ohmic dissipation at all temperatures. Collective effects appear for spins larger one half. For a strong bias, we find a superradiance-like behavior. The influence of the nonresonant bosons of the environment becomes visible in beats in the coherent oscillations of the spin. Finally, we study the equilibrium values of the large spin.

3.1 The Large-Spin Model

Different theoretical models were presented in the previous chapter which study the influence of a dissipative environment on the dynamics of a spin. These models are basically limited to the smallest possible spin, a spin one half. The spin-boson model is by definition restricted to a spin 1/2. The same applies to the Bloch equations: Their derivation is strictly valid at low temperatures only for spin 1/2. An exception is the Dicke model, which deals with an arbitrary spin. However, this model lacks generality as it does not include tunneling in the unperturbed system.

In many real systems, however, a spin larger than one half occurs. This may be a nuclear spin. The elements gallium and arsenic used in the majority of modern solid state experiments have a nuclear spin of 3/2. We also mention molecule magnets which have been investigated in a number of recent experiments, cf. Sec. 2.1.3. The most prominent examples of which, Mn_{12} and Fe_8, are believed to have a total spin of 10. Moreover, we showed in section 2.3 how a large pseudo-spin describes collective effects of an ensemble of two-level systems. These systems are assumed to be independent of each other apart from the coupling to the same environment which introduces an indirect interaction. Realizations of this model include double quantum dots, two-level systems in glasses, and registers of solid state qubits all of which interacting with phonons. In order to investigate such dissipation-induced collective effects, we employ a generalization of the spin-boson model to larger spins. The Hamiltonian of this model, referred to as the *large-spin model* in the following, is given by

$$H = \varepsilon\, J_z + 2T_c\, J_x + J_z \sum_q \gamma_q\, (a_q^\dagger + a_{-q}) + \sum_q \omega_q\, a_q^\dagger a_q. \tag{3.1}$$

The crucial point is that J_λ are components of a spin operator $\boldsymbol{J}$ obeying the spin or angular momentum commutation relations,

$$\left[J_\lambda, J_\mu\right] = i\,\varepsilon^{\lambda\mu\nu}\, J_\nu, \qquad \text{with } \lambda, \mu, \nu \in \{x, y, z\}. \tag{3.2}$$

We use the Levi-Civita symbol $\varepsilon^{\lambda\mu\nu}$ and set $\hbar = 1$. The eigenstates $|JM\rangle$ of J_z and $\boldsymbol{J}^2$ are employed to discuss the Hamiltonian,

$$\boldsymbol{J}^2\,|J, M\rangle = J(J+1)\,|J, M\rangle\,, \qquad J_z\,|J, M\rangle = M\,|J, M\rangle\,. \tag{3.3}$$

The quantum number M takes the $2J{+}1$ values from $-J$ to J. The size J of the spin is arbitrary but in general larger than one half. If the spin describes an ensemble of N identical two-level systems, its size is given by $J = N/2$. The first term in the Hamiltonian (3.1) describes a ladder of energetically equidistant states with a bias ε between adjacent states. The next term can be expressed as $2T_cJ_x = T_c(J_+ + J_-)$ where $J_\pm$ are defined as

$$J_\pm = J_x \pm iJ_y. \tag{3.4}$$

Their effect on the states $|J, M\rangle$ is to raise or to lower M by one,

$$J_\pm |J, M\rangle = c^\pm_{J,M} |J, M\pm 1\rangle , \qquad \text{with } c^\pm_{J,M} = \sqrt{J(J+1) - M(M\pm 1)}. \tag{3.5}$$

Thus, the second term introduces a tunnel coupling between neighboring states with strength T_c. The tunnel matrix elements, however, are not constant but do depend on the value M via the prefactor $c^\pm_{J,M}$. In fact, all collective effects exhibited by the large-spin model can be traced back to this M-dependent tunnel rate.

The environment and the coupling between the spin and the environment in the large-spin model (3.1) are similar to the spin-boson Hamiltonian (2.13). The dissipative environment is modeled by a continuum of harmonic oscillators, hence obeying Bose statistics. A boson in mode q with eigenenergy ω_q is created by the operator $a^\dagger_q$. The coupling between the spin and a boson in mode q has the strength γ_q. It will turn out that a single function, the spectral function, is sufficient to describe the properties of the environment. The coupling is linear in the spin as well as in the environment. The fact that the environment is coupled to the z-component of the spin is referred to as diagonal coupling. Naturally, one could also imagine nondiagonal realizations of the coupling, for instance to the x-component of the spin [69]. In this chapter, however, we do not have a specific system in mind requiring a nondiagonal coupling. Therefore, we use the diagonal form as in the standard spin-boson model.

The large-spin model reduces to the spin-boson model for spin one half. However, this is not the only conceivable generalization of the latter to larger system sizes. Another possibility is the dissipative tight-binding model. There, the tunnel amplitudes between adjacent states are constant. For ohmic dissipation at zero temperature this model shows a transition from diffusion to localization as a function of the coupling strength [63, 64, 65, 70, 71]. By definition, no collective effects exist. In the large-spin model, such effects are incorporated due to the spin algebra (3.2).

From the point of view of a many body system, the large-spin model is closely related to the Dicke model (2.8). The Dicke model employs a large spin to describe collective effects of an ensemble of identical two-level atoms. The difference between the large-spin model and the Dicke Hamiltonian is that the latter does not include tunneling and that the environment is coupled to the x-component of the spin. For zero bias, $\varepsilon = 0$, the large-spin model can be mapped exactly on the Dicke Hamiltonian (2.8) by rotation. This will be discussed in detail in section 3.5.

We conclude that the model of a large spin with coupling to a dissipative environment is closely related to the spin-boson model as well as to the Dicke model. While the spin-boson model exhibits an extremely rich variety of single particle physics, the Dicke model shows collective effects. The investigation of a combination of both systems is a promising undertaking. Yet, it is obvious that a closed solution in the whole parameter space is an unattainable task. Therefore we concentrate our studies

on two cases. In this chapter a weak coupling between the spin and the environment is considered. The strong-coupling limit is investigated in the next chapter. In both cases the main focus is on the dynamics of the z-component of the spin, J_z, since this corresponds to the physical observable in most realizations. For an ensemble of two-level atoms, J_z gives information on the total inversion as explained in Sec. 2.3.

3.2 The Master Equation

The dynamics of the large spin is completely described by its density matrix. We employ a master equation to determine the time evolution of the density matrix and thereby the behavior of the spin system. Due to the interactions between the spin and the environment it is not possible to derive an exact master equation for only the subsystem of the large spin. Instead, we derive the master equation within the Born-Markov approximation. This takes into account the interactions to the environment up to second order. We start with the solution for the spin expectation values in the noninteracting case. Then, the Hamiltonian is transformed into the interaction picture, which will be necessary in the course of the derivation of the master equation.

3.2.1 Free Solution and the Interaction Picture

Let us begin with the dynamics of the large spin in the noninteracting case, given by $H_0 = \varepsilon J_z + 2T_c J_x$. The Heisenberg equations of motion for the expectation values of the spin components read

$$\begin{aligned} \langle \dot{J}_x \rangle &= -\varepsilon \langle J_y \rangle , \\ \langle \dot{J}_y \rangle &= \varepsilon \langle J_x \rangle - 2T_c \langle J_z \rangle , \\ \langle \dot{J}_z \rangle &= 2T_c \langle J_y \rangle . \end{aligned} \tag{3.6}$$

Initial conditions have to be specified in order to solve this set of differential equations. Choosing the wave function at $t = 0$ as an eigenstate $|J, M\rangle$ of J_z, cf. (3.3), we find

$$\begin{aligned} \langle J_x \rangle_t &= M \, \frac{2T_c \, \varepsilon}{\Delta^2} \big(1 - \cos(\Delta t)\big), \\ \langle J_y \rangle_t &= -M \, \frac{2T_c}{\Delta} \, \sin(\Delta t), \\ \langle J_z \rangle_t &= M \, \frac{1}{\Delta^2} \big(\varepsilon^2 + 4T_c^2 \cos(\Delta t)\big). \end{aligned} \tag{3.7}$$

All expectation values oscillate with a frequency Δ, which is defined as

$$\Delta = \sqrt{\varepsilon^2 + 4T_c^2} \, . \tag{3.8}$$

The meaning of Δ becomes clear if we identify the unperturbed system as a spin in a magnetic field with magnitude ε in z direction and $2T_c$ in x direction. The total magnetic field adds up to $\sqrt{\varepsilon^2 + 4T_c^2}$. Thus, Δ is the constant level spacing of H_0. For a two-state system, Δ is the hybridization energy. The free time evolution of the large spin does not depend on the size of the spin, J, and only trivially on the initial value $\langle J_z \rangle_0 = M$. Clearly, no collective effects are expected for the non interacting case.

The set of equations (3.6) is actually the most simple example for Bloch equations, as introduced in Sec. (2.2.1). It will turn out that the corresponding equations do not form a closed set if the coupling to the environment is taken into account. The description of the dissipative dynamics in a manner similar to (3.6) is not possible for spins larger one half.

The next step is to transform the Hamiltonian (3.1) of the large-spin system into the interaction picture. We write the Hamiltonian as a sum of the free part and the interaction, $H = H_0 + V$, with

$$V = J_z \sum_q \gamma_q \, (a_q^\dagger + a_{-q}). \tag{3.9}$$

The interaction representation $\tilde{A}(t)$ of a time-independent operator A is defined as

$$\tilde{A}(t) = e^{iH_0 t} A \, e^{-iH_0 t} \, . \tag{3.10}$$

This transformation can be calculated with help of the Baker-Hausdorff identity,

$$\begin{aligned} \tilde{A}(t) &= A + \big[iH_0 t, A\big] + \frac{1}{2!} \, \big[iH_0 t, \big[iH_0 t, A\big]\big] + \dots \\ &= \sum_{\nu=0}^{\infty} \frac{1}{\nu!} \, \underbrace{\big[iH_0 t, \dots \big[iH_0 t}_{\nu-\text{times}}, A\big]\big]. \end{aligned} \tag{3.11}$$

For the spin operator J_z, the ν-fold commutator follows directly from the spin commutation relations (3.2),

$$\underbrace{\big[H_0, \dots \big[H_0}_{\nu-\text{times}}, J_z\big]\big] = \begin{cases} -i \, 2T_c \, \Delta^m J_y, & \nu = 2m{+}1, \; m \in \mathbb{N}_0 \\ 2T_c \, \Delta^{m-1} \big(2T_c J_z - \varepsilon J_x\big), & \nu = 2m, \; m \in \mathbb{N} \end{cases} \tag{3.12}$$

Thus, the z-component of the spin becomes

$$\tilde{J}_z(t) = J_x \, \frac{2T_c \, \varepsilon}{\Delta^2} \big(1 - \cos(\Delta t)\big) + J_y \, \frac{2T_c}{\Delta} \, \sin(\Delta t) + J_z \, \frac{1}{\Delta^2} \big(\varepsilon^2 + 4T_c^2 \cos(\Delta t)\big). \tag{3.13}$$

In the noninteracting case, the interaction picture is identical to the Heisenberg picture where the full time evolution of the system is carried by the operators. Then, we can retrieve the free solution (3.7) using the initial state $|J, M\rangle$,

$$\langle J_z \rangle_t = \langle J, M | \, \tilde{J}_z(t) \, | J, M \rangle = M \, \frac{1}{\Delta^2} \left(\varepsilon^2 + 4T_c^2 \cos(\Delta t) \right). \tag{3.14}$$

A similar calculation gives for the boson operators in the interaction picture

$$\tilde{a}_q^\dagger(t) = e^{i\omega_q t} \, a_q^\dagger \,, \qquad\qquad \tilde{a}_q(t) = e^{-i\omega_q t} \, a_q \,. \tag{3.15}$$

Hence, the interaction representation $\tilde{V}(t)$ of the coupling term follows by inserting $\tilde{J}_z(t)$ from (3.13) and $\tilde{a}_q^\dagger(t)$ from (3.15) into (3.9).

3.2.2 Born-Markov Approximation

Let us now turn to the master equation for the reduced density matrix of the spin in the limit of a weak interaction with the dissipative environment. We apply the Born-Markov approximation to derive the master equation. The Born-Markov approximation is typically employed in the field of quantum optics to describe the atom-light interactions [19, 72]. Starting point is the von Neumann equation which describes the time evolution of the density matrix $\chi(t)$ of the whole system consisting of the large spin and the environment,

$$\dot{\tilde{\chi}}(t) = -i \, \big[\tilde{V}(t), \tilde{\chi}(t) \big]. \tag{3.16}$$

Again, the tilde denotes the interaction picture. The reduced density matrix of the large spin, $\rho(t)$, follows from tracing over the degrees of freedom of the environment, also referred to as the reservoir,

$$\rho(t) = \mathrm{Tr}_{\mathrm{Res}} \big\{ \chi(t) \big\}. \tag{3.17}$$

Due to the interaction between the spin and the environment, correlations of these subsystems arise and consequently the total density matrix $\chi(t)$ cannot be written as a direct product of $\rho(t)$ and some density matrix of the environment. As we do not know the exact form of the correlated state, it is pointless to trace over the reservoir in the present form of the von Neumann equation (3.16). Instead, the von Neumann equation is integrated and the result for $\tilde{\chi}(t)$ is inserted on the right hand side of the very same equation,

$$\dot{\tilde{\chi}}(t) = -i \, \big[\tilde{V}(t), \chi(0) \big] - \int_0^t dt' \, \big[\tilde{V}(t), \big[\tilde{V}(t'), \tilde{\chi}(t') \big] \big]. \tag{3.18}$$

We assume that the spin is prepared in its initial condition and brought into contact with the environment at time $t = 0$. Then, the initial density matrix of the total

system factorizes, $\chi(0) = \rho(0) \otimes R_0$, where R_0 is the density matrix of the environment. As a consequence, the first term in (3.18) vanishes if the trace over the environment is carried out. The reason is that the interaction acting on the environment, $V_{\mathrm{Res}} = \sum_q \gamma_q (a_q^\dagger + a_{-q})$, changes the particle number while R_0 is assumed to keep the particle number fixed. This is true if R_0, describing in general a mixed state, has no addition that is a superposition of states of different particle number. In particular, the thermal equilibrium fulfills that condition. Hence, we obtain the following equation for the reduced density matrix of the spin,

$$\dot{\tilde{\rho}}(t) = -\int_0^t dt' \, \mathrm{Tr}_{\mathrm{Res}}\Big\{\big[\tilde{V}(t), \big[\tilde{V}(t'), \tilde{\chi}(t')\big]\big]\Big\}. \tag{3.19}$$

Moreover, we assume that the correlations evolving between the spin and the environment are of the order of the interaction strength,

$$\tilde{\chi}(t) = \tilde{\rho}(t) \otimes R_0 + \mathcal{O}(V). \tag{3.20}$$

The other assumption made in this equation is that the density matrix R_0 of the environment is not influenced by the interaction with the spin and therefore time-independent. This is the intrinsic property of a heat bath: it can have severe influence on the system but changes on the bath itself caused by the interaction are negligible. Later, we will assume that the environment is always in thermal equilibrium. The decomposition of the total density matrix in the fashion of (3.20) enables us to actually calculate the trace over the environment whereas equation (3.19) by itself is merely a formal statement. Inserting (3.20) into (3.19) shows that the correlations lead to terms of third order in the interaction strength. The second order *Born approximation* consists in neglecting these terms. The resulting master equation reads

$$\dot{\tilde{\rho}}(t) = -\int_0^t dt' \, \mathrm{Tr}_{\mathrm{Res}}\Big\{\big[\tilde{V}(t), \big[\tilde{V}(t'), \tilde{\rho}(t') \otimes R_0\big]\big]\Big\}, \tag{3.21}$$

which takes into account the interactions up to second order. It would have been futile to apply the decomposition (3.20) directly to the von Neumann equation (3.16), since all first-order terms vanish.

The *correlation function* of the environment, $K(t-t')$, is defined according to

$$K(t-t') = \mathrm{Tr}_{\mathrm{Res}}\big\{\tilde{V}_{\mathrm{Res}}(t)\, \tilde{V}_{\mathrm{Res}}(t')\, R_0\big\}, \tag{3.22}$$

where V_{Res} is that part of the interaction V which acts on the Hilbert space of the environment. The correlation function depends only on the time difference $t-t'$ for any time-independent form of the interaction, as implied in the definition. With the specific realization of the interaction as given in (3.9), we find

$$K(t-t') = \sum_q |\gamma_q|^2 \left(e^{i\omega_q(t-t')}\, \mathrm{Tr}_{\mathrm{Res}}\big\{a_q^\dagger a_q R_0\big\} + e^{-i\omega_q(t-t')}\, \mathrm{Tr}_{\mathrm{Res}}\big\{a_q a_q^\dagger R_0\big\}\right), \tag{3.23}$$

where all combinations of boson operators are neglected that do not conserve the particle number. The correlation function fulfills $K(-t) = K(t)^*$. In section 3.3, we will discuss the correlation function in more detail. The master equation (3.21) can be written with the correlation function as

$$\dot{\tilde{\rho}}(t) = -\int_0^t dt' \left(\left[\tilde{J}_z(t), \tilde{J}_z(t')\,\tilde{\rho}(t') \right] K(t-t') - \left[\tilde{J}_z(t), \tilde{\rho}(t')\,\tilde{J}_z(t') \right] K(t-t')^* \right). \quad (3.24)$$

The great achievement of the Born approximation becomes visible in this form of the master equation: the entire effect of the dissipative environment appears as one single function $K(t)$. The second approximation to be applied is the *Markov approximation*. For this purpose we have a closer look at (3.24). This equation states how the changes on the spin subsystem, given by $\dot{\tilde{\rho}}(t)$, depend on the state of the same system at earlier times, $\rho(t')$. Loosely speaking, the spin passes information about its state to the environment at time t', which is then returned after a delay $t-t'$ and weighted by the correlation function $K(t-t')$. Thus, the function $K(t)$ acts as a memory function of the environment describing how long information is preserved in the environment. Here, we consider a dissipative environment with a huge number of degrees of freedom. The influence of the spin on the environment is expected to be very small and quickly vanishing. Correspondingly, the memory of the environment is very short and the function $K(t)$ is peaked around $t-t'=0$. The Markov approximation consists in assuming that the width of the function $K(t)$ is much smaller than the timescale on which the system changes, i.e. the timescale of $\tilde{\rho}(t)$. Then one can replace $\tilde{\rho}(t')$ in the master equation (3.24) by $\tilde{\rho}(t)$,

$$\dot{\tilde{\rho}}(t) = -\int_0^t dt' \left(\left[\tilde{J}_z(t), \tilde{J}_z(t')\,\tilde{\rho}(t) \right] K(t-t') - \left[\tilde{J}_z(t), \tilde{\rho}(t)\,\tilde{J}_z(t') \right] K(t-t')^* \right). \quad (3.25)$$

It is essential to apply the Markov approximation in the interaction picture, where the time evolution of the density matrix is exclusively due to the interaction, as can be seen from the von Neumann equation (3.16). The free time evolution which is typically much faster is with the operators, cf. Sec. 3.2.1. Note that the Markov approximation is not unique and that also other forms appear in the literature. Sometimes, the Markov approximation is performed by replacing the correlation function by a delta function, $K(t) \to \delta(t)$, e.g. [73]. The quality of the approximation, however, depends crucially on the precise realization of the Markov approximation. In the above form, Eq. (3.25), there is still the integral over dt' to be evaluated, only that $\tilde{\rho}(t)$ is now outside this integral. Apparently, we would have obtained the same result if $\tilde{\rho}(t')$ was replaced by $\tilde{\rho}(t)$ already in (3.21). The latter form will be used as a starting point for the calculations in chapter 5 of this thesis.

The last step is to transform the master equation (3.25) back into the Schrödinger picture. We prefer to solve the master equation in the Schrödinger picture since this

will enable us to calculate the expectation value of any operator without having to transform that operator into the interaction picture first. Therefore, the relation (3.10) between the density matrix in Schrödinger and in interaction representation is differentiated with respect to time, yielding

$$\frac{d}{dt}\,\tilde{\rho}(t) = i\,e^{iH_0 t}\big[H_0, \rho(t)\big]e^{-iH_0 t} + e^{iH_0 t}\dot{\rho}(t)e^{-iH_0 t}. \tag{3.26}$$

Here, H_0 is only the spin part of the unperturbed Hamiltonian. Solving this equation for $\dot{\rho}(t)$ and substituting $\dot{\tilde{\rho}}(t)$ by (3.25), we find the master equation in Schrödinger representation,

$$\begin{aligned}\dot{\rho}(t) = i\,\big[\rho(t), H_0\big] - \int_0^t dt'\,\Big(&\big[J_z, \tilde{J}_z(t'-t)\,\rho(t)\big]\,K(t-t') \\ &- \big[J_z, \rho(t)\,\tilde{J}_z(t'-t)\big]\,K(t-t')^*\Big).\end{aligned} \tag{3.27}$$

Still, one operator, $\tilde{J}_z(t'-t)$, enters this equation in its interaction representation. To obtain an expression with all operators given in the Schrödinger picture, we insert the interaction representation (3.13) of $\tilde{J}_z(t)$, resulting in the final form of the master equation for the large spin,

$$\begin{aligned}\dot{\rho}(t) = i\,\big[\rho(t), H_0\big] &- \frac{1}{\Delta^2}\,(\varepsilon^2\,\Gamma + 4T_c^2\,\Gamma_c)\,\big[J_z, J_z\,\rho(t)\big] \\ &- \frac{2T_c\,\varepsilon}{\Delta^2}\,(\Gamma - \Gamma_c)\,\big[J_z, J_x\,\rho(t)\big] + \frac{2T_c}{\Delta}\,\Gamma_s\,\big[J_z, J_y\,\rho(t)\big] \\ &+ \frac{1}{\Delta^2}\,(\varepsilon^2\,\Gamma^* + 4T_c^2\,\Gamma_c^*)\,\big[J_z, \rho(t)\,J_z\big] \\ &+ \frac{2T_c\,\varepsilon}{\Delta^2}\,(\Gamma^* - \Gamma_c^*)\,\big[J_z, \rho(t)\,J_x\big] - \frac{2T_c}{\Delta}\,\Gamma_s^*\,\big[J_z, \rho(t)\,J_y\big].\end{aligned} \tag{3.28}$$

The integrals over the correlation function are defined as

$$\begin{aligned}\Gamma &= \int_0^\infty K(t)\;dt, \\ \Gamma_c &= \int_0^\infty K(t)\,\cos(\Delta t)\;dt, \\ \Gamma_s &= \int_0^\infty K(t)\,\sin(\Delta t)\;dt.\end{aligned} \tag{3.29}$$

The upper limit of the integration is extended to infinity since $K(t)$ is assumed to be peaked around $t = 0$ within the Markov approximation. The integrals will be evaluated in the next section. In the noninteracting case, all bosonic factors vanish,

$\Gamma = \Gamma_c = \Gamma_s = 0$. Then, only the first commutator remains in the master equation and we retrieve the von Neumann equation for the unperturbed spin in the Schrödinger picture. From the mathematical point of view, the master equation (3.28) is a first-order ordinary differential equation for the density matrix $\rho(t)$. With the specification of an initial value, the master equation has a definite solution. Since the Hilbert space of the large spin has the dimension $2J+1$, the solution of the master equation requires the integration of a set of $(2J+1)^2$ coupled equations. Although not all equations are independent of each other as the density matrix is an hermitean operator, the analytical solution of the master equation is in general unattainable. Numerically, however, the integration is a small challenge and the solution can be obtained with standard routines.

3.2.3 Master Equation for the Matrix Elements

For the numerical integration of the master equation it is preferable to express the density matrix by its elements instead of the operator form (3.28). Then, the master equation gives a set of $(2J+1)^2$ coupled differential equations. We choose the eigenstates $|J, M\rangle$ of J_z as a basis and express J_x and J_y by combinations of J_+ and J_- (3.4). Thus, the master equation (3.28) yields for $\rho_{M,N} = \langle J, M| \, \rho \, |J, N\rangle$,

$$\begin{aligned}
\dot{\rho}_{M,N}(t) = {} & i\,\varepsilon\,(N-M)\,\rho_{MN}(t) \\
& + i\,T_c\left(c^+_{J,N}\,\rho_{M,N+1} + c^-_{J,N}\,\rho_{M,N-1} - c^+_{J,M}\,\rho_{M+1,N} - c^-_{J,M}\,\rho_{M-1,N}\right) \\
& + \frac{1}{\Delta^2}\,(N-M)\left(\varepsilon^2\,\Gamma M - \varepsilon^2\,\Gamma^* N + 4T_c^2\,\Gamma_c M - 4T_c^2\,\Gamma_c^* N\right)\rho_{M,N}(t) \\
& + \frac{T_c}{\Delta^2}\,c^-_{J,M}\,(N-M)\left(\varepsilon\,\Gamma - \varepsilon\,\Gamma_c + i\Delta\,\Gamma_s\right)\,\rho_{M-1,N}(t) \\
& - \frac{T_c}{\Delta^2}\,c^+_{J,N}\,(N-M)\left(\varepsilon\,\Gamma^* - \varepsilon\,\Gamma_c^* + i\Delta\,\Gamma_s^*\right)\,\rho_{M,N+1}(t) \\
& + \frac{T_c}{\Delta^2}\,c^+_{J,M}\,(N-M)\left(\varepsilon\,\Gamma - \varepsilon\,\Gamma_c - i\Delta\,\Gamma_s\right)\,\rho_{M+1,N}(t) \\
& - \frac{T_c}{\Delta^2}\,c^-_{J,N}\,(N-M)\left(\varepsilon\,\Gamma^* - \varepsilon\,\Gamma_c^* - i\Delta\,\Gamma_s^*\right)\,\rho_{M,N-1}(t).
\end{aligned} \tag{3.30}$$

For a reasonable spin size J, this equation can be solved numerically with standard routines. We employ a fourth-order Runge-Kutta method with adaptive step size control [74].

3.3 The Bath Correlation Function

We have seen in the previous section that the entire influence of the dissipative environment on the large spin reduces to a single function, the bath correlation function $K(t)$. This section is devoted to the evaluation and discussion of the correlation function as well as the calculation of the corresponding rates Γ, Γ_c, and Γ_s.

Let us return to the correlation function in the form of (3.23). We assume that the dissipative environment is a macroscopic system so that the effects of the large spin on the environment are negligible. Moreover, we consider the simplest case, where the environment is in thermal equilibrium. This is justified in the majority of realizations. Then, the trace over the boson operators gives the Bose distribution,

$$\mathrm{Tr}_{\mathrm{Res}}\{a_q^\dagger a_q R_0\} \;=\; \frac{1}{e^{\beta\omega_q}-1}\,, \tag{3.31}$$

where β is the inverse temperature of the environment, $\beta{=}1/k_BT$. The other trace in (3.23) follows from the boson commutation relations, $a_q a_q^\dagger = 1 - a_q^\dagger a_q$. It will turn out helpful to rewrite equation (3.23) with an extra integration and delta function as

$$\begin{aligned} K(t) &= \int_0^\infty d\omega \sum_q |\gamma_q|^2\,\delta(\omega-\omega_q)\,\frac{e^{-\beta\omega}e^{i\omega t}+e^{-i\omega t}}{1-e^{-\beta\omega}} \\ &= \int_0^\infty d\omega\;\rho(\omega)\,\frac{e^{-\beta\omega}e^{i\omega t}+e^{-i\omega t}}{1-e^{-\beta\omega}}\,. \end{aligned} \tag{3.32}$$

In the second line, the *spectral function* of the environment, $\rho(\omega)$, is inserted which is defined as

$$\rho(\omega) = \sum_q |\gamma_q|^2\,\delta(\omega-\omega_q). \tag{3.33}$$

This function contains all relevant information on the environment and the coupling to the spin, apart from the temperature. The definition suggests that the spectral function is a highly discontinuous function jumping between zero and infinity, in fact, not a regular function at all. However, the environment was introduced as a macroscopic system with a continuous spectrum. Then, the sum over the modes q in the definition (3.33) of $\rho(\omega)$ becomes an integral and the spectral function appears as a well defined function. Naturally, this function depends on the specific realization of the environment namely the density of states and the distribution of the coupling strength $|\gamma_q|^2$. But since we are not concerned with the details of a certain environment in this chapter, we prefer to model the spectral function in the standard way as a power law with an exponential cutoff ω_c,

$$\rho(\omega) = g\,\omega^s e^{-\omega/\omega_c}\,. \tag{3.34}$$

The overall interaction strength is given by g and one distinguishes the cases

$$\begin{aligned} s < 1 \quad & \text{sub-ohmic,} \\ s = 1 \quad & \text{ohmic,} \\ s > 1 \quad & \text{super-ohmic.} \end{aligned}$$

The linear spectral density is called ohmic, because of the analogy to an electric circuit with induction, capacitor and resistor [75]: The equation of motion for a particle in contact to a dissipative environment with a linear spectral function shows a constant damping term. The same effect is caused by an ohmic resistor in the electric circuit. We will focus on the ohmic case in the following. In the spin-boson model, the ohmic dissipation is the most interesting case. It leads to all different kinds of dynamics, from coherent oscillations to localization, cf. Sec (2.2.3). In chapter 5, we will also meet a different type of spectral function. There, bulk acoustic phonons are considered which interact with electrons in double quantum dots. For $s \neq 1$, the interaction strength g in (3.34) is not dimensionless. This can be cured by an additional factor $\omega_c^{(1-s)}$ in the definition. We will however use the previous definition (3.34) in the following.

3.3.1 Calculation of $K(t)$

For spectral functions of the form of equation (3.34), the correlation function $K(t)$ can readily be evaluated even at finite temperatures. The integral over $d\omega$ in (3.32) is led back to tabulated ones, e.g. Gradshteyn-Ryzhik [76], and for $s>0$ we find

$$K(t) = g\,\beta^{-(s+1)}\,\Gamma(s+1)\Big[\,\zeta\Big(s{+}1, \frac{1+\beta\omega_c - i\omega_c t}{\beta\omega_c}\Big) + \zeta\Big(s{+}1, \frac{1+i\omega_c t}{\beta\omega_c}\Big)\Big]. \quad (3.35)$$

Here, $\zeta(z,a)$ is the generalized zeta function which can be represented as a series (see Magnus et al. [77] for further properties of this function),

$$\zeta(z,\alpha) = \sum_{n=0}^{\infty} \frac{1}{(n+\alpha)^z}\,, \qquad \alpha \notin \big\{0,-1,-2,\dots\big\}. \quad (3.36)$$

Consistent with the definition (3.23), the function $K(t)$ has the dimension of energy squared. Note that we do not distinguish between rates and energies as $\hbar$ is set to one. Fig. 3.1 shows the correlation function for the ohmic case at different temperatures. Both real and imaginary part are clearly peaked around $t=0$ as assumed in the Markov approximation. The real part of $K(t)$ is symmetric while the imaginary is antisymmetric, $K(-t) = K(t)^*$. This follows directly from the definition (3.22). Moreover, the imaginary part does not depend on the temperature, which becomes

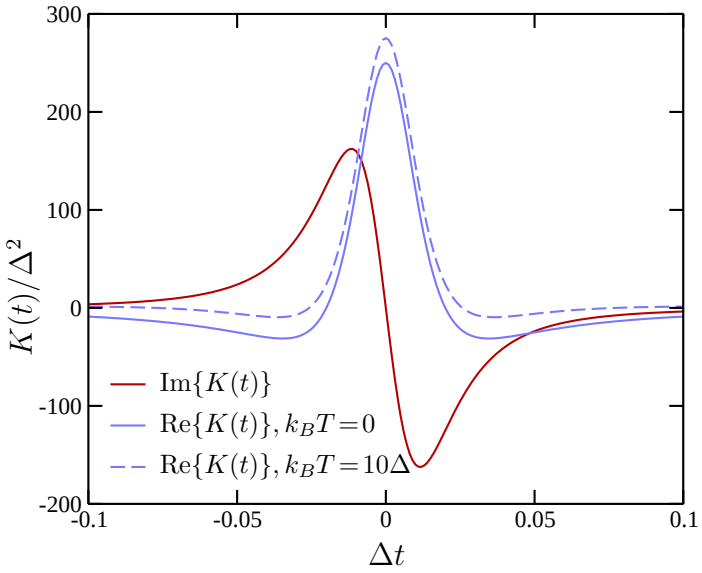

Figure 3.1: Real and imaginary part of the correlation function $K(t)$, Eq. (3.35), for an ohmic dissipation ($s=1$) at different temperatures. Δ is an arbitrary unit of the energy and we used $g=0.1$ and $\omega_c=50\Delta$.

obvious by rewriting equation (3.32) as

$$K(t) = \int_0^\infty d\omega\ \rho(\omega) \left[\cos(\omega t)\ \coth\!\left(\frac{\beta\omega}{2}\right) - i\ \sin(\omega t) \right]. \tag{3.37}$$

In the limit of zero temperature, the bath correlation function can be simplified considerably. With the help of

$$\lim_{T\to 0} \frac{e^{-\beta\omega}}{1-e^{-\beta\omega}} = 0, \qquad \lim_{T\to 0} \frac{1}{1-e^{-\beta\omega}} = 1, \tag{3.38}$$

the integration in equation (3.32) yields

$$K_{T=0}(t) = g\,\Gamma(s+1)\left(\frac{1}{\omega_c} + it\right)^{-(s+1)}. \tag{3.39}$$

This result can also be obtained directly from the finite temperature expression (3.35). In order to do that, we consider the two zeta functions separately. The second argument of the first zeta function in (3.35) goes to one in the limit of zero temperature. Then, the generalized zeta function reduces to the Riemann zeta function,

$$\zeta(z,1) = \zeta(z). \tag{3.40}$$

The Riemann zeta function is a meromorphic function with a simple pole at $z=1$, cf. [77]. In particular, $\zeta(s+1)$ is limited for $s>0$ and we find

$$\lim_{T\to 0}\ \beta^{-(s+1)}\,\zeta\Big(s+1,\frac{1+\beta\omega_c-i\omega_c t}{\beta\omega_c}\Big)=0. \tag{3.41}$$

For the second zeta function, we use the lemma

$$\lim_{\varepsilon\to 0}\ \varepsilon^z\,\zeta(z,\varepsilon u)\ =\ \frac{1}{u^z}\,,\qquad \mathrm{Re}\{z\}>0. \tag{3.42}$$

This can be proven with the series representation (3.36) of the generalized zeta function. Applying the lemma to the second zeta function in (3.35) yields

$$\lim_{T\to 0}\ \beta^{-(s+1)}\,\zeta\Big(s+1,\frac{1+i\omega_c t}{\beta\omega_c}\Big)\ =\ \Big(\frac{1}{\omega_c}+it\Big)^{-(s+1)}. \tag{3.43}$$

Thus, we recover the result of the direct calculation (3.39). This expression shows that the width of the correlation function scales with the inverse of the cutoff frequency ω_c of the spectral function $\rho(\omega)$. For large cutoffs, the width of the peak will be small – a necessary condition for the validity of the Markov approximation. For smaller cutoffs, however, the correlation function becomes broader and the Markov approximation will eventually break down.

3.3.2 Derivation of the Rates

In the final form of the master equation (3.28), the correlation function $K(t)$ does not enter directly but in form of the rates Γ, Γ_c, and Γ_s which are defined as integrals over the correlation function (3.29). These rates are to be calculated in this section. First of all, we show that the rates consist of two contributions: one describing the resonant interaction of the large spin with the environment, the other the nonresonant interaction. For an arbitrary spectral density, an expression for the resonant part is derived. In order to calculate the nonresonant parts of the rates, we concentrate on spectral densities modeled in the fashion of equation (3.34). Then, analytical expressions can be found for all rates at zero temperature. The generalization to finite temperatures is discussed for the ohmic case.

Let us first consider an arbitrary spectral function $\rho(\omega)$. The calculation of the rates (3.29) amounts to computing integrals of the form

$$\int_0^\infty dt\,K(t)\,e^{\pm i\Delta t}=\int_0^\infty dt\,\int_0^\infty d\omega\,\rho(\omega)\,\frac{e^{-\beta\omega}e^{i(\omega\pm\Delta)t}+e^{-i(\omega\mp\Delta)t}}{1-e^{-\beta\omega}}\,. \tag{3.44}$$

On the right hand side, $K(t)$ was inserted in the form of equation (3.32). The time integral can be solved using

$$\int_0^\infty dt\,e^{i\omega t}=\pi\,\delta(\omega)+iP\,\frac{1}{\omega}\,, \tag{3.45}$$

which follows from the Dirac identity. P denotes the Cauchy principal value. Hence, we obtain for the rates

$$\begin{aligned}\Gamma_c &= \frac{\pi}{2}\,\rho(\Delta)\,\coth\Big(\frac{\beta\Delta}{2}\Big) - \frac{i}{2}\,\fint_0^\infty d\omega\,\rho(\omega)\,\Big(\frac{1}{\omega+\Delta}+\frac{1}{\omega-\Delta}\Big),\\ \Gamma_s &= \frac{1}{2}\,\fint_0^\infty d\omega\,\rho(\omega)\,\coth\Big(\frac{\beta\omega}{2}\Big)\,\Big(\frac{1}{\omega+\Delta}-\frac{1}{\omega-\Delta}\Big) - i\,\frac{\pi}{2}\,\rho(\Delta).\end{aligned} \tag{3.46}$$

The remaining rate Γ follows from Γ_c in the limit of $\Delta\to 0$. Equation (3.46) shows that the imaginary parts of the rates do not depend on the temperature – consistent with the correlation function $K(t)$ (3.37). The physical meaning of the real and imaginary parts of the rates becomes clear from (3.46). The spectral function $\rho(\omega)$ is only evaluated at the resonant energy $\omega=\Delta$ in the real parts of Γ and Γ_c as well as in the imaginary part of Γ_s. These parts describe the interaction with bosons of the environment whose energy is identical to the level spacing Δ of the large spin. The other parts, the imaginary parts of Γ and Γ_c, and the real part of Γ_s account for the influence of the nonresonant bosons on the spin system. They typically result in a renormalization of the spin energy Δ. For the correct description of the dynamics of the large spin, it is important to take into account also the nonresonant bosons. On the other hand, the transport properties of quantum dots which are considered in chapter 5 have been shown to depend negligibly on the nonresonant parts [78]. Consequently, we will only consider the resonant interaction in chapter 5. A peculiarity occurs for the real part of the rate Γ: Since this rate results as the limit $\Delta\to 0$ of the rate Γ_c it appears that the real part of Γ gives the influence of bosons with energy zero on the spin. We will also neglect this part in chapter 5 and find for the rates in that case

$$\begin{aligned}\Gamma &= 0,\\ \Gamma_c &= \frac{\pi}{2}\,\rho(\Delta)\,\coth\Big(\frac{\beta\Delta}{2}\Big),\\ \Gamma_s &= -i\,\frac{\pi}{2}\,\rho(\Delta).\end{aligned} \tag{3.47}$$

Let us now turn to the case in which the spectral function is modeled according to equation (3.34). Then, we aim to calculate the complete rates including the nonresonant parts. We begin with the rate Γ which follows from Γ_c in the limit $\Delta\to 0$, cf. (3.29). In this limit, equation (3.46) leads to the Gamma function $\Gamma(s)$ for the imaginary part of the rate Γ at $s>0$. The delta function in (3.45) is counted only half for the real part due to the lower limit of the integration. Because of the divergence of the hyperbolic cotangent at $\omega=0$, the real part of Γ depends crucially on the behavior of the spectral function at small energies, i.e. on the value of the

exponent s, yielding

$$\mathrm{Im}\{\Gamma\} = -g\,\omega_c^s\,\Gamma(s), \qquad \mathrm{Re}\{\Gamma\} = \begin{cases} \infty & s<1, \\ g\pi/\beta & s=1, \\ 0 & s>1. \end{cases} \tag{3.48}$$

Apparently, the Markov approximation breaks down for sub-ohmic spectral functions for which the rate Γ diverges. The result indicates that the ohmic case is of special significance and that $s=1$ is a critical value of the environment. Only then, the real part of Γ is finite and non-zero. We do not neglect the real part in the calculations of this chapter. But we made sure that this part does not lead to any qualitative difference of the results presented in the following.

The rates Γ_c and Γ_s are given in principle by (3.46). Yet, the calculation of the principal value integrals with a spectral function $\rho(\omega)$ as in (3.34) is not possible at finite temperatures. Instead, we restrict ourselves to zero temperature and use the correlation function $K(t)$ in the form (3.39). An additional exponential cutoff has to be added to the correlation function for convergence which is later extended to infinity. Thus, we find from the definition (3.29) at zero temperature

$$\begin{aligned} \Gamma_c &= \frac{i^{-(s+1)}}{2}\, g\,\Delta^s\,\Gamma(s+1)\left[(-i)^s\, e^{-\Delta/\omega_c}\,\Gamma\Big(-s,-\frac{\Delta}{\omega_c}-i0\Big) + i^s\, e^{\Delta/\omega_c}\,\Gamma\Big(-s,\frac{\Delta}{\omega_c}\Big)\right], \\ \Gamma_s &= \frac{i^{-(s+2)}}{2}\, g\,\Delta^s\,\Gamma(s+1)\left[(-i)^s\, e^{-\Delta/\omega_c}\,\Gamma\Big(-s,-\frac{\Delta}{\omega_c}-i0\Big) - i^s\, e^{\Delta/\omega_c}\,\Gamma\Big(-s,\frac{\Delta}{\omega_c}\Big)\right]. \end{aligned} \tag{3.49}$$

The infinitesimal negative imaginary part of the second argument of the incomplete Gamma function $\Gamma(-s,z)$ is important since $\Gamma(-s,z)$ has a branch cut for negative real z [79]. The result can be simplified for positive integer s. This applies to the majority of physical models. Then, the incomplete Gamma function can be represented as a series [76],

$$\Gamma(-n,x) = \frac{(-1)^n}{n!}\left[\Gamma(0,x) - e^{-x}\sum_{m=0}^{n-1}(-1)^m\frac{m!}{x^{m+1}}\right], \tag{3.50}$$

and for a vanishing first argument it is expressed in terms of exponential integrals $\mathrm{Ei}(x)$ and $E_1(x)$ [80],

$$\Gamma(0,x\pm i0) = \begin{cases} E_1(x) & x>0, \\ -\mathrm{Ei}(-x)\mp i\pi & x<0. \end{cases} \tag{3.51}$$

Thus, equation (3.49) becomes for $s=n$

$$\Gamma_c = -\frac{i}{2}\, g\,\Delta^n\,(\Lambda_+ + \Lambda_-), \qquad \Gamma_s = -\frac{1}{2}\, g\,\Delta^n\,(\Lambda_+ - \Lambda_-), \tag{3.52}$$

with Λ_+ and Λ_- defined as

$$\begin{aligned}\Lambda_+ &= e^{-\Delta/\omega_c}\Big[-\mathrm{Ei}\Big(\frac{\Delta}{\omega_c}\Big)+i\pi-e^{\Delta/\omega_c}\sum_{m=0}^{n-1}(-1)^m\,m!\,\Big(-\frac{\omega_c}{\Delta}\Big)^{m+1}\Big],\\ \Lambda_- &= (-1)^n\,e^{\Delta/\omega_c}\Big[E_1\Big(\frac{\Delta}{\omega_c}\Big)-e^{-\Delta/\omega_c}\sum_{m=0}^{n-1}(-1)^m\,m!\,\Big(\frac{\omega_c}{\Delta}\Big)^{m+1}\Big].\end{aligned} \tag{3.53}$$

A further simplification follows for the ohmic case, $s=1$, as the sum vanishes,

$$\begin{aligned}\Gamma_c &= \frac{\pi}{2}\,g\,\Delta\,e^{-\Delta/\omega_c}+\frac{i}{2}\,g\,\Delta\Big[e^{-\Delta/\omega_c}\,\mathrm{Ei}\Big(\frac{\Delta}{\omega_c}\Big)+e^{\Delta/\omega_c}E_1\Big(\frac{\Delta}{\omega_c}\Big)-\frac{2\omega_c}{\Delta}\Big],\\ \Gamma_s &= -\frac{1}{2}\,g\,\Delta\Big[-e^{-\Delta/\omega_c}\,\mathrm{Ei}\Big(\frac{\Delta}{\omega_c}\Big)+e^{\Delta/\omega_c}E_1\Big(\frac{\Delta}{\omega_c}\Big)\Big]-i\,\frac{\pi}{2}\,g\,\Delta\,e^{-\Delta/\omega_c}.\end{aligned} \tag{3.54}$$

The agreement of the real part of Γ_c and the imaginary part of Γ_s with the general result (3.46) in the limit of zero temperature is immediately seen. Since the imaginary parts of the rates do not depend on temperature, the imaginary part of Γ_c as given in equation (3.54) is at the same time valid for all temperatures. This argument, however, does not apply to the real part of Γ_s. Thus, for an ohmic spectral density at finite temperatures, we have found analytical expressions for all rates except the real part of Γ_s. This remains to be evaluated numerically at finite temperatures.

3.4 The Spin-Boson Limit

For the smallest possible value of the spin, $J=1/2$, the large-spin Hamiltonian (3.1) reduces to the spin-boson model, cf. Sec. 2.2.3. The latter has been studied by many authors in great detail and results for most regimes of parameters can be found in the literature. This enables us to compare and to judge the Born-Markov approximation for $J=1/2$. It turns out that the Born-Markov approximation gives reliable results for weak ohmic dissipation at all temperatures.

For easy reference, we repeat the spin-boson Hamiltonian (2.13),

$$H=\frac{\varepsilon}{2}\,\sigma_z-\frac{\Delta_s}{2}\,\sigma_x-\frac{1}{2}\,\sigma_z\sum_q\gamma_q(a_q+a_q^\dagger)+\sum_q\omega_q\,a_q^\dagger a_q. \tag{3.55}$$

The overall interaction strength of the spin-boson model is denoted in the following by α. Due to a different definition of the spectral function in the spin-boson literature, this value differs by a factor of two from the interaction strength g in our notation (3.34). Thus, the relations between the spin-boson model and the large-spin model for $J=1/2$ are

$$\Delta_s=2T_c,\qquad \alpha=\frac{g}{2}\,, \tag{3.56}$$

while the bias ε and the cutoff ω_c are identical in both models. Due to the minus sign in the tunnel term, $-\Delta_s\sigma_x/2$ in (3.55), the x-components of the spins have opposite signs in the two models, $\sigma_x = -2J_x$. The different signs of the interaction terms have no consequence as only the square of the interaction coefficient γ_q enters the definition of the spectral function.

3.4.1 Results for the Spin-Boson Model

An overview of the spin-boson model was given in section 2.2.3. In this section, we present the results for small couplings between the spin and the environment, $\alpha \ll 1$. It is a priori clear, that the Born-Markov approximation which is perturbative in the coupling should only be applied in that regime. We follow the work of Weiss [10, 73] who gives approximative solutions for the dynamics of the spin components for weak ohmic dissipation. Two regimes have to be distinguished: The so-called Markov regime at intermediate temperatures and the non-Markov regime at low temperatures. A smooth transition between the two regimes occurs around the temperature $T_b = \sqrt{\Delta_r^2 + \varepsilon^2}/k_B$, with Δ_r as defined below.

The solution in the Markov regime, $T \gtrapprox T_b$, is obtained by the *noninteracting-blip approximation* (NIBA) [9, 10]. For the initial conditions $\langle\sigma_z\rangle_0 = 1$ and $\langle\sigma_x\rangle_0 = \langle\sigma_y\rangle_0 = 0$, the solution reads

$$\begin{aligned} \langle\sigma_z\rangle_t &= a_1\, e^{-\gamma_r t} + \big[(1-a_1-\langle\sigma_z\rangle_\infty)\cos\Omega t + a_2 \sin\Omega t\big] e^{-\gamma t} + \langle\sigma_z\rangle_\infty\,, \\ \langle\sigma_x\rangle_t &= b_1\, e^{-\gamma_r t} + \big[-(b_1+\langle\sigma_x\rangle_\infty)\cos\Omega t + b_2 \sin\Omega t\big] e^{-\gamma t} + \langle\sigma_x\rangle_\infty\,. \end{aligned} \tag{3.57}$$

The dynamics of the y-component of the spin follows as the time derivative of the z-component, $\langle\sigma_y\rangle_t = \langle\dot\sigma_z\rangle_t / \Delta_s$, which can be seen directly from the Heisenberg equations of motion. The parameters in equation (3.57) are defined as

$$\begin{aligned} \Delta_r &= \Delta_s \left(\frac{\Delta_s}{\omega_c}\right)^{\alpha/(1-\alpha)}, & \Delta_T &= \Delta_r \left(\frac{2\pi k_B T}{\Delta_r}\right)^{\alpha}, \\ \gamma_r &= \frac{2\pi\,\alpha\, k_B T \Delta_T^2}{\Delta_T^2 + \varepsilon^2 + (2\pi\,\alpha\, k_B T)^2}\,, & \gamma &= 2\pi\,\alpha\, k_B T - \frac{\gamma_r}{2}, \\ \Omega &= \sqrt{\varepsilon^2 + \Delta_T^2 + \frac{\gamma_r^2}{4} - \gamma\gamma_r}\,, & D &= \Omega^2 + (\gamma-\gamma_r)^2, \\ a_1 &= \frac{\Omega^2 + \gamma^2 - \Delta_T^2 - (\Omega^2+\gamma^2)\,\langle\sigma_z\rangle_\infty}{D}\,, & a_2 &= \frac{(\gamma_r-\gamma)a_1 + \gamma\big(1-\langle\sigma_z\rangle_\infty\big)}{\Omega}\,, \\ b_1 &= \frac{-1}{D}\left(\frac{\varepsilon\Delta_T^2}{\Delta_s} + \frac{\varepsilon^2(\gamma^2+\Omega^2)}{\gamma^2+\Omega^2-\Delta_T^2}\,\langle\sigma_x\rangle_\infty\right), & b_2 &= \frac{\pi\alpha\Delta_T^2/\Delta_s + (\gamma_r-\gamma)b_1 - \gamma\,\langle\sigma_x\rangle_\infty}{\Omega}. \end{aligned} \tag{3.58}$$

The expressions for γ_r, γ, and Ω apply to the biased system with $\varepsilon > \Delta_T/2\sqrt{2}$. The equilibrium values follow as

$$\langle\sigma_z\rangle_\infty = -\tanh\left(\frac{\varepsilon}{2k_BT}\right), \qquad \langle\sigma_x\rangle_\infty = \frac{\Delta_s}{\varepsilon}\tanh\left(\frac{\varepsilon}{2k_BT}\right). \tag{3.59}$$

Apparently, these expressions for $\langle\sigma_z\rangle_\infty$ and $\langle\sigma_x\rangle_\infty$ do not agree with the thermodynamic results (2.28) at low temperatures. In fact, the NIBA results become unphysical in that regime and indicate that the method fails at low temperatures: The value of $\langle\sigma_x\rangle_\infty$ for instance exceeds the maximum possible value of +1 for $0 < \varepsilon < \Delta_s$. The equilibrium value $\langle\sigma_z\rangle_\infty$ on the other hand predicts a fully localized spin for an arbitrary small bias.

The regime of low temperatures, $T \lessapprox T_b$, is often described as the non-Markov regime. It should be emphasized, however, that it does not necessarily mean that the Markov approximation fails in this regime. The quality of the Markov approximation depends on the exact realization as discussed in section 3.2.2. The solution in the non-Markov regime is derived by considering interblip correlations [10], yielding

$$\begin{aligned}\langle\sigma_z\rangle_t = &\left(\frac{\Delta_{\text{eff}}^2}{\tilde\Omega^2}\cos\tilde\Omega t + \frac{\tilde\gamma_r\varepsilon^2 + \tilde\gamma\Delta_{\text{eff}}^2 - \tilde\gamma_r\tilde\Omega^2\langle\sigma_z\rangle_\infty}{\tilde\Omega^3}\sin\tilde\Omega t\right)e^{-\tilde\gamma t}\\ &+\left(\frac{\varepsilon^2}{\tilde\Omega^2} - \langle\sigma_z\rangle_\infty\right)e^{-\tilde\gamma_r t} + \langle\sigma_z\rangle_\infty\,,\end{aligned} \tag{3.60}$$

$$\langle\sigma_x\rangle_t = \left(\frac{\varepsilon\Delta_{\text{eff}}^2}{\Delta_s\tilde\Omega^2}\cos\tilde\Omega t + \tilde b_2\sin\tilde\Omega t\right)e^{-\tilde\gamma t} - \left(\frac{\varepsilon\Delta_{\text{eff}}^2}{\Delta_s\tilde\Omega^2} + \langle\sigma_x\rangle_\infty\right)e^{-\tilde\gamma_r t} + \langle\sigma_x\rangle_\infty\,.$$

The parameters in these expressions are defined as

$$\begin{aligned}&\Delta_{\text{eff}} = \Delta_r\big[\Gamma(1-2\alpha)\cos(\pi\alpha)\big]^{1/2(1-\alpha)}, && \Delta_b = \sqrt{\Delta_{\text{eff}}^2 + \varepsilon^2}\,,\\ &\tilde\Omega^2 = \Delta_b^2 + 2\alpha\left[\operatorname{Re}\psi\Big(\frac{i\,\Delta_b}{2\pi k_BT}\Big) - \ln\Big(\frac{\Delta_b}{2\pi k_BT}\Big)\right], && \tilde\gamma = \frac{\tilde\gamma_r}{2} + \frac{2\pi\,\alpha\,\varepsilon^2\,k_BT}{\Delta_b^2}\,,\\ &\tilde b_2 = \frac{\Delta_{\text{eff}}^2}{\Delta_s\tilde\Omega}\left[\pi\alpha + \frac{\varepsilon(\tilde\gamma - \tilde\gamma_r)}{\tilde\Omega^2}\right] - \frac{\tilde\gamma_r\,\langle\sigma_x\rangle_\infty}{\tilde\Omega}\,, && \tilde\gamma_r = \pi\alpha\,\coth\Big(\frac{\Delta_b}{2k_BT}\Big)\frac{\Delta_{\text{eff}}^2}{\Delta_b}\,,\end{aligned} \tag{3.61}$$

where $\psi(z)$ is the digamma function. The equilibrium values in the non-Markov regime are given by

$$\langle\sigma_z\rangle_\infty = -\frac{\varepsilon}{\Delta_b}\tanh\left(\frac{\Delta_b}{2k_BT}\right), \qquad \langle\sigma_x\rangle_\infty = \frac{\Delta_{\text{eff}}^2}{\Delta_s\Delta_b}\tanh\left(\frac{\Delta_b}{2k_BT}\right). \tag{3.62}$$

These values match with the thermodynamic results (2.28) in the limit of zero coupling to the environment, $\alpha \to 0$. The different solutions (3.60) and (3.57) agree for intermediate temperatures, $T \approx T_b$. We will use these solutions as a reference for the results of the Born-Markov approximation.

3.4.2 Born-Markov Approximation for $J=1/2$

We now return to the master equation (3.28) for the large spin in Born-Markov approximation. A peculiarity occurs for spin one half: In that case, a closed set of equations for the expectation values of the spin components follows from the master equation, comparable to the Bloch equations as presented in section 2.2.1. This set is found by multiplying the master equation (3.28) with the corresponding spin operator and tracing over the spin degrees of freedom. The products of spin operators which appear in the course of doing so reduce for $J=1/2$ to single spin operators or the (2×2) unity matrix $\mathbb{1}$. The reason is that the Pauli spin matrices together with the unity matrix form a closed group with respect to the multiplication. Thus, we find for $J=1/2$ the Bloch equations

$$\begin{aligned}
\langle \dot{J}_x \rangle &= -\frac{1}{\Delta^2}\left(\varepsilon^2 \operatorname{Re}\{\Gamma\} + 4T_c^2 \operatorname{Re}\{\Gamma_c\}\right)\langle J_x\rangle - \varepsilon \langle J_y\rangle \\
&\quad + \frac{2T_c\,\varepsilon}{\Delta^2}\left(\operatorname{Re}\{\Gamma\} - \operatorname{Re}\{\Gamma_c\}\right)\langle J_z\rangle + \frac{T_c}{\Delta}\operatorname{Im}\{\Gamma_s\}, \\
\langle \dot{J}_y \rangle &= \varepsilon \langle J_x\rangle - \frac{1}{\Delta^2}\left(\varepsilon^2 \operatorname{Re}\{\Gamma\} + 4T_c^2 \operatorname{Re}\{\Gamma_c\}\right)\langle J_y\rangle \\
&\quad - \left(2T_c + \frac{2T_c}{\Delta}\operatorname{Re}\{\Gamma_s\}\right)\langle J_z\rangle + \frac{T_c\,\varepsilon}{\Delta^2}\left(\operatorname{Im}\{\Gamma\} - \operatorname{Im}\{\Gamma_c\}\right), \\
\langle \dot{J}_z \rangle &= 2T_c \langle J_y\rangle .
\end{aligned} \tag{3.63}$$

A similar set of Bloch equations was recently published by Hartmann et al. [81]. It is, however, not possible to extend these equations to a larger spin without additional approximations. This was already remarked in the original works by Bloch [48, 49]. The difficulty arises because products of spin operators cannot be replaced by a single spin operator for spins larger than one half. The corresponding equations do not form a closed set anymore. Hence, we can only transform the master equation into Bloch equations for spin one half. For larger spins we will have to come back to the master equation (3.28).

Let us first consider the unbiased system, $\varepsilon=0$. Then, the equations for $\langle J_y\rangle$ and $\langle J_z\rangle$ decouple from $\langle J_x\rangle$ and we find the equation of a damped harmonic oscillator for $\langle J_z\rangle$,

$$\langle \ddot{J}_z \rangle + \operatorname{Re}\{\Gamma_c\}\langle \dot{J}_z\rangle + 4T_c^2\left(1 + \frac{\operatorname{Re}\{\Gamma_s\}}{2T_c}\right)\langle J_z\rangle = 0. \tag{3.64}$$

This result clearly shows the influence of the dissipative environment on the spin dynamics: First of all damping is introduced by the interaction with the resonant bosons, expressed by $\operatorname{Re}\{\Gamma_c\}$. Moreover, the influence of the nonresonant bosons, $\operatorname{Re}\{\Gamma_s\}$, leads to a shift of the oscillation frequency. The equation for $\langle J_x\rangle$ on the other hand describes an exponential decay to its equilibrium value.

For an arbitrary bias, $\varepsilon \geq 0$, the equilibrium values of the spin components follow from the Bloch equations (3.63). It is readily seen that $\langle J_y \rangle_\infty$ vanishes. The other two components are

$$\begin{aligned} \langle J_z \rangle_\infty &= \frac{\varepsilon \,\mathrm{Re}\{\varepsilon^2 \,\Gamma + 4T_c^2 \,\Gamma_c\} \,\mathrm{Im}\{\Gamma - \Gamma_c\} + \varepsilon \Delta^3 \,\mathrm{Im}\{\Gamma_s\}}{2\Delta \,\mathrm{Re}\{\varepsilon^2 \,\Gamma + 4T_c^2 \,\Gamma_c\}(\Delta + \mathrm{Re}\{\Gamma_s\}) - 2\varepsilon^2 \Delta^2 \mathrm{Re}\{\Gamma - \Gamma_c\}}\,, \\ \langle J_x \rangle_\infty &= \frac{T_c \Delta^2 \,\mathrm{Im}\{\Gamma_s\}(\Delta + \mathrm{Re}\{\Gamma_s\}) + \varepsilon^2 T_c \,\mathrm{Re}\{\Gamma - \Gamma_c\} \,\mathrm{Im}\{\Gamma - \Gamma_c\}}{\Delta \,\mathrm{Re}\{\varepsilon^2 \,\Gamma + 4T_c^2 \,\Gamma_c\} \,(\Delta + \mathrm{Re}\{\Gamma_s\}) - \varepsilon^2 \Delta^2 \,\mathrm{Re}\{\Gamma - \Gamma_c\}}\,. \end{aligned} \tag{3.65}$$

These expressions simplify considerably in the limit of zero coupling, $g \to 0$. Neglecting products of the rates in the nominator as well as in the denominator yields with (3.46)

$$\langle J_z \rangle_\infty = -\frac{\varepsilon}{2\Delta} \tanh\left(\frac{\beta\Delta}{2}\right), \qquad \langle J_x \rangle_\infty = -\frac{T_c}{\Delta} \tanh\left(\frac{\beta\Delta}{2}\right). \tag{3.66}$$

These results agree with the thermodynamic results (2.28). Since the Born-Markov approximation gives the correct equilibrium values in the limit of zero coupling for all temperatures, we have no indication at this point that the Born-Markov approximation breaks down below a certain temperature similar to the noninteracting-blip approximation.

3.4.3 Comparison of the Different Approaches

After having presented the Born-Markov approximation for a spin one half and the solution of the spin-boson model with weak ohmic dissipation in the previous sections, we now compare the two methods for different parameters. Therefore, the Bloch equations (3.63) which follow from the master equation in Born-Markov approximation (3.28) are solved numerically. We use the initial conditions $\langle J_z \rangle_0 = 1/2$, $\langle J_x \rangle_0 = \langle J_y \rangle_0 = 0$, corresponding to an initially localized system, throughout this section. Three different regimes of the parameters are investigated, a large bias, a zero bias, and an intermediate bias. Depending on the temperature, the NIBA solution or the non-Markov solution of the spin-boson model applies.

We begin with a system of intermediate bias, $\varepsilon = T_c$, at a finite temperature $k_B T = 2T_c$. The cutoff frequency for the ohmic spectral density is chosen as $\omega_c = 50 T_c$ throughout this chapter. With an interaction strength of $g = 0.1$, corresponding to $\alpha = 0.05$, cf. (3.56), the transition temperature between the Markov and the non-Markov regime of the spin-boson model becomes $k_B T_b \approx 2.0 T_c$. Thus, the system is in the Markov regime and the solution of the spin-boson model is given by the NIBA results (3.57). These results are plotted in Fig. 3.2 as $\langle J_z \rangle = \langle \sigma_z \rangle /2$ and $\langle J_x \rangle = -\langle \sigma_x \rangle /2$ together with the solution of the Bloch equations (3.63). The different

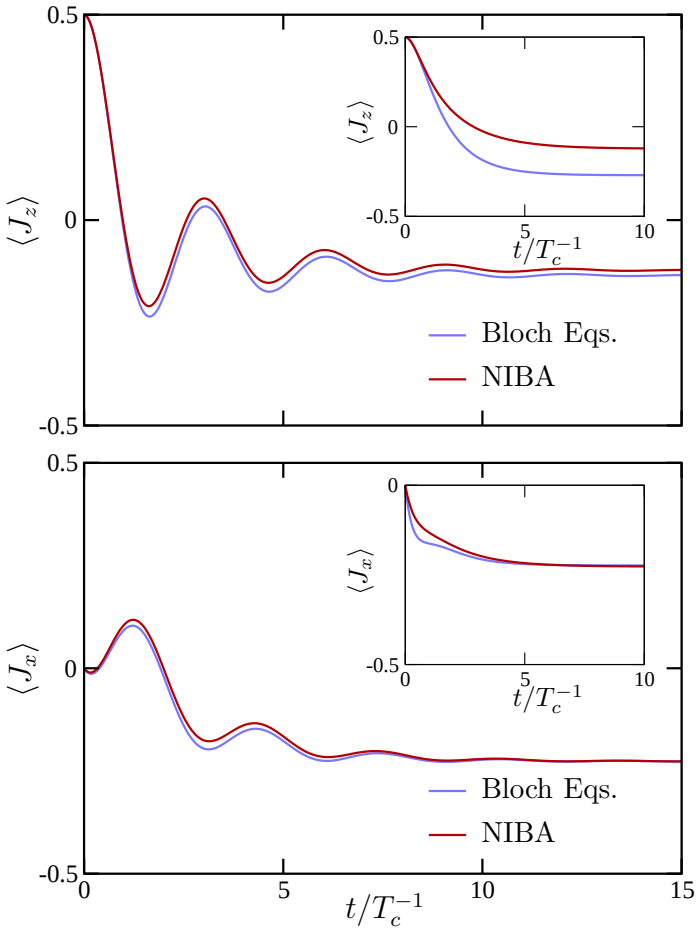

Figure 3.2: Dynamics of the spin-boson model for $\varepsilon = T_c$, $\omega_c = 50T_c$, $k_BT = 2T_c$, and $g = 0.1$ (inset $g = 0.4$) according to the NIBA (3.57) and the Bloch equations (3.63).

methods are in excellent agreement both for $\langle J_z \rangle$ and for $\langle J_x \rangle$. For an increased coupling strength, $g = 0.4$, deviations between the different solutions become evident as shown in the inset of Fig. 3.2. However, this is not surprising as the Bloch equations are perturbative in the coupling strength and by definition only valid for small couplings. Apparently, the Born-Markov approximation gives correct results in the regime of intermediate temperatures and weak interaction.

Next, we investigate the regime of low temperatures, the non-Markov regime, where the NIBA is not reliable anymore. We consider a symmetric system, $\varepsilon = 0$, at zero temperature. With the other parameters as above, the transition temperature is finite, $k_BT_b \approx 1.7T_c$, so that the system is clearly in the non-Markov regime. Then, we have to compare the results of the Bloch equations with the low temperature solution (3.60) of the spin-boson model. For zero bias, the Bloch equations decouple

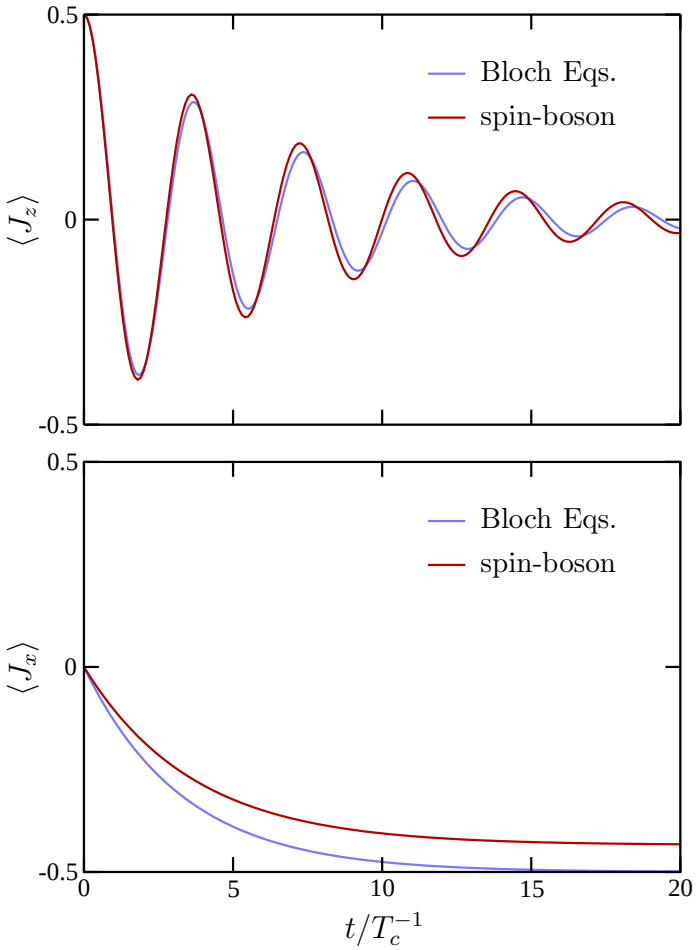

Figure 3.3: Dynamics of the spin components resulting from the Bloch equations (3.63) and the low temperature solution of the spin-boson model (3.60) for $\varepsilon = 0$, $k_B T = 0$, $g = 0.1$, and $\omega_c = 50 T_c$.

and we find the equation of a damped harmonic oscillator for the z-component of the spin, $\langle J_z \rangle$, while $\langle J_x \rangle$ decays exponentially to the equilibrium value, as derived in the previous section. These results agree well with the low temperature solution (3.60) as can be seen from Fig. 3.3. It should be emphasized that the Born-Markov approximation yields the correct oscillation frequency for weak interaction. For a smaller coupling, e.g. $g = 0.05$, the different results for $\langle J_z \rangle$ cannot be distinguished (not shown). The equilibrium value $\langle J_x \rangle_\infty$ of the Bloch equations appears too large as compared to the low temperature solution in Fig. 3.3. However, it was mentioned in the previous section that both equilibrium values, i.e. (3.65) and (3.62), approach the thermodynamic result (2.28) in the limit of zero coupling and hence coincide in that limit. Thus, we find that the results of the Born-Markov approximation are

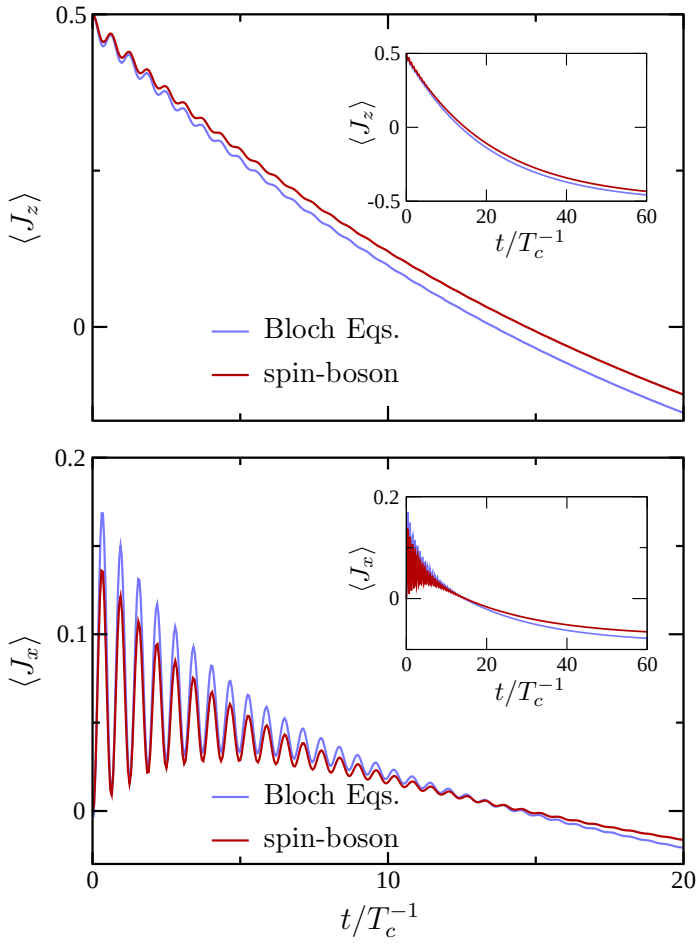

Figure 3.4: Spin dynamics for a large-biased system according to the Bloch equations (3.63) and the low temperature solution of the spin-boson model (3.60) for $\varepsilon = 10T_c$, $k_BT = T_c$, $g = 0.1$, and $\omega_c = 50T_c$.

reliable for low temperatures down to $k_BT = 0$.

Finally, we compare the different results for a system with a large bias, $\varepsilon = 10T_c$. At a temperature of $k_BT = T_c$ also this system is in the non-Markovian regime, since the transition temperature results as $k_BT_b \approx 10.1T_c$. Again, the result of the Bloch equations is in good agreement with the solution of the spin-boson model (3.60), as can be seen from Fig. 3.4. The insets of that figure show that also the long-time behavior of the two methods agree.

We conclude that the Born-Markov approximation which is perturbative in the system-environment coupling correctly describes the dynamics of the spin-boson model for weak ohmic dissipation. This applies to all temperatures down to zero temperature. Both in the intermediate and in the low temperature regime the results are in good agreement with the respective solutions of the spin boson system. With

increasing coupling strength, the deviations grow as expected from a perturbative method. Hence, the spin-boson system is correctly described by the set of Bloch equations (3.63) for a weak interaction to the environment. This is corroborated by recent results for the driven two-state system [81]. Moreover, there is no reason to assume that the Born-Markov approximation breaks down for larger spins. We expect that the master equation (3.28) is a reliable description for the large-spin model with weak dissipation.

3.5 Relation to the Dicke Hamiltonian

The close relation between the large-spin model and the Dicke Hamiltonian was already mentioned at the beginning of this chapter. We will now discuss the connection between these two models in detail. In particular, we consider the effect of superradiance that is characteristic of the Dicke Hamiltonian, cf. Sec. 2.2.2.

Superradiance is the collective spontaneous emission of an ensemble of initially excited two-level systems. The indirect interaction between the two-level systems leading to this effect is caused by the coupling of all two-level systems to the common radiation field. In the description of a large spin the superradiance effect becomes visible in an accelerated decay of the z-component of the spin: The time J_z needs to decay from the initial value $\langle J_z\rangle_0 = +J$ to the ground state is typically inverse proportional to the size of the total spin, J. The decay becomes faster with increasing spin size. In a semiclassical approximation, the dynamics of $\langle J_z\rangle$ is given by equation (2.12) which is repeated here for easy reference,

$$\langle J_z\rangle_t = \frac{2J(J+1) - J\, e^{\Gamma(2J+1)t}}{2J + e^{\Gamma(2J+1)t}}\,, \tag{3.67}$$

with Γ as defined in (2.10). The two most severe approximations made in the derivation of the semiclassical solution are the secular approximation and the disregarding of the nonresonant bosonic modes. The secular approximation ignores operator combinations J_+J_+ and J_-J_- in the master equation.

The large-spin model can be mapped exactly on the Dicke Hamiltonian for zero bias, $\varepsilon = 0$. Then, one model is transformed into the other by rotation around the y-axis. Suppose, we rotate the frame of reference of the large-spin model by $\pi/2$. Then, any operator A is expressed in the rotated frame as

$$\bar{A} = e^{i\pi/2\, J_y} A\, e^{-i\pi/2\, J_y}\,. \tag{3.68}$$

The rotation gives for the spin operators $\bar{J}_x = J_z$ and $\bar{J}_z = -J_x$. Thus, the large spin Hamiltonian reads in the rotated frame

$$\bar{H} = 2T_c\, J_z - J_x \sum_q \gamma_q\, (a_q^\dagger + a_{-q}) + \sum_q \omega_q\, a_q^\dagger a_q. \tag{3.69}$$

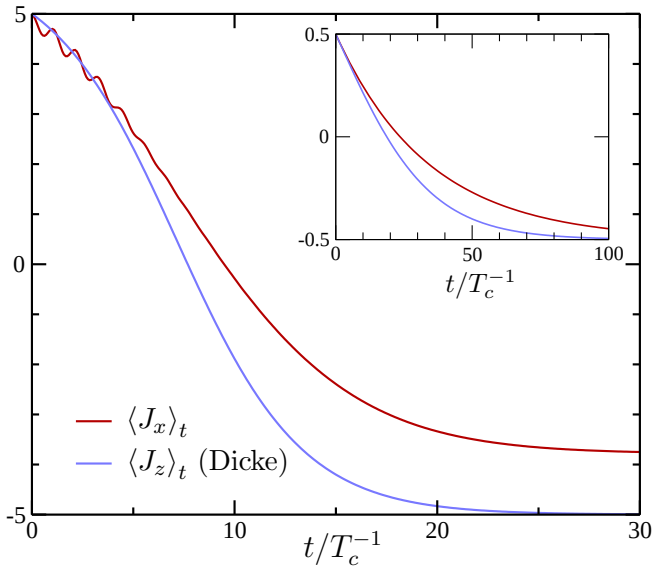

Figure 3.5: Superradiant decay of J_x in the large-spin model together with the semiclassical solution (3.67) for J_z in the Dicke model ($J=5$ (inset: $J=0.5$), $\varepsilon=0$, $g=0.01$, $\omega_c=30T_c$, and $k_BT=0$).

This form is identical to the Dicke Hamiltonian (2.8) with $\omega_0=2T_c$. Consequently, the large-spin model exhibits superradiance in its *original* J_x component.

The superradiant decay of J_x in the large-spin model is best observed if the initial density matrix ρ_0 is chosen such that $\langle J_x\rangle_0=J$ and $\langle J_y\rangle_0=\langle J_z\rangle_0=0$. This is in contrast to the previous section where $\langle J_z\rangle_0$ was chosen maximum. The initial density matrix is constructed as $\rho_0=|\psi\rangle\langle\psi|$ where $|\psi\rangle$ is the eigenstate of J_x with the maximum eigenvalue J. Since the master equation for the matrix elements of the density matrix (3.30) is expressed with respect to the eigenstates of J_z, one has to diagonalize J_x in that basis to construct ρ_0. This can easily be done numerically for a reasonable spin size, J.

Figure 3.5 shows the time evolution of the x-component of the large spin, $\langle J_x\rangle$, together with the semiclassical solution of the Dicke Hamiltonian (3.67) for a total spin of size $J=5$ and $J=0.5$ (inset) with ohmic dissipation. The deviations are caused by the additional approximations in the derivation of the semiclassical solution. Both curves exhibit the typical superradiance property that the time of the decay decreases with increasing spin size. Moreover, also the form of the curves change. We showed in the previous section for spin one half and zero bias that the decay of $\langle J_x\rangle$ is purely exponential. This changes for larger spins, as can be seen from Fig. 3.5. Then, the decay only starts after some delay time. For a large spin, $\langle J_x\rangle$ does not decay completely anymore, in contrast to the semiclassical solution which approaches $-J$ for large times. This is caused by the interaction

of the large spin with the nonresonant bosons, which are not considered in the semiclassical solution. Moreover, the numerical solution for $\langle J_x \rangle$ shows an oscillatory behavior at the beginning of the decay. These oscillations are caused by the operator combinations $J_+ J_+$ and $J_- J_-$ in the master equation which are neglected in the secular approximation. They describe two boson processes. One can show from the master equation of the Dicke model that the frequency of these oscillations is approximately given by $2\omega_0 = 4T_c$. We find numerically that the amplitude as well as the frequency of the oscillations is increased due to the influence of the nonresonant bosons.

We conclude that for zero bias, $\varepsilon = 0$, the large-spin model becomes identical to the Dicke Hamiltonian, however in a rotated frame of reference. Therefore, the effect of superradiance occurs in the decay of the x-component of the large spin, J_x. For an ohmic dissipation, the time evolution is not satisfactorily described by the semiclassical solution (3.67). In particular, we find that the decay of J_x is not complete due to the influence of the nonresonant bosons.

3.6 Results for the Large-Spin Model

In the previous sections, we considered two limits in which the large spin reduces to familiar models, first the dissipative two-state system and then the Dicke model. We shall now leave these grounds and turn to the investigation of the large-spin model with weak ohmic dissipation. Thereby, we focus on collective effects and the question how the behavior of the large spin changes as the spin size increases. Three different regimes are studied: a zero bias, $\varepsilon = 0$, a strong bias, $\varepsilon = 10T_c$, and finally an intermediate bias, $\varepsilon = T_c$.

3.6.1 Superradiant Dynamics

We saw in section 3.5 that the large-spin model becomes identical to the Dicke Hamiltonian for zero bias. As a consequence, the x-component of the spin, J_x, exhibits superradiance. It seems reasonable to ask if a similar statement is also valid for the z-component: Does J_z decay in a superradiant fashion for appropriate parameters? The answer is yes, as we will show in the following. We choose a large bias, $\varepsilon = 10T_c$, to ensure the decay of J_z and calculate the dynamics for different spin sizes J. We find a superradiance-like behavior which can be seen in Fig. 3.6. The decay of the normalized z-component $\langle J_z \rangle / J$ is plotted in that figure for the spin sizes $J = 1/2$, 2, 5, and 10 for an initially polarized spin, $\langle J_z \rangle_0 = J$. It is clearly visible that the time in which the spin decays decreases with increasing spin size, similar to the Dicke superradiance. The change of the form of the curves becomes apparent if the interaction strength in the Hamiltonian (3.1) is renormalized as

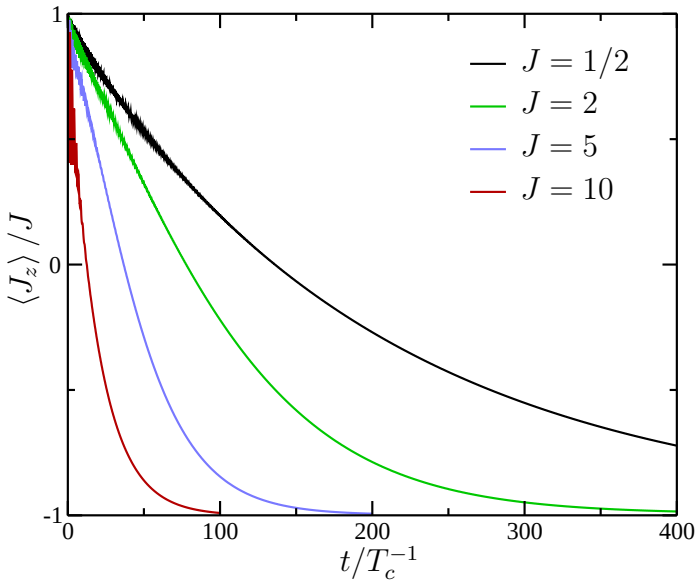

Figure 3.6: Decay of J_z for different spin sizes; The parameters are chosen as $\varepsilon = 10T_c$, $g = 0.01$, $\omega_c = 50T_c$, and $k_B T = T_c$.

$\tilde{g} = g/\sqrt{2J}$. The advantage of the renormalization is that the time scale of the decay becomes approximately independent of the spin size J. The resulting dynamics of J_z is shown in Fig. 3.7. For an increasing spin size, the decay is delayed and takes place more rapidly. The identical behavior is observed from the Dicke superradiance, cf. Sec 2.2.2.

In summary, we find that the large-spin model exhibits the characteristic features of the Dicke superradiance for a large bias, $\varepsilon \gg T_c$. Naturally, the exact dynamics of the large spin differs from the Dicke model as the Hamiltonians are not identical. In contrast to the Dicke model the coupling to the environment is diagonal and a tunnel term exists in the unperturbed Hamiltonian. Yet, despite these differences, the basic results are the same. The reason is that the superradiance is driven by the spin algebra on which both models rely. This is expressed in particular by the state dependent transition rate $c^{\pm}_{J,M}$ (3.5) which is at maximum for states $|J, M = 0\rangle$, corresponding to $\langle J_z \rangle = 0$. From the point of view of the spin-boson system it appears that the spin shows collective effects, namely a superradiance-like behavior, once it is generalized to spins larger one half.

3.6.2 Quantum Beats

We shall return once again to the symmetric case, $\varepsilon = 0$. It was shown in section 3.5 that the x-component of the spin shows superradiant behavior. For spin one half, on the other hand, the dynamics of the z-component is given by a damped oscilla-

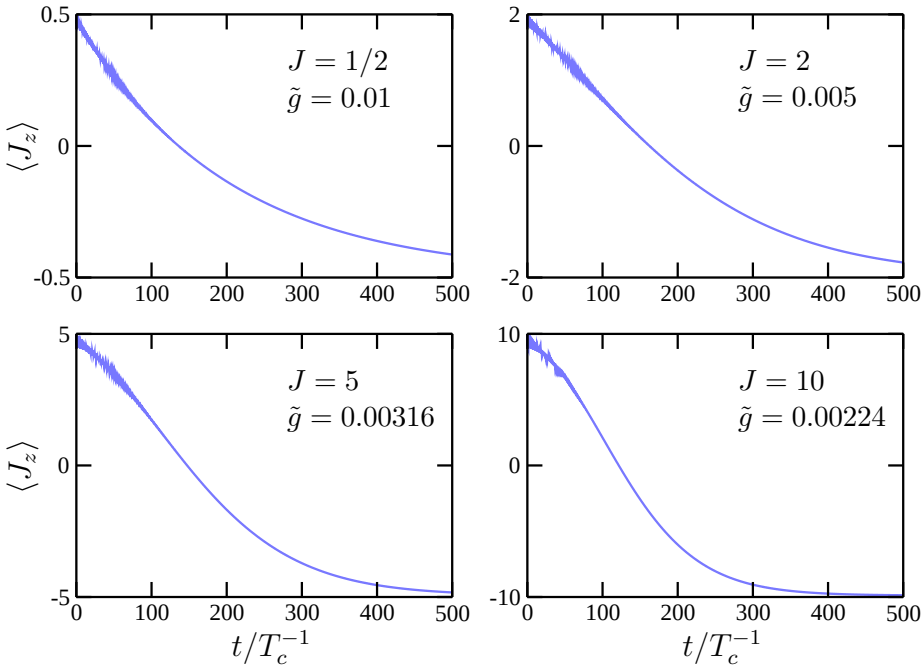

Figure 3.7: Decay of J_z with renormalized interaction $\tilde{g} = g/\sqrt{2J}$. The other parameters agree with Fig. 3.6.

tion (3.64). Already for the next higher spin, $J = 1$, a new feature appears in the time evolution of J_z. Figure 3.8 shows the expectation values of J_z and J_x for spin one at different interaction strengths. A clear beat pattern is visible on top of the damped oscillations of J_z. With increasing interaction to the environment, the beat pattern dissolves to a seemingly chaotic behavior. The decay of J_x is superposed with oscillations of doubled frequency, $4T_c$, due to two-boson processes, as explained in section 3.5. We shall investigate the beat pattern in the following and find that this is caused by the different corrections to the eigenenergies of the spin resulting from the coupling to the nonresonant bosons.

Consider a spin one corresponding to a three level system. Without interaction to the environment, the eigenstates of J_z are degenerate since we assume $\varepsilon = 0$. This degeneracy is lifted by the tunnel coupling in the unperturbed Hamiltonian, $2T_c\, J_x$. We refer to the eigenstates of H_0 as $|+\rangle$, $|0\rangle$, and $|-\rangle$ with the corresponding eigenenergies $2T_c$, 0, and $-2T_c$, respectively. The initial state is chosen as an eigenstate of J_z and hence not a stationary state of the system. The time evolution is then given by an oscillation with frequency $2T_c$ (3.7). Apparently, the unperturbed spin does not show any beats in the dynamics of J_z. In a second step, the influence of the dissipative environment is considered. We use second-order perturbation theory to determine how the eigenenergies of the spin are affected by the environment. There

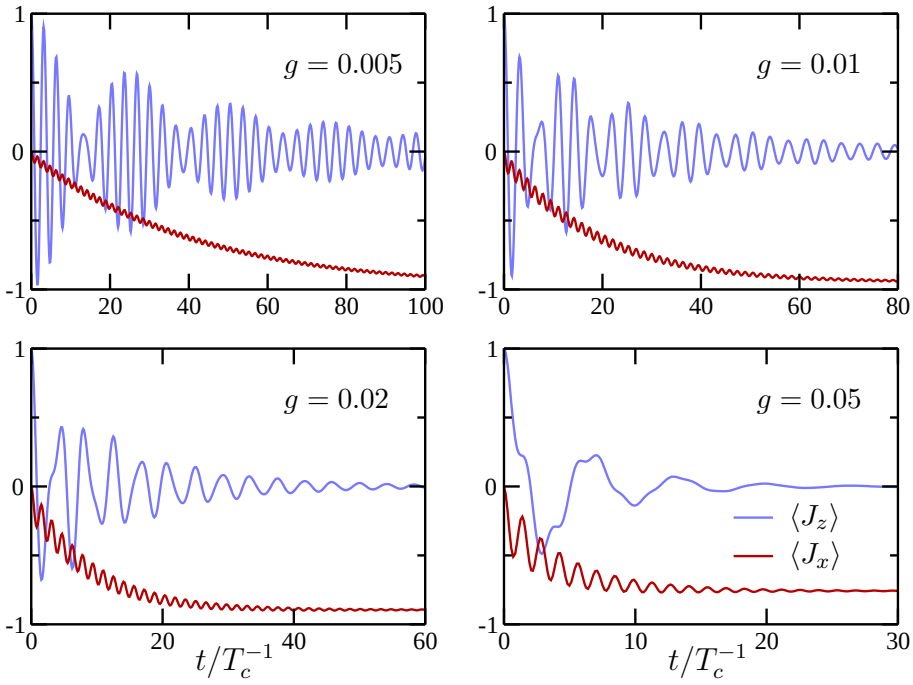

Figure 3.8: Time evolution of J_z and J_x for different interaction strengths to the environment, $J=1$, $\varepsilon=0$, $\omega_c=50T_c$, and $k_BT=0$.

are no contributions from the first order. The influence of the environment on the eigenstates is neglected. The correction to the energy E_n of the state $|n\rangle$ is given in second order as

$$E_n^{(2)} = \sum_{m\neq n} \frac{|\langle m|\, V\, |n\rangle\,|^2}{E_n - E_m}\,, \tag{3.70}$$

where V is the coupling term (3.9) in the Hamiltonian and the sum runs over all eigenstates $|m\rangle$ of the unperturbed system. We still have to specify the state of the environment since $|n\rangle$ and $|m\rangle$ are states of the total system, spin plus environment. Consistent with the considerations of this chapter, the environment of the initial state $|n\rangle$ is assumed to be in thermal equilibrium. Thus, in order to calculate the corrections to the eigenenergy of the spin state $|+\rangle$, we use

$$|n\rangle = |+\rangle \otimes |\Omega_T\rangle\,, \tag{3.71}$$

where $|\Omega_T\rangle$ is the equilibrium state of the environment at temperature T. Then, the correction to the energy $E_{|+\rangle}$ of this state follows from equation (3.70) as

$$E_{|+\rangle}^{(2)} = \frac{1}{2}\sum_q \frac{|\gamma_q|^2}{(e^{\beta\omega_q}-1)^2}\left(\frac{e^{2\beta\omega_q}}{2T_c-\omega_q} + \frac{1}{2T_c+\omega_q}\right). \tag{3.72}$$

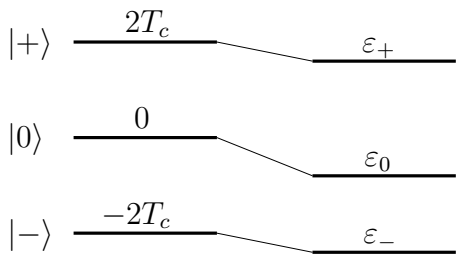

Figure 3.9: Corrections to the eigenenergies of the spin due to the interaction with the environment.

For the sake of simplicity we restrict ourselves to zero temperature. Hence, the second term in the brackets vanishes. Rewriting the sum as an integration and using the definition (3.33) of the spectral function $\rho(\omega)$, yields

$$E^{(2)}_{|+\rangle} = -\frac{1}{2}\fint_0^\infty d\omega\, \rho(\omega)\, \frac{1}{\omega - 2T_c}\,. \tag{3.73}$$

The integral is written as a principal value integral as we do not consider the influence of the resonant bosons, $\omega_q = 2T_c$. They lead to dissipation and thus to the damping of the oscillations of $\langle J_z\rangle$ which is not our concern in the present calculation. If one wants to take into account also the resonant bosons, an infinitesimal imaginary part has to be added to the denominator in equation (3.70), cf. [82, 83]. Similarly, we find for the energy corrections to the other two states, $|0\rangle$ and $|-\rangle$,

$$\begin{aligned} E^{(2)}_{|0\rangle} &= -\frac{1}{2}\fint_0^\infty d\omega\, \rho(\omega)\, \Big(\frac{1}{\omega - 2T_c} + \frac{1}{\omega + 2T_c}\Big)\,, \\ E^{(2)}_{|-\rangle} &= -\frac{1}{2}\int_0^\infty d\omega\, \rho(\omega)\, \frac{1}{\omega + 2T_c}\,. \end{aligned} \tag{3.74}$$

These results show that the corrections to the eigenenergies of the three states differ from each other. In other words, the eigenenergies are not equidistant anymore, as depicted schematically in Fig. 3.9. The corrected eigenenergies of the spin are labeled as

$$\varepsilon_+ = 2T_c + E^{(2)}_{|+\rangle}\,, \qquad \varepsilon_0 = E^{(2)}_{|0\rangle}\,, \qquad \varepsilon_- = -2T_c + E^{(2)}_{|-\rangle}\,. \tag{3.75}$$

Let us consider the effects on the dynamics of the spin. We assume that the initial state, $\langle J_z\rangle_0 = J$, is still given by the same superposition of eigenstates as in the unperturbed case. Then, we find for the time evolution of the z-component,

$$\langle J_z\rangle_t = \cos\Big(\frac{\varepsilon_+ - \varepsilon_-}{2}\, t\Big)\, \cos\Big(\frac{\varepsilon_+ - 2\varepsilon_0 + \varepsilon_-}{2}\, t\Big). \tag{3.76}$$

For the unperturbed spin, the second cosine becomes identical to one and we recover the dynamics as given in (3.7). However, as soon as the spacings between

the eigenenergies become slightly different due to the coupling to the environment, equation (3.76) predicts an oscillation with beats for the dynamics of J_z. The oscillation frequency $\omega_0 = (\varepsilon_+ - \varepsilon_-)/2$ and the beat frequency $\omega_b = (\varepsilon_+ - 2\varepsilon_0 + \varepsilon_-)/2$ follow as

$$\begin{aligned} \omega_0 &= 2T_c + \frac{1}{4}\fint_0^\infty d\omega\, \rho(\omega) \Big(\frac{1}{\omega + 2T_c} - \frac{1}{\omega - 2T_c} \Big)\,, \\ \omega_b &= \frac{1}{4}\fint_0^\infty d\omega\, \rho(\omega) \Big(\frac{1}{\omega + 2T_c} + \frac{1}{\omega - 2T_c} \Big)\,. \end{aligned} \tag{3.77}$$

For an ohmic spectral function, the frequencies can be expressed by exponential integrals [76] as

$$\begin{aligned} \omega_0 &= 2T_c + \frac{1}{2}\, g\, T_c \Big[e^{2T_c/\omega_c}\, \mathrm{Ei}\Big(\frac{-2T_c}{\omega_c}\Big) + e^{-2T_c/\omega_c}\, \mathrm{Ei}\Big(\frac{2T_c}{\omega_c}\Big) \Big], \\ \omega_b &= \frac{1}{2}\, g\, \omega_c + \frac{1}{2}\, g\, T_c \Big[e^{2T_c/\omega_c}\, \mathrm{Ei}\Big(\frac{-2T_c}{\omega_c}\Big) - e^{-2T_c/\omega_c}\, \mathrm{Ei}\Big(\frac{2T_c}{\omega_c}\Big) \Big]. \end{aligned} \tag{3.78}$$

For a large cutoff frequency, $\omega_c \gg T_c$, the term in the bracket in the expression for the beat frequency ω_b is of the order of T_c/ω_c. This can be seen from the series expansion of the exponential integral function. Hence, the beat frequency is given in good approximation as

$$\omega_b = \frac{1}{2}\, g\, \omega_c\,. \tag{3.79}$$

The resulting dynamics (3.76) of the z-component of the spin is shown in Fig. 3.10 together with the numerical solution of the master equation. The curves are in excellent agreement. Naturally, equation (3.76) does not include damping since dissipative effects of the resonant bosons are not considered in the derivation.

We conclude that the beat pattern in the time evolution of the expectation value of J_z is caused by the nonresonant bosons of the dissipative environment. They lead to different corrections to the spin eigenenergies which lift the constant level spacing. For small interaction strengths, $g \ll 1$, this results in a beat pattern in the dynamics of J_z. It turns out that the beat frequency is approximately proportional to the interaction strength g as well as to the cutoff frequency ω_c of the spectral function, cf. (3.79). It should be remarked that this effect is not restricted to zero temperature and spin one. Similar beat patterns occur for larger spins, $J > 1$, and finite temperatures. The pattern dissolves for high temperatures or high spins. Even for a finite bias, $\varepsilon > 0$, a beat pattern can be observed. Then, the oscillations are no longer completely suppressed at certain points like in the unbiased case. This is comparable to a superposition of two waves with slightly different frequencies but unequal amplitudes.

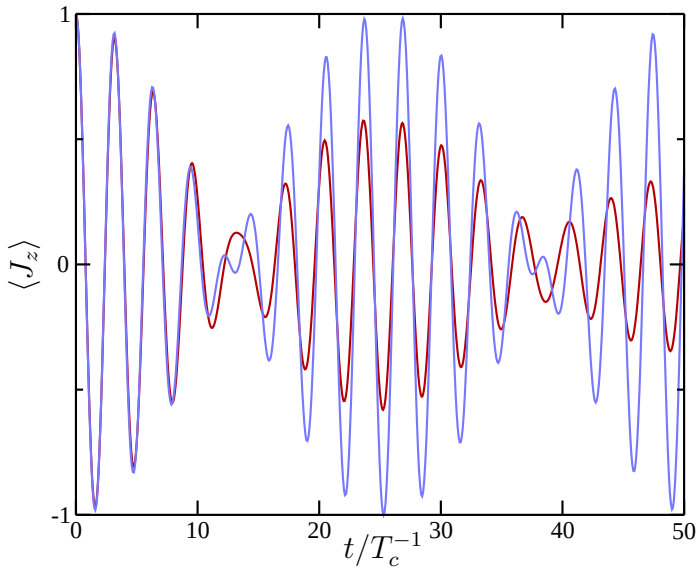

Figure 3.10: Blue: Time evolution (3.76) of J_z with frequencies $\omega_0 = 1.987$ and $\omega_b = 0.124$, Eq. (3.78). Red: Numerical solution of the master equation ($J=1$, $\varepsilon=0$, $g=0.005$, $\omega_c=50T_c$, $k_BT=0$).

3.6.3 Equilibrium Values

Finally, we turn to the equilibrium values of the large spin for a finite bias. In that case, the equilibrium values cannot be readily predicted from symmetry considerations as in the unbiased case. Yet, it is well-known, that the thermodynamic results for a large spin in contact to a heat bath are given by Brillouin functions (2.26). We compare the numerical results of the Born-Markov approximation with the thermodynamic expressions in the following. It turns out that the results agree for a very small coupling to the environment.

The equilibrium values $\langle J_z \rangle_\infty$ and $\langle J_z \rangle_\infty$ for a spin $J=2$ with intermediate bias, $\varepsilon = T_c$, are shown in Fig. 3.11 as a function of the temperature. The results of the Born-Markov approximation are in good agreement with the Brillouin functions but deviate slightly at low temperatures. However, this is not an implication that the Born-Markov approximation breaks down. The Brillouin functions are derived for a large spin in contact with a heat bath. Neither the form of the interaction nor the realization of the bath itself are specified. Consequently, this is only a valid description for very small coupling strengths. Then, it is justified to neglect the details of the contact to the heat bath. Indeed, we find that the results of the Born-Markov approximation agree with the thermodynamic equilibrium values in the limit of zero coupling, $g \to 0$, as shown in the inset of Fig. 3.11. For increasing interaction, the Born-Markov approximation goes away from the thermodynamic approach, which does not depend on the interaction strength g. A similar behavior

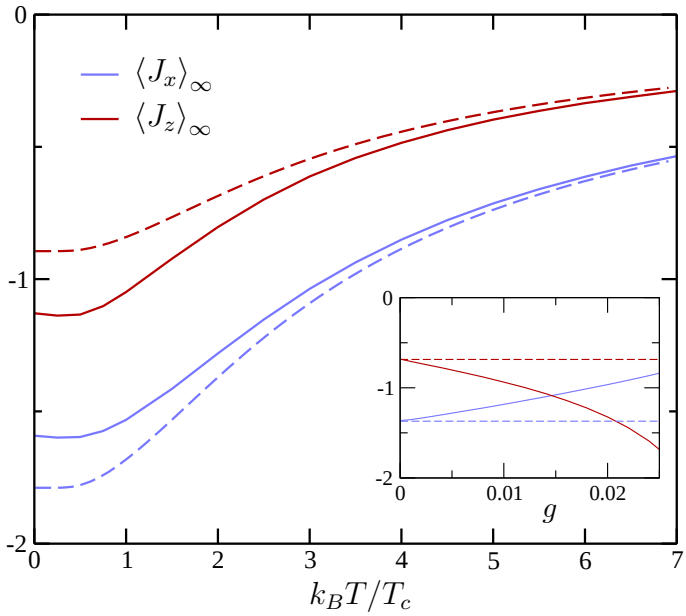

Figure 3.11: Equilibrium values according to the Born-Markov approximation (solid line) and to the thermodynamic calculation (2.26) (dashed line) for $g = 0.005$. The inset shows $\langle J_x \rangle_\infty$ and $\langle J_z \rangle_\infty$ for $k_B T = 2T_c$ as a function of g ($J = 2$, $\varepsilon = T_c$, $\omega_c = 50T_c$).

was observed for spin one half. In that case it is possible to show analytically, that the equilibrium values resulting from the Born-Markov approximation reduce to the thermodynamic predictions in the limit of zero coupling, cf. Sec. 3.4.2.

3.7 Conclusion

In this chapter, we have investigated the large-spin model in the regime of weak dissipation. The model is a generalization of the spin-boson model and allows to study the influence of a dissipative environment on a spin of arbitrary size. This is not only of interest for intrinsic large spins but applies at the same time to dissipation induced collective effects. Such effects arise in an ensemble of identical two-level systems due to the indirect interaction caused by the coupling to the same environment.

We employ the Born-Markov approximation to derive a master equation for the large spin. The Born-Markov approximation is perturbative in the system-environment coupling. It is sometimes argued that a perturbative treatment of the spin-boson system is only possible for finite temperatures and breaks down below a certain critical temperature. We find, however, that the numerical solution of

the master equation for a spin one half with weak ohmic dissipation is in excellent agreement with the solution of the spin-boson model for all temperatures down to zero temperature. We conclude that the Born-Markov approximation gives a reliable description of the spin-boson model with weak dissipation for all temperatures.

The large-spin model is closely related to the Dicke Hamiltonian. For zero bias, the large-spin model can be mapped exactly on the latter by rotation. This implies that the x-component of the unbiased large spin exhibits superradiant behavior. A similar effect is observed in the dynamics of the z-component of the spin for large bias.

The influence of the resonant and of the nonresonant modes of the environment can be distinguished. The nonresonant bosons lift the constant level spacing of the unperturbed spin. This leads to a beat pattern in the coherent oscillations of the large spin which is best observed in the unbiased system.

The numerical results of this chapter are calculated for an ohmic spectral density of the environment. However, the master equation (3.28) applies for an arbitrary spectral function. So do the Bloch equations (3.63) for the spin one half and the resulting equilibrium values (3.65). Other realizations of a dissipative environment can readily be investigated using the same method. Only the rates are to be calculated for different spectral functions. In fact, for spectral functions with a power law dependence on the frequency as modeled in equation (3.34) the rates are already given by equations (3.49) and (3.52).

Chapter 4

The Large-Spin Model in the Strong-Coupling Regime

We will continue to study the large-spin model in this chapter. While the previous chapter was devoted to the investigation of the large spin with weak dissipation we shall now turn to the opposite limit and consider a spin which is strongly coupled to a dissipative environment. As a matter of fact, we employ the same approximation for the derivation of the master equation as in the weak-coupling regime, the Born-Markov approximation. Instead of the spin-reservoir interaction, however, we consider the tunneling as the perturbation. The basis of this approach is that the interacting system without tunneling can be solved exactly. The solution follows from a polaron transformation.

For an ohmic dissipation, the master equation takes a particularly simple form since some of the bosonic expectation values vanish. This is shown in appendix A. Only the Fourier transform of one bosonic correlation function enters the master equation. This is evaluated in two regimes of parameters, first, at zero temperature and second, for a constant coupling strength between spin and environment, $g=1$.

The combination of the polaron transformation and the second-order Born approximation is equivalent to the noninteracting blip approximation for a spin one half. Consequently, the comparison of the solution of the spin-boson model with the master equation shows that the latter gives incorrect results for those parameters where the NIBA fails. For other parameters the results are in good agreement with the solution of the spin-boson model.

For greater spins, $J>1/2$, the dynamics of the spin turns out to differ completely from the two-state system. Depending on the initial value, the z-component of the large spin relaxes towards one of two possible equilibrium values. These are given by the polarized states where the spin is parallel or antiparallel to the z-axis. The relaxation is approximately logarithmic.

4.1 Polaron Transformation

This chapter deals with the perturbative treatment of the tunneling in the large-spin model. The point of departure is the solution of the free Hamiltonian without tunneling to be presented in this section. The solution follows from a canonical transformation, the *polaron* transformation. Again, we write the Hamiltonian of the large-spin model (3.1) as a sum of an unperturbed part and a perturbation, $H = H_0 + V$. In contrast to the previous chapter, however, the tunnel term is chosen as the perturbation, $V = 2T_c\, J_x$. This leaves the unperturbed Hamiltonian

$$H_0 = \varepsilon\, J_z + J_z \sum_q \gamma_q\, (a_q^\dagger + a_{-q}) + \sum_q \omega_q\, a_q^\dagger a_q. \tag{4.1}$$

The basis of the considerations of this chapter is that the unperturbed Hamiltonian can be solved exactly. This is most easily seen by applying the polaron transformation to H_0. The polaron transformation $\bar{A}$ of an operator A is defined as

$$\bar{A} = e^{\sigma J_z} A\, e^{-\sigma J_z}\,, \tag{4.2}$$

with σ acting on the bosonic field defined as

$$\sigma = \sum_q \frac{\gamma_q}{\omega_q}\, (a_q^\dagger - a_{-q}). \tag{4.3}$$

The transformation is unitary if we require $\gamma_q^* = \gamma_{-q}$ and $\omega_q = \omega_{-q}$ (ω_q is assumed to be real), yielding $\sigma^\dagger = -\sigma$. It is readily seen that the z-component of the spin stays unchanged by the transformation, $\bar{J}_z = J_z$. The other terms are calculated with help of the identity (3.11). Then, the transformed Hamiltonian reads

$$\bar{H}_0 = \varepsilon J_z - \kappa J_z^2 + \sum_q \omega_q\, a_q^\dagger a_q. \tag{4.4}$$

The new parameter κ is defined as

$$\kappa = \sum_q \frac{|\gamma_q|^2}{\omega_q} = g\, \omega_c^s\, \Gamma(s). \tag{4.5}$$

The expression on the right-hand side follows for spectral densities of the form of (3.34). In particular, we find for ohmic spectral densities $\kappa = g\omega_c$. As a result of the transformation, the interaction term between the spin and the environment has vanished. Instead, we find a new term, $-\kappa J_z^2$. This reminds of the spin-spin interaction in the Ising model [84] favoring parallel order of the individual spins which constitute the large spin. The new term will turn out to be of great importance to the behavior of the large spin in the strong-coupling regime.

The solution of the transformed Hamiltonian (4.4) becomes trivial since the two subsystems, spin and environment, are now separated. The eigenstates of $\bar{H}_0$ are products of eigenstates of J_z and Fock states of the bosonic field. The solution of the original Hamiltonian H_0 ensues from the back-transformation of these product states. We will, however, not undertake this task since the result is not required for the further proceeding. The spectrum, on the other hand, is identical in the original and in the transformed picture. In the latter, the eigenenergies E_M of the large spin follow immediately from (4.4) as

$$E_M = \varepsilon M - \kappa M^2, \qquad -J \leq M \leq J. \tag{4.6}$$

Finally, we give the perturbation, V, in the transformed picture,

$$\bar{V} = T_c \, (J_+ \, X + J_- \, X^\dagger), \tag{4.7}$$

where the bosonic operator X is defined as

$$X = e^{\sigma} \, . \tag{4.8}$$

The perturbation V acting exclusively on the spin in the original Hamiltonian acquires a bosonic part as a result of the transformation. Thus, the tunnel term reintroduces an interaction between the spin and the environment in the transformed representation.

The polaron transformation employed in this section has many applications in solid state physics. The Hamiltonian of an electron interacting with the phonons of a crystal is solved by a similar transformation [85]. The solution is a *polaron* or dressed electron, namely an electron surrounded by a cloud of phonons, which explains the name of the transformation.

4.2 Born-Markov Approximation

Again, we employ the Born-Markov approximation to derive a master equation for the large spin. The starting point, however, is the transformed Hamiltonian $\bar{H}$. The system-reservoir interaction which is treated perturbatively within the Born-Markov approximation is now given by the transformed tunnel term $\bar{V}$ (4.7). We restrict the investigation to the case of an ohmic dissipation where the master equation takes a particularly simple form. First, we transform the Hamiltonian into the interaction picture. This is defined for any operator A as, cf. (3.10),

$$\tilde{A}(t) = e^{i\bar{H}_0 t} \, \bar{A} \, e^{-i\bar{H}_0 t} \, . \tag{4.9}$$

It will turn out to be a great simplification that J_z stays unchanged,

$$\tilde{J}_z = \bar{J}_z = J_z. \tag{4.10}$$

The perturbation $\bar{V}$ (4.7) becomes in the interaction picture

$$\begin{aligned}\tilde{V}(t) &= T_c\,(\tilde{J}_+(t)\,X_t + \tilde{J}_-(t)\,X_t^\dagger) \\ &= T_c\,(e^{i\varepsilon t}e^{-i\kappa J_z^2 t}\,J_+\,e^{i\kappa J_z^2 t}\,X_t + e^{-i\varepsilon t}e^{-i\kappa J_z^2 t}\,J_-\,e^{i\kappa J_z^2 t}\,X_t^\dagger),\end{aligned} \tag{4.11}$$

where the interaction representation of X is denoted by X_t. We begin the derivation of the master equation from the integro-differential equation (3.18) for the density matrix $\chi(t)$ of the total system. This follows directly from the von-Neumann equation and no approximations have been made so far. Similar to the previous chapter, we assume that the initial density matrix factorizes in a system and a reservoir part, $\bar{\chi}(0) = \bar{\rho}(0) \otimes \bar{R}_0$. Yet, the meaning is a different one in the transformed picture. The assumption corresponds to a situation in which the spin without tunneling and the environment have been in contact for a long time such that they are in mutual equilibrium. Then, at $t=0$, the tunneling is switched on. Again, it is assumed that the environment always stays in thermal equilibrium. The trace over the reservoir degrees of freedom yields among others the expectation values $\langle X_t\rangle = \mathrm{Tr}_{\mathrm{Res}}\{X_t\bar{R}_0\}$ and $\langle X_t^\dagger\rangle$. It is shown in the appendix A that these terms vanish for spectral functions of the form of (3.34) with $s \leq 1$. Thus, in second-order Born approximation and for ohmic dissipation, we find an equation for the spin density matrix that is formally identical to equation (3.21) of the weak-coupling regime. The remaining bosonic contributions to that equation are the four combinations $\langle X_t^\dagger X\rangle$, $\langle X_t X^\dagger\rangle$, $\langle X_t^\dagger X^\dagger\rangle$, and $\langle X_t X\rangle$. It is possible to assign the time dependency exclusively to the first of the X operators, since the unperturbed Hamiltonian $\bar{H}_0$ commutes with the equilibrium density matrix of the environment, $\bar{R}_0$, and due to the cyclic invariance property of the trace. Let us first consider the terms $\langle X_t^\dagger X^\dagger\rangle$ and $\langle X_t X\rangle$ where either both or none of the operators are adjoint. Also these terms vanish for $s \leq 1$ as derived in appendix A, that is, in particular for ohmic dissipation,

$$\langle X_t^\dagger X^\dagger\rangle = \langle X_t X\rangle = 0. \tag{4.12}$$

The calculation of the other two bosonic expectation values is given in the next section. We anticipate that they give identical results and define the correlation function

$$C(t) = \langle X_t^\dagger X\rangle = \langle X_t X^\dagger\rangle. \tag{4.13}$$

Naturally, this function differs from the correlation function in the weak-coupling regime, $K(t)$. It follows from the definition that $C(t)$ fulfills

$$C(-t) = C(t)^*. \tag{4.14}$$

Then, the master equation reads in second-order Born approximation

$$\begin{aligned}\dot{\tilde{\rho}}(t) = -T_c^2 \int_0^t dt' \Big\{ &\big[\tilde{J}_+(t)\,\tilde{J}_-(t')\,\tilde{\rho}(t') + \tilde{J}_-(t)\,\tilde{J}_+(t')\,\tilde{\rho}(t') \\ &- \tilde{J}_+(t')\,\tilde{\rho}(t')\,\tilde{J}_-(t) - \tilde{J}_-(t')\,\tilde{\rho}(t')\,\tilde{J}_+(t)\big]\, C(t-t') \\ &+ \big[\tilde{\rho}(t')\,\tilde{J}_+(t')\,\tilde{J}_-(t) + \tilde{\rho}(t')\,\tilde{J}_-(t')\,\tilde{J}_+(t) \\ &- \tilde{J}_+(t)\,\tilde{\rho}(t')\,\tilde{J}_-(t') - \tilde{J}_-(t)\,\tilde{\rho}(t')\,\tilde{J}_+(t')\big]\, C(t-t')^* \Big\}.\end{aligned} \tag{4.15}$$

It is well-known that the master equation in second-order Born approximation is equivalent to the noninteracting-blip approximation (NIBA) for the spin-boson model with ohmic dissipation. This was first pointed out by Aslangul, Pottier, and Saint-James [86].

Within the Markov approximation, $\tilde{\rho}(t')$ is replaced by $\tilde{\rho}(t)$ and the upper limit of the integration is extended to infinity, cf. Sec. 3.2.2. The resulting equation simplifies further if we consider the diagonal elements of the density matrix, $\tilde{\rho}_{M,M}$. The integrals over the correlation function $C(t)$ can be replaced by its Fourier transform $\mathcal{F}_C(\omega)$ using (4.14),

$$\int_0^\infty dt\ \mathrm{Re}\big\{C(t)e^{i\omega t}\big\} = \frac{1}{2}\int_{-\infty}^\infty dt\ C(t)e^{i\omega t} = \frac{1}{2}\,\mathcal{F}_C(\omega). \tag{4.16}$$

Finally, we arrive at the master equation for the large spin with ohmic dissipation,

$$\begin{aligned}\dot{\tilde{\rho}}_{M,M}(t) = &- T_c^2\ {c^-_{J,M}}^2\ \mathcal{F}_C\big(\varepsilon - \kappa(2M-1)\big)\ \tilde{\rho}_{M,M}(t) \\ &- T_c^2\ {c^+_{J,M}}^2\ \mathcal{F}_C\big(-\varepsilon + \kappa(2M+1)\big)\ \tilde{\rho}_{M,M}(t) \\ &+ T_c^2\ {c^-_{J,M}}^2\ \mathcal{F}_C\big(-\varepsilon + \kappa(2M-1)\big)\ \tilde{\rho}_{M-1,M-1}(t) \\ &+ T_c^2\ {c^+_{J,M}}^2\ \mathcal{F}_C\big(\varepsilon - \kappa(2M+1)\big)\ \tilde{\rho}_{M+1,M+1}(t).\end{aligned} \tag{4.17}$$

We like to add some remarks regarding the master equation. In contrast to the weak-coupling regime, we abstain from the back-transformation of the master equation into the Schrödinger picture. The reason is that J_z takes the same form in all pictures, cf. (4.10). Hence, its expectation value follows directly from the density matrix in the interaction picture,

$$\langle J_z\rangle_t = \sum_{M=-J}^{+J} M\,\tilde{\rho}_{M,M}(t). \tag{4.18}$$

Apparently, the diagonal elements of the density matrix correspond in any picture to the probability that the large spin is in the state $|J,M\rangle$. We note that the normalization of the probability, i.e. the trace of the density matrix, is conserved by

the master equation (4.17), $\mathrm{Tr}\{\dot{\tilde{\rho}}\}=0$. The master equation only couples the diagonal elements of the density matrix. Thus, it corresponds to a set of $2J+1$ coupled differential equations for a spin of size J. The solution of the full density matrix including the nondiagonal matrix elements requires the integration of a set of $(2J+1)^2$ equations. The nondiagonal matrix elements are necessary for the calculation of the other spin components, in particular J_x. We shall, however, concentrate on the investigation of J_z in the following. The knowledge of the diagonal matrix elements is sufficient for this task.

As the diagonal elements of the density matrix, $\tilde{\rho}_{M,M}$, correspond to probabilities, we can identify gain and loss terms in the master equation: The probability of the state $|J,M\rangle$ is increased by transitions from the neighboring states, $|J,M\pm1\rangle \to |J,M\rangle$, weighted with the respective probabilities, $\tilde{\rho}_{M\pm1,M\pm1}$. It is decreased by the reverse transitions, $|J,M\rangle \to |J,M\pm1\rangle$, weighted with the probability $\tilde{\rho}_{M,M}$. The influence of the environment on the large spin is described by the Fourier transform of the correlation function, $\mathcal{F}_C(\omega)$. The argument of which, $\omega=\pm\big(\varepsilon-\kappa(2M\pm1)\big)$, is precisely the energy difference between neighboring states of the unperturbed large spin, cf. (4.6). Hence, the Fourier transform gives the rate for the emission or absorption of bosons with the necessary energy for the respective transition. We can already guess that no absorption is possible at zero temperature. Note that the Fourier transform $\mathcal{F}_C(\omega)$ is identical to the function $P(E)$ which appears in the context of a dissipative tunnel junction [26]. The function $P(E)$ determines the current-voltage characteristics of the junction.

The spin algebra responsible for collective effects in the weak-coupling regime appears here in form of the coefficients $c^{\pm}_{J,M}$ (3.5). The effect of the perturbation strength T_c is merely a scaling of the time, $t \to T_c^2\, t$. The final remark concerns the validity of the Born-Markov approximation. It was already remarked that the second-order Born approximation is equivalent to the noninteracting-blip approximation for a spin one half. In the course of the derivation of the master equation (4.17), we applied one additional approximation, the Markov approximation. Thus, the master equation cannot be expected to yield correct results for parameters where the NIBA fails.

4.3 The Bath Correlation Function and its Fourier Transform

We saw in the previous section that the influence of the dissipative environment on the spin is expressed by a correlation function, similar to the weak-coupling regime. Moreover, only its Fourier transform appears in the master equation in Born-Markov approximation (4.17). Both, the correlation function and its Fourier transform are

calculated for an ohmic dissipation in this section. Since it is not possible to give a closed expression for the Fourier transform we concentrate on two regimes. First, we consider an environment at zero temperature with arbitrary coupling strength to the spin and, second, a constant coupling, $g = 1$, at finite temperatures. At this interaction strength, the spin-boson model becomes equivalent to the so-called *Toulouse limit* of the anisotropic Kondo model [10].

It is well-known that the definition (4.13) of the correlation function $C(t)$ can be rewritten as, see e.g. Mahan [85],

$$C(t) = e^{-\Phi(t)}, \tag{4.19}$$

with

$$\Phi(t) = \int_0^\infty d\omega \, \frac{\rho(\omega)}{\omega^2} \Big[\big(1 - \cos(\omega t)\big) \, \coth\Big(\frac{\beta\omega}{2}\Big) + i \sin(\omega t) \Big]. \tag{4.20}$$

The spectral function of the environment, $\rho(\omega)$, was defined in (3.33). As a matter of fact, the function $\Phi(t)$ resembles the correlation function $K(t)$ of the weak-coupling regime (3.37). We shall, however, not pursue this fact any further for it does not simplify the following calculations. At zero temperature, the integral in (4.20) is calculated directly and the correlation function becomes

$$C_{T=0}(t) = (1 + i\omega_c t)^{-g}. \tag{4.21}$$

Apparently, this result is nonperturbative in the spin-reservoir interaction since the coupling strength g enters in the exponent. Only the real part of $\Phi(t)$ depends on the temperature, as follows from the definition (4.20). The calculation of this function at finite temperatures is given in [87]. The trick is to differentiate $\Phi(t)$ with respect to time and then perform the integration over $d\omega$. The result is integrated over the time yielding the correlation function at finite temperatures,

$$C(t) = (1 + i\omega_c t)^{-g} \left| \frac{\Gamma(1 + 1/\beta\omega_c + it/\beta)}{\Gamma(1 + 1/\beta\omega_c)} \right|^{2g}. \tag{4.22}$$

Thus, the temperature dependence is expressed by an additional factor which reduces to unity at zero temperature. Before proceeding with the Fourier transform of this function, we shall have a closer look at the zero temperature result (4.21). The absolute value of $C_{T=0}(t)$ is peaked around $t = 0$ where it takes the value one. For an increasing argument, the function approaches zero. The Markov approximation requires that the width of the correlation function is the smallest time scale of the system. The time $t_{1/2}$ in which the absolute value of the correlation function decreases to one half may serve as a measure of this feature. From (4.21) we find $\omega_c \, t_{1/2} = \sqrt{4^{1/g} - 1}$. Similar to the weak-coupling regime the width scales with the inverse cutoff frequency ω_c justifying the Markov approximation for large cutoffs.

For small interaction strengths, however, the Markov approximation is definitely not applicable within the polaron picture. This may be clarified by inserting some typical values used in the previous chapter, $g=0.01$ and $\omega_c=50T_c$. Then, the width of the peak, $t_{1/2}$, is of the order of $10^{28}\,T_c^{-1}$ – a preposterous result far beyond the applicability of the Markov approximation. This underlines that our approach is only sensible in the strong-coupling regime where g is at least of the order of one. The conclusion is fully consistent with the assumptions made at the beginning of this chapter. The derivation of the master equation starts from the interacting system taking into account the tunneling perturbatively. This implies that the effects of the interaction are stronger than the tunneling.

4.3.1 Fourier Transform

The correlation function enters the master equation (4.17) as a Fourier transform which is calculated in this paragraph. We restrict ourselves to two regimes of parameters depicted in Fig. 4.1. First, the Fourier transform is determined for zero temperature. It is known from the spin-boson model that the NIBA fails for $1<g<2$ at zero temperature, indicated by the dashed line in Fig. 4.1, see [10]. The second regime is of interest since the spin-boson model becomes equivalent to the Toulouse limit of the anisotropic Kondo model for $g=1$. Then, analytical results can be obtained for the spin-boson model. We will discuss this in more detail in the subsequent section. The two regimes intersect at the point $g=1$, $k_BT=0$.

At zero temperature, the correlation function $C_{T=0}(t)$ (4.21) can be transformed using standard integrals. We find for its Fourier transform $\mathcal{F}_C(\omega)$, cf. (4.16),

$$\mathcal{F}_C(\omega) = \frac{2\pi\,\omega^{g-1}}{\omega_c^g\,\Gamma(g)}\,e^{-\omega/\omega_c}\,\theta(\omega), \qquad g>1, \tag{4.23}$$

where $\theta(\omega)$ is the Heaviside step function. For $\omega=0$, the integral only converges if g is greater than one, underlining once more the restriction of our approach to the strong-

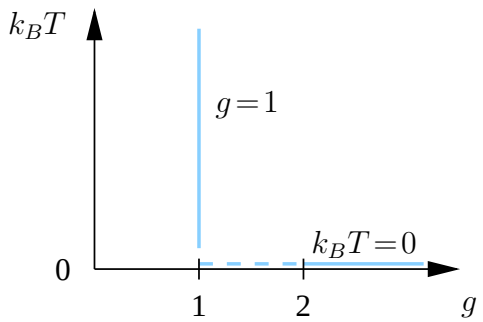

Figure 4.1: The Fourier transform $\mathcal{F}_C(\omega)$ is calculated in the two regimes $g=1$ and $k_BT=0$, indicated by the blue lines.

coupling regime. The function $\mathcal{F}_C(\omega)$ vanishes for negative frequencies as already suspected previously. We have seen from the master equation that $\mathcal{F}_C(\omega)$ then accounts for absorption of energy from the environment which becomes impossible at zero temperature.

In the second regime, $g=1$, the Fourier transform can be calculated with the residue theorem. Positive, negative and zero frequency have to be considered separately. We recall the property of the Gamma function $\Gamma(z^*)=\Gamma(z)^*$ [80] and rewrite the Fourier transform (4.16) as

$$\mathcal{F}_C(\omega) = \frac{-i}{\omega_c\,\Gamma(1+1/\beta\omega_c)^2} \int_{-i\infty}^{i\infty} dz\, \frac{1}{z+1/\beta\omega_c}\,\Gamma\Big(1+\frac{1}{\beta\omega_c}+z\Big)\,\Gamma\Big(1+\frac{1}{\beta\omega_c}-z\Big)\,e^{\beta\omega z}. \tag{4.24}$$

For positive frequencies, $\omega>0$, the contour can be closed in the negative real half plane. The pole at $z=-1/\beta\omega_c$ lies inside the contour. Moreover, the Gamma function $\Gamma(z)$ has simple poles at $z=-n$, $n\in\mathbb{N}_0$, with residues $(-1)^n/n!$, cf. [80]. Thus, the poles of the first Gamma function in (4.24) are also inside the path of integration while all poles of the second Gamma function are outside. Then, the Fourier transform can be expressed as a sum,

$$\mathcal{F}_C(\omega) = \frac{2\pi\,e^{-\omega/\omega_c}}{\omega_c\,\Gamma(1+1/\beta\omega_c)^2} \sum_{n=0}^{\infty} \frac{(-1)^n}{n!}\,\Gamma\Big(n+1+\frac{2}{\beta\omega_c}\Big)\,e^{-\beta\omega n}, \qquad \omega>0. \tag{4.25}$$

In the limit of zero temperature, we retrieve the respective result for $k_BT=0$, (4.23) with $g\to 1$. At low temperatures, $k_BT\ll\omega_c$, the sum can be approximated by the geometric series,

$$\mathcal{F}_C(\omega) \approx \frac{2\pi\,e^{-\omega/\omega_c}}{\omega_c\,\Gamma(1+1/\beta\omega_c)^2\,(1+e^{-\beta\omega})}, \qquad \omega>0. \tag{4.26}$$

The calculation for negative frequencies, $\omega<0$, proceeds similarly, only that the contour has to be closed in the positive real half plane. Then, the poles of the second Gamma function in (4.24) lie inside the contour, yielding

$$\mathcal{F}_C(\omega) = \frac{2\pi\,e^{\omega(\beta+1/\omega_c)}}{\omega_c\,\Gamma(1+1/\beta\omega_c)^2} \sum_{n=0}^{\infty} \frac{(-1)^n}{n!}\,\Gamma\Big(n+1+\frac{2}{\beta\omega_c}\Big)\,e^{\beta\omega n}, \qquad \omega<0. \tag{4.27}$$

Also for negative frequencies, we retrieve the zero temperature result (4.23) for $g\to 1$. Again, the sum can be approximated by the geometric series at low temperatures, $k_BT\ll\omega_c$,

$$\mathcal{F}_C(\omega) \approx \frac{2\pi\,e^{\omega(\beta+1/\omega_c)}}{\omega_c\,\Gamma(1+1/\beta\omega_c)^2\,(1+e^{\beta\omega})}, \qquad \omega<0. \tag{4.28}$$

The results for positive and negative frequencies, (4.25) and (4.27), are related by

$$\mathcal{F}_C(-\omega) = e^{-\beta\omega}\,\mathcal{F}_C(\omega). \tag{4.29}$$

This relation is known as the detailed balance symmetry [26]. Hence, the absorption is suppressed at low temperatures, $k_BT \ll \omega$. At high temperatures, $k_BT \gg \omega$, on the other hand, absorption and emission become approximately equivalent as one would expect intuitively.

Finally, the Fourier transform is calculated for zero frequency, $\omega = 0$. The value accounts for transitions without energy transfer between the spin and the environment, involving some rearrangement of the bosonic state. Due to the absence of the exponential function, the contour cannot be closed on neither side,

$$\mathcal{F}_C(\omega=0) = \frac{1}{\Gamma(1+1/\beta\omega_c)^2}\int_{-\infty}^{\infty} dt\,\frac{1}{1+i\omega_c t}\,\Gamma\Big(1+\frac{1}{\beta\omega_c}+\frac{it}{\beta}\Big)\,\Gamma\Big(1+\frac{1}{\beta\omega_c}-\frac{it}{\beta}\Big). \tag{4.30}$$

Instead, we insert the definition of the Gamma function, valid for a positive real part of the argument [80],

$$\Gamma(z) = \int_0^\infty \tau^{z-1}\,e^{-\tau}d\tau, \qquad \mathrm{Re}\{z\} > 0. \tag{4.31}$$

Then, the integral in (4.30) is of the same form as the one calculated in the previous paragraph (4.23). The remaining two integrations can be solved elementary. The second of which results again in a Gamma function and we find for the Fourier transform at zero frequency

$$\mathcal{F}_C(\omega=0) = \frac{\pi\,\Gamma(1+2/\beta\omega_c)}{\omega_c\,4^{1/\beta\omega_c}\,\Gamma(1+1/\beta\omega_c)^2}\,. \tag{4.32}$$

Apparently, the zero temperature limit of this expression exists. It is, however, *not* identical to the $g \to 1$ limit of the zero temperature result (4.23). In fact, the derivation of the latter is not valid at $g = 1$. We infer that the validity of the Born-Markov approximation is doubtful at the point $g = 1$, $k_BT = 0$. We will have to treat this point with caution.

The Fourier transform of the correlation function at $g = 1$ and finite temperatures is given by (4.25), (4.27), and (4.32). Figure 4.2 shows $\mathcal{F}_C(\omega)$ for three different temperatures. We employ the exact expressions (4.25) and (4.27) and calculate the series numerically. This method is applied throughout this chapter. It can be seen from Fig. 4.2 that the absorption is suppressed at low temperatures, cf. (4.29). With increasing temperature, the absorption grows and the maximum of the emission side is shifted to higher frequencies.

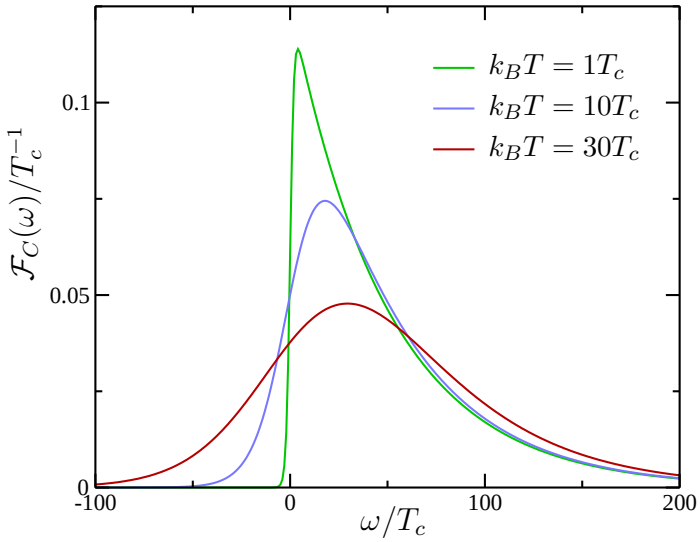

Figure 4.2: Fourier transform of the correlation function for different temperatures ($g=1$, $\omega_c=50T_c$, where T_c is an arbitrary unit of energy).

4.4 The Spin-Boson Limit

Similar to the proceeding in the weak-coupling regime, Sec. 3.4, we will compare our results for a spin one half with ohmic dissipation to the spin-boson literature. The case of a spin one half, $J=1/2$, plays a special part in our approach to the strong-coupling regime. This becomes obvious in the transformed Hamiltonian $\bar{H}_0$ (4.4) where a new term appears, $-\kappa J_z^2$. The term is constant for $J=1/2$ and hence has no bearing on the physics of a spin one half. Only for greater spins, $J>1/2$, this term is expected to affect the dynamics.

4.4.1 Solution of the Master Equation

For a spin one half, the master equation (4.17) reduces to two coupled differential equations for the matrix elements $\tilde{\rho}_{1/2,\,1/2}$ and $\tilde{\rho}_{-1/2,\,-1/2}$,

$$\begin{aligned}\dot{\tilde{\rho}}_{1/2,\,1/2} &= T_c^2\left(-\mathcal{F}_C(\varepsilon)\;\tilde{\rho}_{1/2,\,1/2} + \mathcal{F}_C(-\varepsilon)\;\tilde{\rho}_{-1/2,\,-1/2}\right),\\ \dot{\tilde{\rho}}_{-1/2,\,-1/2} &= T_c^2\left(\mathcal{F}_C(\varepsilon)\;\tilde{\rho}_{1/2,\,1/2} - \mathcal{F}_C(-\varepsilon)\;\tilde{\rho}_{-1/2,\,-1/2}\right).\end{aligned} \tag{4.33}$$

The parameter κ does not appear anymore since the J_z^2 term drops out. The meaning of this master equation is evident. The probability of the states $|J,M\rangle = |1/2,\pm 1/2\rangle$ changes by transitions to and from the respective other state. The rate of these transitions is given by the function $\mathcal{F}_C(\pm\varepsilon)$, accounting for the exchange of the

necessary energy ε with the environment. The dynamics of J_z follows from the solution of the master equation. For an initially polarized spin, $\langle J_z\rangle_0 = 1/2$, we find with (4.18)

$$\langle J_z\rangle_t = \left(\frac{1}{2} - \langle J_z\rangle_\infty\right) e^{-\gamma t} + \langle J_z\rangle_\infty \ , \tag{4.34}$$

where the equilibrium value $\langle J_z\rangle_\infty$ and the relaxation rate γ are defined as

$$\begin{aligned} \langle J_z\rangle_\infty &= -\frac{1}{2}\,\frac{\mathcal{F}_C(\varepsilon) - \mathcal{F}_C(-\varepsilon)}{\mathcal{F}_C(\varepsilon) + \mathcal{F}_C(-\varepsilon)} \ , \\ \gamma &= T_c^2\,\big(\mathcal{F}_C(\varepsilon) + \mathcal{F}_C(-\varepsilon)\big). \end{aligned} \tag{4.35}$$

Thus, the master equation (4.33) predicts an exponential relaxation of J_z to its equilibrium value. The only exception occurs if $\mathcal{F}_C(\varepsilon)$ as well as $\mathcal{F}_C(-\varepsilon)$ become zero. Then, the spin remains in its initial state. We shall consider in detail the two regimes in which the Fourier transform $\mathcal{F}_C(\varepsilon)$ has been evaluated (Fig. 4.1).

4.4.2 Zero Temperature

The Fourier transform $\mathcal{F}_C(\varepsilon)$ for strong couplings, $g > 1$, at zero temperature is given by equation (4.23). Up to this point, there is no indication that our approach may fail for these parameters. It is however known that the NIBA gives incorrect results for $1 < g < 2$, see [10]. Since the Born approximation employed in the derivation of the master equation corresponds to the NIBA, cf. Sec. 4.2, the master equation cannot be expected to yield reliable results in that regime. Therefore, we restrict the investigation at zero temperature to stronger couplings, $g \geq 2$.

For the symmetric two-state system, the rates vanish, $\mathcal{F}_C(\varepsilon = 0) = 0$, (4.23). Then, the master equation (4.33) predicts that the spin stays in its initial state. This is the well-known localization of the spin-boson model appearing at zero temperature for interaction strength $g \geq 2$. It was first derived by Chakravarty [88] and Bray and Moore [89] using an imaginary-time path integral method. The results were later confirmed by Hakim et. al. [90] with a renormalization group treatment. They apply the polaron transformation and consider the tunneling as a perturbation similar to the approach of this chapter. Hence, the master equation (4.33) reproduces the correct result at zero temperature and zero bias for couplings $g \geq 2$ though it does not predict the critical value at which the transition to the localization occurs.

For a finite bias, $\varepsilon > 0$, the Fourier transform does not vanish anymore. It is finite for positive arguments, $\mathcal{F}_C(\varepsilon) > 0$, but it is still suppressed for negative arguments as absorption is not possible at zero temperature, $\mathcal{F}_C(-\varepsilon) = 0$, cf. (4.23). Thus, the equilibrium value (4.35) becomes $\langle J_z\rangle_\infty = -1/2$. In equilibrium, the spin is in the

state of lower energy with probability one. The relaxation rate (4.35) follows as

$$\gamma = \frac{2\pi\, T_c^2\, \varepsilon^{g-1}}{\omega_c^g\, \Gamma(g)}\; e^{-\varepsilon/\omega_c}. \tag{4.36}$$

In leading order in ε/ω_c the exponential function is replaced by unity and we find

$$\gamma \approx \frac{\pi\, (2T_c)^2\, \varepsilon^{g-1}}{2\,\omega_c^g\, \Gamma(g)}\,. \tag{4.37}$$

The same result follows from a path integral formalism for the spin-boson model [9, 91, 92].

We conclude that the approach based on a polaron transformation combined with the Born-Markov approximation yields correct results for the spin-boson model at zero temperature with strong interaction to the environment, $g \geq 2$.

4.4.3 Finite Temperatures

For the interaction strength $g = 1$, the spin-boson model with ohmic dissipation corresponds to the Toulouse limit of the anisotropic Kondo model. This case is of special significance to the spin-boson model as it marks the coherent-incoherent transition at zero temperature in the limit $T_c/\omega_c \to 0$ [10]. Again, we first consider the symmetric system. The Fourier transform $\mathcal{F}_C(\varepsilon = 0)$ is now given by equation (4.32). The equilibrium value (4.35) becomes zero, as expected for a symmetric system, $\langle J_z \rangle_\infty = 0$. The relaxation rate reads

$$\gamma = 4^{-k_B T/\omega_c}\; \frac{2\pi\, T_c^2\, \Gamma(1+2k_BT/\omega_c)}{\omega_c\, |\Gamma(1+k_BT/\omega_c)|^2}\,. \tag{4.38}$$

In the limit of zero temperature, this rate reduces to

$$\gamma_{T=0} = \frac{\pi\, (2T_c)^2}{2\,\omega_c}\,. \tag{4.39}$$

This is the correct result for the spin-boson model in the limit of zero temperature. It can be derived for instance by the direct summation of the exact formal solution [93]. The reason why we can reproduce this result is that the NIBA becomes exact in that limit [10].

For a finite bias, we employ the relation (4.29) between absorption and emission yielding the equilibrium value

$$\langle J_z \rangle_\infty = -\frac{1}{2} \tanh\Big(\frac{\varepsilon}{2k_BT}\Big). \tag{4.40}$$

This, however, is just the NIBA result (3.59) that we have already met in the weak-coupling regime. It demonstrates once again the close relation between our approach and the noninteracting-blip approximation. It has been discussed in chapter 3 that this result becomes unphysical at low temperatures as it predicts an entirely localized equilibrium value, $\langle J_z\rangle_\infty = -1/2$, for an infinitesimal small bias ε in the limit of zero temperature. Hence, the master equation (4.33) is not reliable for a finite bias and $g=1$ at low temperatures. This had to be expected from the failure of the NIBA in that regime.

Weiss gives a solution for the spin-boson model with $g=1$ in the so-called *scaling limit*, $k_BT/\omega_c \to 0$ [10],

$$\begin{aligned} \langle\sigma_z\rangle_t &= e^{-\gamma t} - 2\int_0^t d\tau\, \frac{k_BT\,\sin(\varepsilon\tau)}{\sinh(\pi\tau k_BT)}\,\big[e^{-\gamma\tau/2} - e^{-\gamma t}e^{\gamma\tau/2}\big], \\ \langle\sigma_z\rangle_\infty &= \frac{2}{\pi}\,\mathrm{Im}\Big\{\psi\Big(\frac{1}{2} + \frac{\gamma}{4\pi\,k_BT} - i\,\frac{\varepsilon}{2\pi\,k_BT}\Big)\Big\}. \end{aligned} \tag{4.41}$$

The relaxation rate γ is defined identically to equation (4.39) and $\psi(z)$ is the digamma function. This solution for the equilibrium value is plotted together with the NIBA result (4.40) in Fig. 4.3. It can be seen that the NIBA deviates from (4.41) at low temperatures. The different results converge for increasing temperature, as known from the NIBA. The inset of Fig. 4.3 shows the different solutions for the dynamics of J_z. The exponential decay (4.34) is in good agreement with the solution in the scaling limit (4.41). Thus, the spin-boson model with finite bias is well described by the master equation (4.33) for intermediate temperatures.

From the comparison with the results of the spin-boson model, we learn that the master equation (4.33) gives incorrect results in the regime where the NIBA fails. This is hardly surprising. We noted in section 4.2 that the first steps in the derivation of the master equation, namely the polaron transformation together with the second-order Born approximation, are equivalent to the NIBA. The master equation employs one additional approximation, the Markov approximation. In the other regimes, the master equation reproduces the results of the spin-boson model. For coupling strengths $g \geq 2$ we find the exact analytical expressions for the dynamics of J_z. The same applies for the unbiased system at $g=1$ in the limit of zero temperature. For a finite bias at $g=1$, the numerical evaluation of the solution of the spin-boson model in the scaling limit is in good agreement with the exponential relaxation as predicted by the master equation. We conclude that our approach, the polaron transformation combined with a Born-Markov approximation, yields good results for a spin one half with strong coupling to the environment, $g \geq 2$, at zero temperature and in the Toulouse limit, $g = 1$, at finite temperatures. We expect that the method is likewise reliable for greater spins, $J > 1/2$.

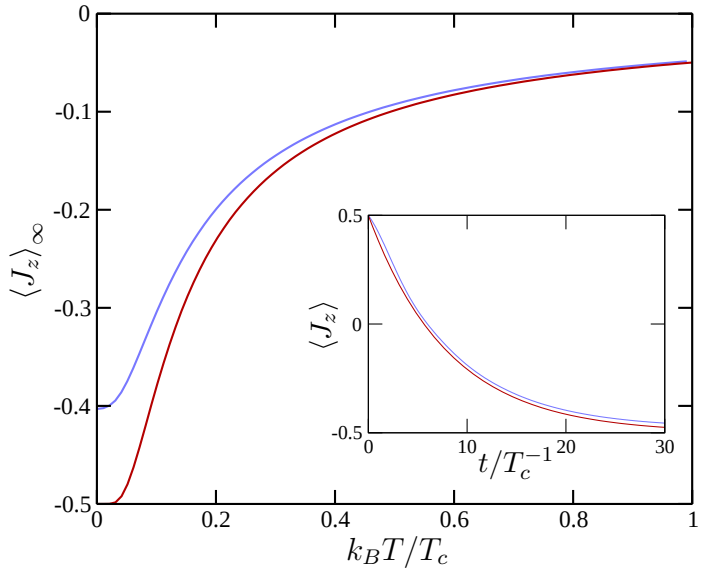

Figure 4.3: Equilibrium value $\langle J_z \rangle_\infty$ and dynamics of J_z (inset); red: master equation (4.33), blue: solution in the scaling limit (4.41), ($\varepsilon = 0.2\,T_c$, $g=1$, $\omega_c=50T_c$; inset: $\varepsilon=T_c$, $k_BT=0.1T_c$).

4.5 The Large-Spin Dynamics

We shall now investigate the influence of the strong dissipation on a spin greater than one half, $J > 1/2$. The dynamics of the spin follows from the solution of the master equation (4.17). The two regimes are considered in which the master equation has been shown to yield correct results for a spin one half, namely $g \geq 2$ at zero temperature and $g=1$ at finite temperatures.

4.5.1 Zero Temperature

It was demonstrated in the previous section that an unbiased spin one half is localized for strong couplings, $g \geq 2$, at zero temperature. Greater spins, however, do not show this phenomenon. This can be seen in Fig. 4.4 which shows the expectation value of J_z derived from the numerical solution of the master equation for a spin $J=3/2$ and different initial values. The most striking feature is the dependence of the long-time behavior on the initial value. Apparently, there are two distinct equilibrium values, $\langle J_z \rangle_\infty = \pm J$.

Actually, we can learn a great deal from the unperturbed system, i.e. the transformed Hamiltonian $\bar{H}_0$ (4.4). The eigenvalues lie on an inverted parabola as sketched in the inset of Fig. 4.4. Since the expectation value of J_z cannot exceed the spin size J the minima of the energy are found at the extreme points, $\langle J_z \rangle = \pm J$.

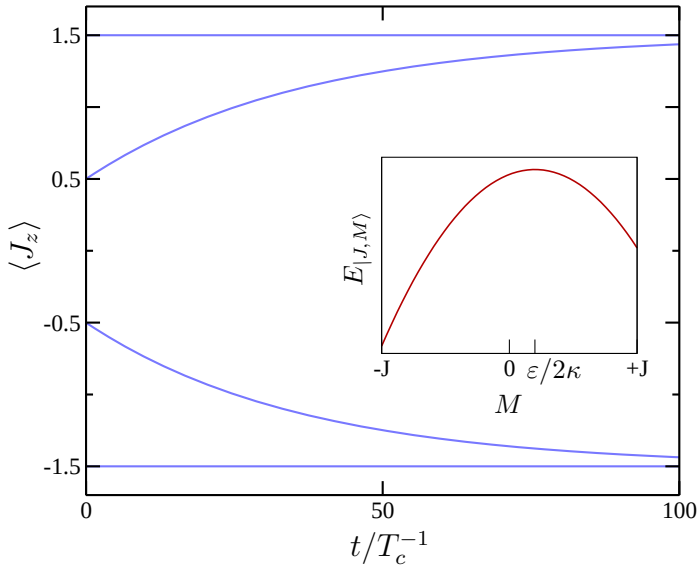

Figure 4.4: Dynamics of J_z for a spin 3/2 with different initial values ($\varepsilon = 0$, $g = 2$, $\omega_c = 50T_c$ and $k_B T = 0$). The inset shows the eigenenergies of the unperturbed system.

Depending on which side of the parabola the initial value is located, the spin will approach either of those states for long times. From that picture we can already guess what the effect of a finite bias will be. A bias shifts the center of the parabola from zero to $\varepsilon/2\kappa$. Thus, we expect that the borderline between initial values relaxing to the different equilibrium values moves accordingly. Even for a finite bias, though, there are in general initial states from which the spin relaxes to the polarized state $\langle J_z \rangle_\infty = +J$. This appears contradictory on the first view since that state has the highest possible eigenenergy for a spin without dissipation. Yet, we must not forget that the spin is strongly coupled to the environment and that the interaction energy and therewith the total energy is minimized for a polarized spin. The eigenenergies of the two polarized states may differ for a finite bias, $E_{+J} > E_{-J}$. However, a transition from one to the other requires to overcome a high energy barrier so that the spin is expected to remain on its side of the parabola.

The dynamics of the large spin as described above also follows directly from the master equation (4.17). We consider an unbiased system, $\varepsilon = 0$. The derivation can be generalized to a finite bias without difficulty. First, we note that the system is symmetric with respect to the quantum number M, i.e. $|J, M\rangle \to |J, -M\rangle$. Thus, we can restrict ourselves to states with positive M. Recalling that absorption is completely suppressed for zero temperature, the master equation (4.17) reads for

positive M

$$\begin{aligned}\dot{\tilde{\rho}}_{M,M}(t) = &- T_c^2 \; {c_{J,M}^+}^2 \; \mathcal{F}_C\big(\kappa(2M+1)\big) \; \tilde{\rho}_{M,M}(t) \\ &+ T_c^2 \; {c_{J,M}^-}^2 \; \mathcal{F}_C\big(\kappa(2M-1)\big) \; \tilde{\rho}_{M-1,M-1}(t).\end{aligned} \tag{4.42}$$

This equation accounts for transitions to higher quantum numbers M, that is $|J,M\rangle \to |J,M+1\rangle$. Hence, the expectation value of J_z increases until the density matrix reaches the stationary solution, $\tilde{\rho}_{M,M} = \delta_{J,M}$, corresponding to the equilibrium value $\langle J_z \rangle_\infty = +J$.

Let us now consider the typical time it takes the spin to relax from a state $|J,M\rangle$ to the next higher state, $|J,M+1\rangle$. Imagine the spin is initially prepared in the state $|J,M_0\rangle$, i.e. $\tilde{\rho}_{M,M} = \delta_{M,M_0}$. According to the master equation (4.42), the probability for that state, $\tilde{\rho}_{M_0,M_0}$, decays exponentially to zero. We assume for the moment that the expectation value of J_z also relaxes exponentially from M_0 to M_0+1. This approximation neglects all further transitions from M_0+1 to states with higher quantum numbers M. The justification will become clear in the following. Then, the transition rate $\Gamma_{M_0 \to M_0+1}$ with which J_z relaxes follows from the Fourier transform (4.23) using $\kappa = g\omega_c$ (4.5) as

$$\Gamma_{M_0 \to M_0+1} = \frac{2\pi \, T_c^2}{\omega_c \, \Gamma(g)} \, \big(J(J+1) - M_0(M_0+1)\big) \, \big(g(2M_0+1)\big)^{g-1} \, e^{-g(2M_0+1)}. \tag{4.43}$$

The important feature of this rate is the exponential dependence on the actual state of the spin, M_0. Hence, each transition $|J,M\rangle \to |J,M+1\rangle$ happens much more slowly than the previous transition, $|J,M-1\rangle \to |J,M\rangle$. It is therefore justified to assume that one transition is basically finished before the next one becomes effective. Thus, we find the following picture for the relaxation of J_z to its equilibrium value. The expectation value rises step by step the ladder of eigenvalues until it reaches the equilibrium value $\langle J_z \rangle_\infty = +J$. Each step is approximately an exponential relaxation while the rate of these transitions becomes exponentially damped with increasing expectation value $\langle J_z \rangle$. This behavior can be observed in Fig. 4.5 which shows the time evolution of J_z for a spin of size $J = 4.5$ for several initial values on different time scales. The half-life of each transition as given in the table follows from the

Transition $M \to M+1$	$1/2 \to 3/2$	$3/2 \to 5/2$	$5/2 \to 7/2$	$7/2 \to 9/2$
Half-life $/T_c^{-1}$	3.1	98	4700	$0.34 \cdot 10^6$

approximate rate $\Gamma_{M \to M+1}$ (4.43). These numbers are indeed in good agreement with the numerical solution of the master equation as presented in Fig 4.5.

Finally, we derive an approximation for the dynamics of J_z. According to the previous paragraph, the time it takes the spin to relax to the state $|J,M\rangle$ is roughly

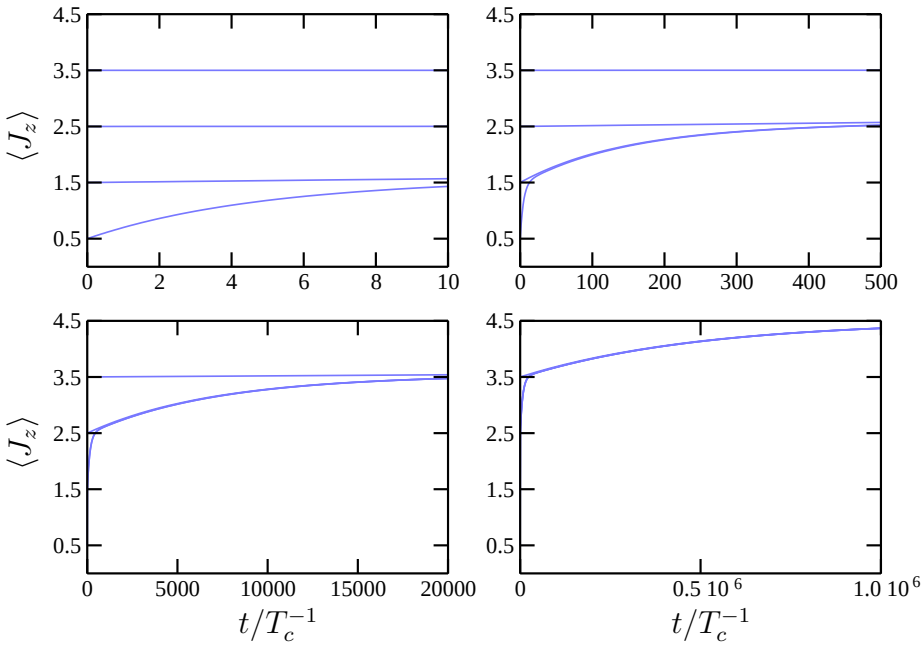

Figure 4.5: Relaxation of a spin of size $J=4.5$ for various initial values on different time scales ($\varepsilon=0$, $g=2$, $\omega_c=50T_c$ and $k_BT=0$).

given by the period of the last transition, $|J, M-1\rangle \to |J, M\rangle$. All previous transitions happen much faster and thus are neglected. We take the inverse of the rate $\Gamma_{M-1\to M}$ (4.43) as a measure for the relaxation time. Then, the time t_M after which the spin is in the state $|J, M\rangle$ is given by

$$t_M = \frac{\omega_c\,\Gamma(g)\,\big(g(2M-1)\big)^{1-g}\,e^{-g}}{2\pi\,T_c^2\,\big(J(J+1)-M(M-1)\big)}\,e^{2gM}. \tag{4.44}$$

Again, the important dependence on the quantum number M is given by the exponential function. Neglecting the dependence of the prefactor on M yields for the expectation value

$$\langle J_z\rangle = M \approx \frac{1}{2g}\ln(t) + C. \tag{4.45}$$

The constant C accounts for the prefactor in equation (4.44). This approximation for the expectation value of J_z gives a good description of the relaxation as can be seen from Fig. 4.6. This figure shows the data of Fig. 4.5 on a logarithmic time scale. The evolution of J_z is well approximated by the logarithmic relaxation (4.45), since both curves are parallel. The constant C describing the offset is of no particular interest and hence is not considered any further. An additional oscillation is visible in the evolution of J_z, Fig. 4.6. This is caused by the step by step relaxation of the expectation value and is not reproduced by the approximation (4.45).

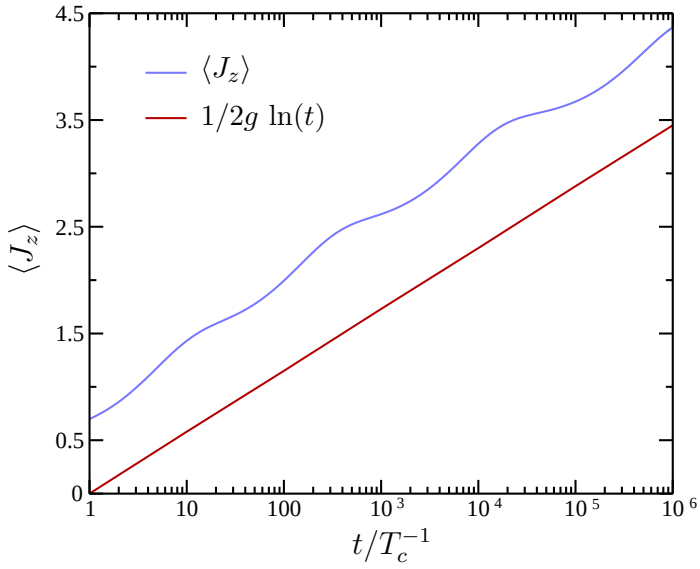

Figure 4.6: Logarithmic plot of the relaxation data of Fig. 4.5 with initial value $\langle J_z \rangle_0 = 1/2$ (blue) and the logarithmic approximation (4.45), without the constant, $C = 0$, (red).

Up to this point, the investigation has been restricted to positive quantum numbers M. This is possible as the unbiased system is symmetric with respect to M. All statements made above equally apply to the negative branch, $M < 0$. We shall now consider the influence of a finite bias on the spin relaxation. For the smallest possible value of the spin, $J = 1/2$, a finite bias changes the spin dynamics from localization to exponential relaxation, as discussed in section 4.4.2. For greater spins, however, the consequences of a finite bias are less spectacular. The bias ε changes the argument of the Fourier transform in the master equation (4.17). It was already mentioned at the beginning of this section, that this leads to a shift of the parabola of eigenvalues to the new center $\varepsilon/2\kappa$. For ohmic dissipation κ is given by $\kappa = g\omega_c$, cf. Sec. 4.1. It is assumed in our model that the cutoff frequency ω_c constitutes the highest energy in the problem, in particular greater than the bias, $\varepsilon < \omega_c$. Thus, the center of the parabola is shifted by less than one half. This change is so small that its influence on the spin dynamics is expected to be insignificant. The exact symmetry between positive and negative quantum numbers M is lifted by a finite bias but the considerations made for zero bias are still valid. In particular, the logarithmic relaxation to the equilibrium values $\pm J$ is equally shown by a spin with finite bias. Altogether, we find that the physics of a dissipative large spin clearly differs from a spin one half at zero temperature in the strong-coupling regime. The different behavior is mainly caused by the J_z^2 term in the transformed Hamiltonian. The peculiarity of the spin one half is that this term becomes constant and has no influence on the spin.

4.5.2 Finite Temperatures

We shall now investigate the dynamics of the large spin in the second regime, $g=1$ at finite temperatures. In contrast to the zero temperature regime absorption of energy from the environment becomes possible such that the large spin is not restricted to transitions in one direction, $|J,M\rangle \to |J,M+1\rangle$ for $M>0$. However, even at intermediate temperatures the absorption rate is much smaller than the emission rate. This can be seen from the master equation (4.17). The argument of the Fourier transform is of the order of $g\omega_c$. Within this model, the temperature is assumed to be smaller than the cutoff, $k_BT<\omega_c$. Hence, the ratio of absorption to emission becomes much smaller than one, according to (4.29). If the absorption is completely neglected, the unbiased large spin is again described by the master equation (4.42). The transition rate $\Gamma_{M\to M+1}$ at finite temperatures follows from (4.25),

$$\Gamma_{M\to M+1} = \frac{2\pi\, T_c^2\, {c^+_{J,M}}^2\, e^{-(2M+1)}}{\omega_c\, \Gamma(1+1/\beta\omega_c)^2} \sum_{n=0}^{\infty} \frac{(-1)^n}{n!}\, \Gamma\Big(n+1+\frac{2}{\beta\omega_c}\Big)\, e^{-\beta n\omega_c(2M+1)}. \quad (4.46)$$

This rate resembles the zero temperature rate (4.43) in one essential point. Both are exponentially suppressed with increasing quantum number M. Thus, the same conclusions can be drawn here as in the zero temperature regime. The large spin relaxes step by step to the equilibrium. At finite temperatures this is only approximately given by the polarized state, $\langle J_z\rangle_\infty \approx \pm J$. In particular, the relaxation is logarithmic. Apparently, the constant in equation (4.45) is different for finite temperatures and we have to insert $g=1$. The relaxation of a spin of size $J=7$ is shown in Fig. 4.7 for different parameters. The dynamics is well described by the logarithmic approximation (4.45). Deviations become visible at the end of the relaxation, $\langle J_z\rangle \approx J$, for the logarithmic approximation does not take into account the finite size of the spin. It can be seen from Fig. 4.7 that a finite bias, $\varepsilon = 20T_c$, or a higher temperature, $k_BT=25T_c$, only weakly modify the dynamics of J_z. The influence of a finite bias was already discussed in the previous section.

We conclude that the dynamics of the large-spin model drastically changes once the spin size becomes greater than one half. We have investigated the behavior in two regimes, $g\geq 2$ at $k_BT=0$ and $g=1$ at $k_BT>0$, and find similar results in both regimes. The spin relaxes to a polarized state, $\langle J_z\rangle_\infty \approx \pm J$ (the equation becomes correct at zero temperatures). Which of the two possible values the spin approaches is determined by its initial value. Positive initial values, $\langle J_z\rangle_0 > 0$, decay to $+J$ and vice versa. This behavior can be understood from the unperturbed Hamiltonian $\bar{H}_0$. Its energy is minimized by a polarized spin. The relaxation to the equilibrium values is logarithmic, $\langle J_z\rangle \approx \ln(t)/2g + C$, where the constant C depends on the other parameters. The influence of the parameters, in particular the bias ε and the temperature k_BT in the second regime, is marginal as long as they are smaller

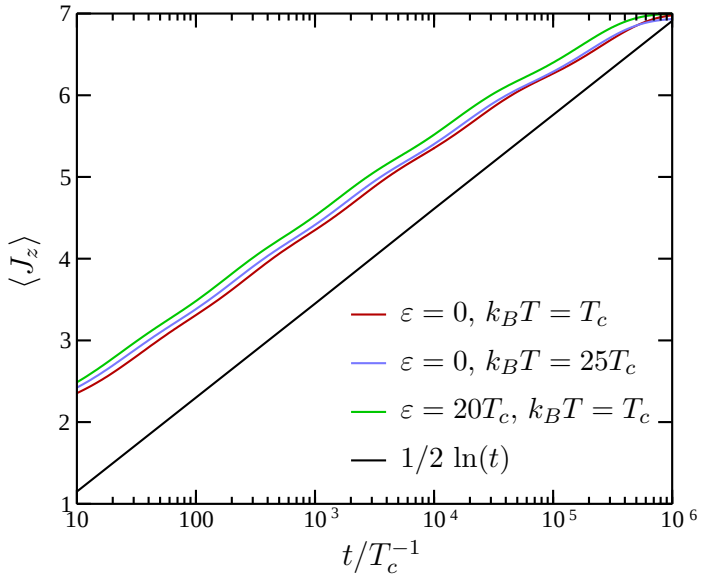

Figure 4.7: Relaxation of a spin $J=7$ ($g=1$, $\omega_c=50T_c$, and $\langle J_z\rangle_0=2$). The logarithmic approximation is plotted in black.

than the cutoff frequency ω_c. From the point of view of the large-spin model, the spin-boson model with spin size $J=1/2$ appears as an exception. The quadratic term in the transformed Hamiltonian, $-\kappa J_z^2$, which governs the dynamics of a large spin becomes constant for $J=1/2$ and consequently does not affect a spin one half. This explains why we find such a different behavior if the spin becomes greater than one half.

4.6 Conclusion

We have studied the large-spin model with strong ohmic dissipation in this chapter. In the strong-coupling regime, the interaction with the environment is expected to predominate the physics of the large spin and we treat the tunneling as a perturbation. The master equation for the large spin is derived by combining the polaron transformation and the Born-Markov approximation. The effect of the polaron transformation on the unperturbed spin without tunneling is to decouple the two subsystems, spin and environment. An interaction is reintroduced by the tunneling. This new interaction is considered as the perturbation within the Born-Markov approximation.

For spin one half the large-spin model reduces to the spin-boson model and the results of the latter are used to check the validity of our approach. It is interesting to note that the combination of the polaron transformation with the second-order

Born approximation is equivalent to the noninteracting-blip approximation for the spin-boson model. Hence, the master equation derived in this chapter is not reliable for parameters where the NIBA is known to give incorrect results. This is for instance the case for intermediate coupling strengths, $1<g<2$, at zero temperature. For higher coupling strengths, the results of the spin-boson model are reproduced. In a second regime, the Toulouse limit, $g=1$, the results of the master equation are in good agreement with the solution of the spin-boson model for intermediate temperatures.

The physics changes drastically if greater spins are considered. The reason is that the strong coupling to the environment favors a polarized spin. The energy of the coupling is minimized if the spin is parallel or antiparallel to that direction to which the dissipative environment couples. Thus, the equilibrium value is not unique and the spin relaxes towards one of the polarized states. The initial condition determines to which of them. This resembles the broken parity symmetry of the one mode Dicke model in the strong-coupling limit [60].

For an ohmic spectral function with exponential cutoff, the relaxation is approximately logarithmic, $\langle J_z\rangle \approx \ln(t)/2g + C$. A different long-time behavior is expected for other forms of the cutoff. The influence of the bias and the temperature on the large spin is marginal. They do not alter the dynamics qualitatively.

We have found similar dynamics of the large spin in the two regimes that are investigated. It seems natural to suspect that these results also apply to other parameters, that is a strong coupling, $g>2$, at finite temperatures. Without further investigation, however, this is merely a speculation. Finally, we note that the dynamics in the strong-coupling regime do not show any similarities to the behavior in the weak-coupling limit as discussed in chapter 3. In fact, the results are quite contrary. While the spin relaxes faster with increasing spin size in the weak-coupling regime the relaxation becomes extremely slow for a strong dissipation. Apparently, the transition between these different behaviors occurs at intermediate coupling strengths, $0<g<1$. This regime, however, is not accessible by the methods chosen in this work since the tunneling and the dissipation become equally important and none can be treated perturbatively.

Chapter 5

Dicke Effect in Two Double Quantum Dots

The previous chapters of this thesis were devoted to the investigation of a dissipative large spin. The spin was used to study collective effects in an ensemble of identical two-level systems which are interacting with the same environment. No assumptions were made on the specific form of the two-level systems to ensure a broad applicability of the results. In this chapter, however, we consider a very specific realization of a two-level system and concentrate on the smallest ensemble which possibly exhibits collective effects: We calculate the tunnel current through two parallel double quantum dots coupled to a phonon environment. The limitation on a small system has several advantages. Most of the assumptions and approximations made in the previous chapters are not necessary anymore. In particular, we are not restricted to identical two-level systems in the following. Furthermore, the product Hilbert space of the double dots is used instead of the large spin basis which describes only a subspace.

Mesoscopic systems as double quantum dots are especially well suited as realizations of two-level systems. They allow tuning of the parameters over a wide range [21, 22]. In double dots, for instance, the level spacing as well as the tunnel rates can be changed continously by adjustment of the gate voltages. Moreover, transport spectroscopy is possible in these systems by connection with leads [4, 5, 27, 94, 95]. The influence of the phonon environment can be seen in the tunnel current [3, 16, 96]. Designing the geometry of a sample even allows to modify the phonon environment [34, 97]. The appearance of collective effects in mesoscopic transport has gained a considerable interest recently. Shahbazyan and Raikh first predicted the Dicke effect to occur in resonant tunneling through two impurities [98]. The interaction between the impurities arises due to the coupling to the same leads. No bosonic environment is considered. Brandes and co-workers predicted superradiance of quantum dot arrays resulting in an oscillatory photon emission intensity [99, 100].

The quantum dots in that work are described by a large spin. The investigation of collective effects of double quantum dots is closely related to the evolution of entanglement and hence to quantum dot based qubits [25]. Interactions with phonons, however, are feared to destroy the coherence in qubits [101].

In this chapter, we study two nearby but otherwise independent double quantum dots which are coupled to the same phonon environment. The influence of the resulting indirect interaction on the stationary tunnel current is examined in the non-linear transport regime. Signatures of super- and subradiance of phonons are predicted which show up as an increase or a decrease, respectively, of the stationary electron current. We demonstrate that this effect is directly related to the creation of charge wave function entanglement between the two double dots, which appears in a preferred formation of either a charge-triplet or singlet configuration, depending on the internal level splittings and the tunnel couplings to the external electron leads.

5.1 The Model

We consider two double quantum dots, that are coupled to leads as well as a bosonic environment. No assumptions are made on the specific realization of the quantum dots that can be lateral or vertical. Yet, the different dots of one double dot are referred to as the left and the right dot, respectively. Electrons can tunnel back and forth between the dots of one double dot but tunneling between the different double dots is not possible. The leads serve as electron reservoirs and enable the flow of a current through the system. Each double dot is connected to independent leads, as depicted in Fig. 5.1. This excludes possible collective effects that arise if both systems are connected to the same leads [98]. Moreover, both double dots are coupled to a common bosonic bath describing the interactions of electrons in the dots with phonons that are inherent to any solid state system. The bosonic environment has two purposes. First, the emission of phonons makes a current possible also in the inelastic regime when the energy of electrons tunneling between the quantum dots is not conserved. Furthermore, the environment introduces an indirect coupling between the different double dots which are independent otherwise. The consequences of this coupling are investigated in the present chapter.

The regime of strong Coulomb blockade is considered. Then, the two quantum dots of one double dot cannot be occupied simultaneously by an additional electron. It has been demonstrated for this case, that the Hilbert space of each double dot can by described by a basis of three states only [33]. For the i-th double dot, these states are $|L,i\rangle$, a state with one additional electron in the i-th left dot at eigenenergy $\varepsilon_{L,i}$, $|R,i\rangle$ a state with one additional electron in the i-th right dot at eigenenergy $\varepsilon_{R,i}$, and $|0,i\rangle$ for no additional electron in either of the two dots. The zero of the energy is chosen to be the eigenenergy of $|0,i\rangle$. However, we do not take into account

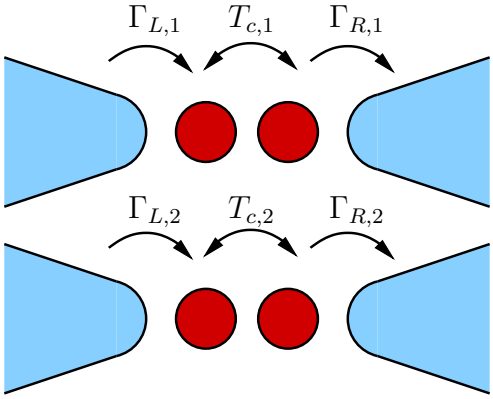

Figure 5.1: Model for two double quantum dots coupled to independent leads and to the same bosonic environment (not shown). The rates T_c, Γ_L, and Γ_R will be defined in the text.

Coulomb blockade between different double dots. This is justified for experimental configurations where the Coulomb interaction between electrons in different double dots is much weaker than the Coulomb interaction inside one double dot. Hence, any collective effects that follow from this model result exclusively from the coupling of both double quantum dots to the same phonons.

Although the system introduced above consists of two double dots we give the Hamiltonian and the subsequent derivation of the master equation for an arbitrary number of N double dots. With the help of the operators

$$\begin{aligned} n_{L,i} &= |L,i\rangle\langle L,i|\,, & n_{R,i} &= |R,i\rangle\langle R,i|\,, \\ p_i &= |L,i\rangle\langle R,i|\,, & p_i^\dagger &= |R,i\rangle\langle L,i|\,, \\ s_{L,i} &= |0,i\rangle\langle L,i|\,, & s_{R,i} &= |0,i\rangle\langle R,i|\,, \end{aligned} \tag{5.1}$$

the Hamiltonian can be written as

$$\begin{aligned} H = \sum_i^N \Big(& \varepsilon_{L,i}\, n_{L,i} + \varepsilon_{R,i}\, n_{R,i} + T_{c,i}(p_i + p_i^\dagger) \\ & + \sum_k V_{k,i}\, c_{k,i}^\dagger s_{L,i} + h.c. + \sum_k \varepsilon_{k,i}^L\, c_{k,i}^\dagger c_{k,i} \\ & + \sum_l W_{l,i}\, d_{l,i}^\dagger s_{R,i} + h.c. + \sum_l \varepsilon_{l,i}^R\, d_{l,i}^\dagger d_{l,i} \\ & + \sum_q \gamma_{q,i}\,(a_q^\dagger + a_{-q})(n_{L,i} - n_{R,i}) \Big) + \sum_q \omega_q\, a_q^\dagger a_q\,. \end{aligned} \tag{5.2}$$

The matrix elements for the tunneling of the additional electron between the dots is $T_{c,i}$. A phonon in mode q with energy ω_q is created by the operator $a_q^\dagger$. The coupling

to the quantum dots is purely diagonal and has the amplitude $\gamma_{q,i}$ for mode q to the i-th double dot. The electrons in the leads are described by creation operators $c^\dagger_{k,i}$ for an electron in mode k with an eigenenergy $\varepsilon^L_{k,i}$ in the left lead and $d^\dagger_{l,i}$ with eigenenergy $\varepsilon^R_{l,i}$ in the right lead of the i-th double quantum dot. The coupling of the double dots to the leads has the matrix elements $V_{k,i}$ and $W_{l,i}$ and $\hbar$ is set to 1.

We consider the limit in which the electron–phonon interaction is identical for all double dots,

$$\gamma_{q,i} = \gamma_q. \tag{5.3}$$

This corresponds to the situation where the distance between different double dots is small as compared to the phonon wavelength. Even if this is not fulfilled, the assumption of equal coupling to the phonons can be realized experimentally by placing the double dots in an appropriate phonon cavity or phonon resonator [97].

The Hamiltonian can be split into an unperturbed part H_0, the coupling to the leads H_e, and the coupling to the phonons H_p,

$$H = H_0 + H_\mathrm{e} + H_\mathrm{p}, \tag{5.4}$$

where

$$\begin{aligned} H_\mathrm{e} &= \sum_{i,k} V_{k,i}\, c^\dagger_{k,i} s_{L,i} + h.c. + \sum_{i,l} W_{l,i}\, d^\dagger_{l,i} s_{R,i} + h.c., \\ H_\mathrm{p} &= \sum_{i,q} \gamma_q\, (a^\dagger_q + a_{-q})(n_{L,i} - n_{R,i}). \end{aligned} \tag{5.5}$$

Note that the states $|L,i\rangle$ and $|R,i\rangle$ are no eigenstates of the unperturbed Hamiltonian H_0 in presence of tunneling $T_{c,i}$ between the dots. Consequently, they take a different form in the interaction picture (3.10),

$$\begin{aligned} \tilde{n}_{L,i}(t) =\ & n_{L,i} \ - \ \frac{i\,T_{c,i}}{\Delta_i}\,\sin(\Delta_i t)\,(p_i - p_i^\dagger) \\ & + \frac{T_{c,i}}{\Delta_i^2}\,(1-\cos(\Delta_i t))\left((\varepsilon_{L,i}-\varepsilon_{R,i})(p_i+p_i^\dagger) - 2T_{c,i}(n_{L,i}-n_{R,i})\right), \\ \tilde{n}_{R,i}(t) =\ & n_{R,i} \ + \ \frac{i\,T_{c,i}}{\Delta_i}\,\sin(\Delta_i t)\,(p_i - p_i^\dagger) \\ & - \frac{T_{c,i}}{\Delta_i^2}\,(1-\cos(\Delta_i t))\left((\varepsilon_{L,i}-\varepsilon_{R,i})(p_i+p_i^\dagger) - 2T_{c,i}(n_{L,i}-n_{R,i})\right). \end{aligned} \tag{5.6}$$

We used the Baker-Hausdorff identity (3.11) to evaluate $\tilde{n}_{L,i}(t)$ and $\tilde{n}_{R,i}(t)$. The hybridization energy Δ_i of the i-th double dot is defined as

$$\Delta_i = \sqrt{\varepsilon_i^2 + 4T_{c,i}^2}\,, \tag{5.7}$$

with the difference of the eigenenergies in the left and in the right dot,

$$\varepsilon_i = \varepsilon_{L,i} - \varepsilon_{R,i}. \tag{5.8}$$

5.2 Master Equation

We derive a master equation for the reduced density matrix $\rho(t)$ of the double quantum dots. The current through the system follows directly from the solution of the density matrix. In principle, it is possible to take into account the coupling to the phonons to arbitrary high orders by applying a polaron transformation and by considering the tunneling between the dots perturbatively, corresponding to the proceeding of chapter 4. A comparison with 2nd order Born-Markov approximation however shows that the results for the stationary current through one double dot, as calculated by the two methods, practically coincide for $T_c \ll \varepsilon$ and small couplings [102]. Hence, we employ the standard Born-Markov approximation as introduced in chapter 3,

$$\frac{d}{dt}\,\tilde{\rho}(t) = -\int_0^t dt'\ \mathrm{Tr}_{\mathrm{Res}}\Big\{\big[\tilde{V}(t),\big[\tilde{V}(t'),\tilde{\rho}(t)\otimes R_0\big]\big]\Big\}\,. \tag{5.9}$$

In contrast to the previous chapters, though, we have to deal now with a system that is coupled to two different environments, the electron leads and the boson bath, $V = H_{\mathrm{e}} + H_{\mathrm{p}}$. The density matrix of the environment is written as a product of the density matrices of the leads and of the phonons, $R_0 = R_{0,\mathrm{e}} \otimes R_{0,\mathrm{p}}$, since we do not consider correlations between the leads and the phonons. The environments' density matrices are assumed to be always in thermal equilibrium, as the influence of the quantum dots on the environments is neglected. Taking into account the special form of the couplings (5.5), we see that the master equation is greatly simplified as the trace over mixed products of phonon and lead operators vanishes. Hence, the master equation can be written as a sum of a lead and a phonon part,

$$\begin{aligned}\frac{d}{dt}\,\tilde{\rho}(t) = -\int_0^t dt'\ &\mathrm{Tr}_{\mathrm{Res,e}}\Big\{\big[\tilde{H}_{\mathrm{e}}(t),\big[\tilde{H}_{\mathrm{e}}(t'),\tilde{\rho}(t)\otimes R_{0,\mathrm{e}}\big]\big]\Big\}\\ &+\mathrm{Tr}_{\mathrm{Res,p}}\Big\{\big[\tilde{H}_{\mathrm{p}}(t),\big[\tilde{H}_{\mathrm{p}}(t'),\tilde{\rho}(t)\otimes R_{0,\mathrm{p}}\big]\big]\Big\}\,.\end{aligned} \tag{5.10}$$

Let us first consider the trace over the electron reservoirs. Inserting H_{e} (5.5) yields

$$\begin{aligned}&\big[\tilde{H}_{\mathrm{e}}(t),\big[\tilde{H}_{\mathrm{e}}(t'),\tilde{\rho}(t)\otimes R_{0,\mathrm{e}}\big]\big]\\ &= \Big[\sum_{i,k} V_{k,i}\,\tilde{c}^{\dagger}_{k,i}(t)\tilde{s}_{L,i}(t) \;+\; h.c. + \sum_{i,l} W_{l,i}\,\tilde{d}^{\dagger}_{l,i}(t)\tilde{s}_{R,i}(t) \;+\; h.c.\ ,\\ &\quad \Big[\sum_{j,k'} V_{k',j}\,\tilde{c}^{\dagger}_{k',j}(t')\tilde{s}_{L,j}(t') \;+\; h.c. \;+ \sum_{j,l'} W_{l',j}\,\tilde{d}^{\dagger}_{l',j}(t')\tilde{s}_{R,j}(t') \;+\; h.c.\ ,\ \tilde{\rho}(t)\otimes R_{0,\mathrm{e}}\Big]\Big].\end{aligned} \tag{5.11}$$

In the interaction picture, the lead operators $c^\dagger_{k,i}$ and $d^\dagger_{l,i}$ acquire an additional time-dependent phase,

$$\tilde{c}^\dagger_{k,i}(t) = c^\dagger_{k,i}\, e^{i\,\varepsilon^L_{k,i}t}, \qquad\qquad \tilde{d}^\dagger_{l,i}(t) = d^\dagger_{l,i}\, e^{i\,\varepsilon^R_{l,i}t}. \tag{5.12}$$

As the trace over the density matrix $R_{0,e}$ of the leads in thermal equilibrium requires particle number conservation in each lead separately, only combinations of creation and annihilation operators in the same lead give a non-zero contribution to the sum. If all double quantum dots were coupled to the same lead, we would find additional terms due to correlations in the lead. However, such processes are not considered in this calculation. Bearing in mind that $c^\dagger_{k,i}c_{k,i}$ is the number operator whose expectation value is the Fermi function,

$$\mathrm{Tr}_{\mathrm{Res,e}}\left\{c^\dagger_{k,i}c_{k,i}\,R_{0,\mathrm{e}}\right\} = n_F(\varepsilon^L_{k,i}), \tag{5.13}$$

we can perform the trace over the electron reservoirs. Since we want to describe transport in the non-linear regime, with a large source-drain voltage between the leads on the left side and on the right side, the chemical potentials are supposed to be infinite in the left leads and zero in the right leads. Thus, the Fermi functions become either one or zero,

$$n_F(\varepsilon^L_{k,i}) = 1, \qquad\qquad n_F(\varepsilon^R_{l,i}) = 0, \tag{5.14}$$

and the trace reads

$$\begin{aligned}
&\mathrm{Tr}_{\mathrm{Res,e}}\left\{\left[\tilde{H}_{\mathrm{e}}(t),\left[\tilde{H}_{\mathrm{e}}(t'),\tilde{\rho}(t)\otimes R_{0,\mathrm{e}}\right]\right]\right\} \\
&\quad= \sum_{k,i}|V_{k,i}|^2\left\{e^{i\,\varepsilon^L_{k,i}(t-t')}\left(\tilde{s}_{L,i}(t)\,\tilde{s}^\dagger_{L,i}(t')\,\tilde{\rho}(t) - \tilde{s}^\dagger_{L,i}(t')\,\tilde{\rho}(t)\,\tilde{s}_{L,i}(t)\right)\right. \\
&\qquad\qquad \left. + e^{-i\,\varepsilon^L_{k,i}(t-t')}\left(\tilde{\rho}(t)\,\tilde{s}_{L,i}(t')\,\tilde{s}^\dagger_{L,i}(t) - \tilde{s}^\dagger_{L,i}(t)\,\tilde{\rho}(t)\,\tilde{s}_{L,i}(t')\right)\right\} \\
&\quad+ \sum_{l,i}|W_{l,i}|^2\left\{e^{i\,\varepsilon^R_{l,i}(t-t')}\left(\tilde{\rho}(t)\,\tilde{s}^\dagger_{R,i}(t')\,\tilde{s}_{R,i}(t) - \tilde{s}_{R,i}(t)\,\tilde{\rho}(t)\,\tilde{s}^\dagger_{R,i}(t')\right)\right. \\
&\qquad\qquad \left. + e^{-i\,\varepsilon^R_{l,i}(t-t')}\left(\tilde{s}^\dagger_{R,i}(t)\,\tilde{s}_{R,i}(t')\,\tilde{\rho}(t) - \tilde{s}_{R,i}(t')\,\tilde{\rho}(t)\,\tilde{s}^\dagger_{R,i}(t)\right)\right\}.
\end{aligned} \tag{5.15}$$

The last step is to rewrite the sum over the states k in the leads as

$$\sum_k |V_{k,i}|^2\, e^{i\,\varepsilon^L_{k,i}(t-t')} = \int d\varepsilon\, \sum_k |V_{k,i}|^2\,\delta(\varepsilon-\varepsilon^L_{k,i})\, e^{i\,\varepsilon(t-t')} \tag{5.16}$$

and to assume the spectral function of the lead to be constant,

$$\Gamma_{L,i} = 2\pi\sum_k |V_{k,i}|^2\,\delta(\varepsilon-\varepsilon^L_{k,i}). \tag{5.17}$$

Similarly, $\Gamma_{R,i}$ is defined as the constant spectral function of the coupling to the i-th right lead. The integral over $d\varepsilon$ then gives a delta-function in the time,

$$\sum_k |V_{k,i}|^2 \; e^{i\,\varepsilon^L_{k,i}(t-t')} = \Gamma_{L,i}\,\delta(t-t'). \tag{5.18}$$

Finally, the first part of the master equation (5.10) takes the form

$$\begin{aligned} -\int_0^t dt'\; \mathrm{Tr}_{\mathrm{Res,e}} \Big\{ \big[\tilde{H}_{\mathrm{e}}(t), \big[\tilde{H}_{\mathrm{e}}(t'), \tilde{\rho}(t)\otimes R_{0,\mathrm{e}}\big]\big] \Big\} \\ = \sum_i \Gamma_{L,i} \left(\tilde{s}^\dagger_{L,i}(t)\,\tilde{\rho}(t)\,\tilde{s}_{L,i}(t) - \frac{1}{2}\,\tilde{s}_{L,i}(t)\,\tilde{s}^\dagger_{L,i}(t)\,\tilde{\rho}(t) - \frac{1}{2}\,\tilde{\rho}(t)\,\tilde{s}_{L,i}(t)\,\tilde{s}^\dagger_{L,i}(t) \right) \\ + \Gamma_{R,i} \left(\tilde{s}_{R,i}(t)\,\tilde{\rho}(t)\,\tilde{s}^\dagger_{R,i}(t) - \frac{1}{2}\,\tilde{s}^\dagger_{R,i}(t)\,\tilde{s}_{R,i}(t)\,\tilde{\rho}(t) - \frac{1}{2}\,\tilde{\rho}(t)\,\tilde{s}^\dagger_{R,i}(t)\,\tilde{s}_{R,i}(t) \right). \end{aligned} \tag{5.19}$$

The trace over the bosonic degrees of freedom differs from the trace over the leads because all double quantum dots couple to the same bosonic bath. This induces a coupling between the otherwise independent double quantum dots and results in collective effects as we will show below. We use the definition (3.22) of the bath correlation function $K(t)$ to write the trace over the environment as

$$\begin{aligned} \mathrm{Tr}_{\mathrm{Res,p}} \Big\{ \big[\tilde{H}_{\mathrm{p}}(t), \big[\tilde{H}_{\mathrm{p}}(t'), \tilde{\rho}(t)\otimes R_{0,\mathrm{p}}\big]\big] \Big\} \\ = \sum_{i,j} \big[(\tilde{n}_{L,i}(t) - \tilde{n}_{R,i}(t)), (\tilde{n}_{L,j}(t') - \tilde{n}_{R,j}(t'))\;\tilde{\rho}(t)\big]\; K(t-t') \\ - \big[(\tilde{n}_{L,i}(t) - \tilde{n}_{R,i}(t)), \tilde{\rho}(t)\;(\tilde{n}_{L,j}(t') - \tilde{n}_{R,j}(t'))\big]\; K^*(t-t'). \end{aligned} \tag{5.20}$$

Then, the master equation in interaction picture is the sum of the terms (5.19) and (5.20) according to equation (5.10). The final step is to transform the master equation back into the Schrödinger picture, using

$$\dot{\rho}(t) = -i\,\big[H_0, \rho(t)\big] + e^{-iH_0 t}\,\dot{\tilde{\rho}}(t)\,e^{iH_0 t}. \tag{5.21}$$

Here, H_0 is the double quantum dot part of the unperturbed Hamiltonian (5.4), as the reservoirs have already been traced out. Hence, the back-transformation of (5.20) results in

$$\begin{aligned} e^{-iH_0 t} \int_0^t dt'\; \mathrm{Tr}_{\mathrm{Res,p}} \Big\{ \big[\tilde{H}_{\mathrm{p}}(t), \big[\tilde{H}_{\mathrm{p}}(t'), \tilde{\rho}(t)\otimes R_{0,\mathrm{p}}\big]\big] \Big\}\; e^{iH_0 t} \\ = \int_0^t dt'\; \sum_{i,j} \big[(n_{L,i} - n_{R,i}), \big(\tilde{n}_{L,j}(t'-t) - \tilde{n}_{R,j}(t'-t)\big)\;\rho(t)\big]\; K(t-t') \\ - \big[(n_{L,i} - n_{R,i}), \rho(t)\;\big(\tilde{n}_{L,j}(t'-t) - \tilde{n}_{R,j}(t'-t)\big)\big]\; K^*(t-t'), \end{aligned} \tag{5.22}$$

with the operators $\tilde{n}_{L,j}(t'-t)$ and $\tilde{n}_{R,j}(t'-t)$ in the interaction picture (5.6). We assume that the correlation function $K(t)$ is peaked around $t=0$ such that the upper limit of the time integral can be extended to infinity. This property of the bath correlation function is a condition for applying the Markov approximation, cf. Sec. 3.2.2. The rates Γ, $\Gamma_{C,i}$, and $\Gamma_{S,i}$ are defined according to (3.29) with Δ replaced by Δ_i. Thus, we find for the master equation of an ensemble of double quantum dots that are coupled to leads and a common bosonic environment:

$$\begin{aligned}
\frac{d}{dt}\,\rho(t) = i\,\Big[\,\rho(t)\,,\sum_i^N\Big(\varepsilon_{L,i}\,n_{L,i}+\varepsilon_{R,i}\,n_{R,i}+T_{c,i}(p_i+p_i^\dagger)\Big)\Big] \\
+\sum_i \Gamma_{L,i}\Big(s_{L,i}^\dagger\,\rho(t)\,s_{L,i}-\frac{1}{2}\,s_{L,i}\,s_{L,i}^\dagger\,\rho(t)-\frac{1}{2}\,\rho(t)\,s_{L,i}\,s_{L,i}^\dagger\Big) \\
+\Gamma_{R,i}\Big(s_{R,i}\,\rho(t)\,s_{R,i}^\dagger-\frac{1}{2}\,s_{R,i}^\dagger\,s_{R,i}\,\rho(t)-\frac{1}{2}\,\rho(t)\,s_{R,i}^\dagger\,s_{R,i}\Big) \\
-\sum_{i,j}\frac{1}{\Delta_j^2}\,\Big[(n_{L,i}-n_{R,i}),\big(\,((\Delta_j^2-4T_{c,j}^2)\,\Gamma+4T_{c,j}^2\Gamma_{C,j})(n_{L,j}-n_{R,j}) \\
+2T_{c,j}(\Gamma-\Gamma_{C,j})\,\varepsilon_j\,(p_j+p_j^\dagger)+i\,2T_{c,j}\Delta_j\Gamma_{S,j}(p_j-p_j^\dagger)\,\big)\,\rho(t)\Big] \\
+\sum_{i,j}\frac{1}{\Delta_j^2}\,\Big[(n_{L,i}-n_{R,i}),\,\rho(t)\,\big(\,((\Delta_j^2-4T_{c,j}^2)\,\Gamma^*+4T_{c,j}^2\Gamma_{C,j}^*)(n_{L,j}-n_{R,j}) \\
+2T_{c,j}(\Gamma^*-\Gamma_{C,j}^*)\,\varepsilon_j\,(p_j+p_j^\dagger)+i\,2T_{c,j}\Delta_j\Gamma_{S,j}^*(p_j-p_j^\dagger)\,\big)\Big].
\end{aligned} \tag{5.23}$$

Note that the mixed terms $i\neq j$ in the summation over the double quantum dots are responsible for possible collective effects. Without these terms, the master equation merely describes an ensemble of N double quantum dots which are completely independent of each other. This corresponds to a situation in which each double quantum dot couples to an independent bosonic environment. Then, the density matrix $\rho(t)$ factorizes and no correlations between different dots evolve. The additional terms, $i\neq j$, on the other hand introduce an interaction between the double dots which is caused by the coupling of the dots to the same environment. For only one double quantum dot, $N=1$, we recover the result given in [102] for the matrix elements of the density operator of such a system.

5.3 Electron-Phonon Interaction

In the derivation of the master equation, we used the definition (3.22) for the correlation function $K(t)$ as already introduced in chapter 3. It was also shown in that

chapter that $K(t)$ can be written as an integral over the spectral function $\rho(\omega)$ of the environment (3.33). It should be emphasized once again that this spectral function is of great importance since all properties of both the environment itself and its interaction to the electrons in the quantum dots enter exclusively into this function. For the calculations of this chapter, we choose the spectral function of bulk acoustic phonons with piezoelectric interaction to lateral quantum dots [33, 102],

$$\rho(\omega) = g\,\omega\left(1 - \frac{\omega_d}{\omega}\sin\left(\frac{\omega}{\omega_d}\right)\right) e^{-\omega/\omega_c}\,, \tag{5.24}$$

where g is the dimensionless interaction strength, ω_c the cut-off frequency and the frequency $\omega_d = c/d$ is determined by the ratio of the the sound velocity c to the distance d between two quantum dots. We checked by separate calculations that the collective effects as presented in the following sections do not depend on the exact form of the spectral function and do equally appear for other spectral functions like that of an ohmic bath.

The correlation function $K(t)$ does not enter the master equation directly but in the form of the rates Γ, $\Gamma_{C,j}$, and $\Gamma_{S,j}$, defined as different integrals over the correlation function (3.29). It will turn out to be useful to define linear combinations of Γ, $\Gamma_{C,j}$, and $\Gamma_{S,j}$,

$$\begin{aligned}
\alpha_j &= 2\Big(1 - \frac{4T_{c,j}^2}{\Delta_j^2}\Big)\,\Gamma + \frac{8T_{c,j}^2}{\Delta_j^2}\,\Gamma_{C,j}\,,\\
\beta_j &= \frac{4T_{c,j}\,\varepsilon_j}{\Delta_j^2}\,(\Gamma - \Gamma_{C,j}) + i\,\frac{4T_{c,j}}{\Delta_j}\,\Gamma_{S,j}\,,\\
\gamma_j &= \frac{4T_{c,j}\,\varepsilon_j}{\Delta_j^2}\,(\Gamma - \Gamma_{C,j}) - i\,\frac{4T_{c,j}}{\Delta_j}\,\Gamma_{S,j}\,.
\end{aligned} \tag{5.25}$$

If we neglect the principal values in the integration over the correlation function $K(t)$ [78], as discussed in section 3.3.2, the expressions for the rates Γ, $\Gamma_{C,j}$, and $\Gamma_{S,j}$ are considerably simplified, see (3.47). Then, we find from (5.25)

$$\begin{aligned}
\alpha_j &= \frac{4\pi T_{c,j}^2}{\Delta_j^2}\,\rho(\Delta_j)\,\coth\Big(\frac{\beta\Delta_j}{2}\Big),\\
\beta_j &= \frac{2\pi T_{c,j}}{\Delta_j}\,\rho(\Delta_j)\left(1 - \frac{\varepsilon_j}{\Delta_j}\,\coth\Big(\frac{\beta\Delta_j}{2}\Big)\right),\\
\gamma_j &= -\frac{2\pi T_{c,j}}{\Delta_j}\,\rho(\Delta_j)\left(1 + \frac{\varepsilon_j}{\Delta_j}\,\coth\Big(\frac{\beta\Delta_j}{2}\Big)\right).
\end{aligned} \tag{5.26}$$

Thus, neglecting the principal values leads to real parameters α_j, β_j, and γ_j. Nevertheless, we will treat them in the following calculations as complex quantities in order not to restrict the validity of the results to that approximation.

5.4 Stationary Current through One Double Dot

The master equation (5.23) describes the general case of N double quantum dots interacting with the same bosonic bath. Before turning to collective effects in the tunnel current through two double quantum dots, we consider the master equation for only one double dot, $N = 1$, and thus without any collective effects. In the stationary case, $\dot{\rho}(t) = 0$, the master equation is solved analytically and the current through the double dot is derived from the density matrix. We show that the inelastic part of the current, which results from the interaction with the phonon bath, can be approximated by a classical rate equation. The transition rate of electrons between the left and the right quantum dot follows from Fermi's Golden Rule.

5.4.1 Master Equation for One Double Dot

As we consider the stationary current, the density matrix becomes time-independent, $\dot{\rho}(t) = 0$, and the master equation reduces to a linear system of equations. The three states $|0\rangle$, $|L\rangle$, and $|R\rangle$ as introduced in section 5.1 of this chapter are chosen as a basis of the density matrix. Then, the equations for the four matrix elements

$$\begin{aligned} \langle n_L \rangle &= \langle L| \rho |L\rangle , & \langle p^\dagger \rangle &= \langle L| \rho |R\rangle , \\ \langle p \rangle &= \langle R| \rho |L\rangle , & \langle n_R \rangle &= \langle R| \rho |R\rangle \end{aligned} \tag{5.27}$$

form a closed set with the exception of the element $\langle 0| \rho |0\rangle$. Since the trace of the density matrix is always equal to 1, this element can be expressed as

$$\langle 0| \rho |0\rangle = 1 - \langle n_L \rangle - \langle n_R \rangle . \tag{5.28}$$

Thus, we arrive at a linear system of four equations which is solved analytically. We find for the density matrix elements in the stationary case

$$\begin{aligned} \langle n_L \rangle &= 1 - \frac{T_c(\Gamma_L + \Gamma_R)}{D} \left\{ \varepsilon(\gamma{+}\gamma^*) - \big(2T_C + i(\gamma{-}\gamma^*)\big)\Big(\frac{\Gamma_R}{2} + \alpha{+}\alpha^*\Big) \right\}, \\ \langle n_R \rangle &= \frac{T_c\Gamma_L}{D} \left\{ \varepsilon(\gamma{+}\gamma^*) - \big(2T_C + i(\gamma{-}\gamma^*)\big)\Big(\frac{\Gamma_R}{2} + \alpha{+}\alpha^*\Big) \right\}, \\ \langle p \rangle &= \frac{\Gamma_L}{D} \left\{ T_c^2(\beta{+}\beta^*{-}\gamma{-}\gamma^*) + iT_c(\beta\gamma{-}\beta^*\gamma^*) + \Gamma_R(iT_c{-}\gamma)\Big(i\varepsilon{+}\frac{\Gamma_R}{2} + \alpha{+}\alpha^*\Big) \right\}. \end{aligned} \tag{5.29}$$

The remaining matrix element follows directly, $\langle p^\dagger\rangle = \langle p\rangle^*$, as the density matrix is a hermitian operator. The denominator D in these equations is defined as

$$\begin{aligned} D = &-\Gamma_L\Gamma_R\Big(\varepsilon^2 + \Big(\frac{\Gamma_R}{2} + \alpha{+}\alpha^*\Big)^2\Big) + \varepsilon T_c\Big(\Gamma_L(\beta{+}\beta^*) + (\Gamma_L{+}\Gamma_R)(\gamma{+}\gamma^*)\Big) \\ &- \Big(2T_c^2(2\Gamma_L{+}\Gamma_R) + iT_c(\Gamma_L{+}\Gamma_R)(\gamma{-}\gamma^*) - iT_c\Gamma_L(\beta{-}\beta^*)\Big)\Big(\frac{\Gamma_R}{2} + \alpha{+}\alpha^*\Big). \end{aligned} \tag{5.30}$$

The expressions for the matrix elements are simplified considerably if the parameters α_j, β_j, and γ_j become real as assumed in the previous section, Eq. (5.26).

5.4.2 Tunnel Current

The tunnel current through one double quantum dot follows from the time derivative of the occupation operator of one of the dots, for instance the left one. The Heisenberg equation of motion gives

$$\langle \dot{n}_L\rangle = -\frac{iT_c}{\hbar}\left(\langle p\rangle - \langle p^\dagger\rangle\right) + \frac{i}{\hbar}\sum_k V_k\,\langle c_k^\dagger s_L\rangle - V_k^*\,\langle c_k s_L^\dagger\rangle\,, \tag{5.31}$$

where we reintroduced $\hbar$ in order to obtain the current in units of Ampère. Two parts can be identified in this expression: The first part ($\propto T_{c,i}$) gives the change in the occupation of the left quantum dot due to tunneling of electrons to or from the right dot. The second part describes the tunneling between the left dot and the lead. In the stationary case, the two contributions equal each other and the current operator can be expressed by the number of electrons tunneling between the two dots,

$$I = \frac{i\,e\,T_c}{\hbar}\,(p - p^\dagger). \tag{5.32}$$

The expectation value of the current results if the solution (5.29) of the master equation is inserted in this equation,

$$\langle I\rangle = \frac{e\,T_c\,\Gamma_L\Gamma_R}{\hbar\,D}\left\{\varepsilon\,(\gamma{+}\gamma^*) - \big(2T_c{+}\,i(\gamma{-}\gamma^*)\big)\Big(\frac{\Gamma_R}{2} + \alpha{+}\alpha^*\Big)\right\}. \tag{5.33}$$

A comparison of this expression with the current as obtained by a polaron transformation is given in [102]. Without interaction to phonons, $\alpha{=}\beta{=}\gamma{=}0$, we recover the result of Stoof and Nazarov [103] for the tunnel current via two discrete states,

$$\langle I\rangle = \frac{e}{\hbar}\,\frac{T_c^2\,\Gamma_R}{T_c^2(2+\Gamma_R/\Gamma_L) + \Gamma_R^2/4 + \varepsilon^2}\,. \tag{5.34}$$

A slightly different result was derived by Gurvitz and Prager [104]. They explain an additional factor 2 connected with the tunnel rate Γ_L in their result by the

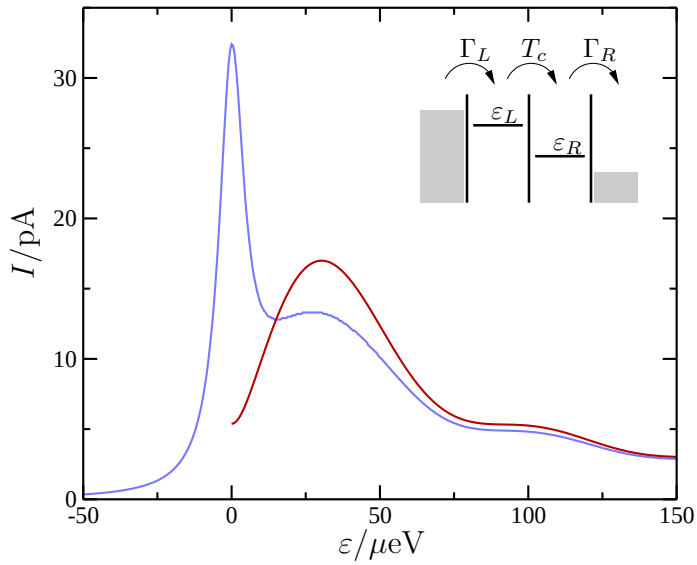

Figure 5.2: Blue: Stationary current through one double quantum dot (5.33) as a function of the energy bias $\varepsilon = \varepsilon_L - \varepsilon_R$. Red: Inelastic current from Fermi's Golden Rule (5.42). The inset shows schematically the energies and tunnel rates in the double quantum dot. The parameters are $T_c = 3\mu$eV, $\Gamma_L = \Gamma_R = 0.4\mu$eV and the spectral function (5.24) with $g = 0.01$, $T = 23$mK, $\omega_d = 10\mu$eV and $\omega_c = 1$meV.

consideration of the spin degree of freedom. Equation (5.34) shows that the current through an ideal double quantum dot which is not coupled to phonons or photons takes the form of a Lorentz-shaped function centered around zero bias, $\varepsilon = 0$. In this case, an additional electron can tunnel elastically between the left and the right quantum dot since its eigenenergy is equal in both dots and consequently the tunnel current becomes maximal. The Lorentz shape of the tunnel current has indeed be found in experiments [3, 27].

For finite bias, $\varepsilon \neq 0$, conservation of energy leads to a vanishing current as the energy of an additional electron is not the same in the left and the right dot. However, interaction with an environment, for instance a phonon bath, enables tunneling also for a finite bias if exchange of energy is possible. For negative bias, $\varepsilon < 0$, an electron in the left dot can gain the necessary energy to tunnel to the right dot by absorption of a phonon. Since this process requires the presence of a sufficient number of phonons, it is restricted to finite temperatures. The reverse process is even possible in the limit of zero temperature, $T \to 0$. The electron in the left dot overcomes a positive bias by emission of a phonon and hence can tunnel to the right dot. Figure 5.2 shows the current through one double dot (5.33) as a function of the bias ε for a small temperature, $T = 23$mK. The elastic peak at $\varepsilon = 0$ is clearly visible.

The broad shoulder on the emission side, $\varepsilon > 0$, is due to the interaction with the bosonic environment. This part of the current is referred to as the inelastic current. The energies for a positive bias are depicted in the inset. The oscillations in the inelastic current are due to the choice of the spectral function (5.24). We will come back to the connection between the spectral function and the inelastic current in the next paragraph. The shape of the current is in good agreement with experimental results [16] that were obtained at the same temperature. The absolute values of the current in Fig. 5.2 are too large as compared to the experiment as we used different parameters.

5.4.3 Rate Equation

The inelastic current caused by interactions with the environment can be approximated by a classical rate equation. A rate equation allows to calculate the probabilities for certain states in the double dot from the transition rates between these states. We introduce this method here not only to give an approximation for the inelastic current through one double dot. The rate equation will turn out to be very useful for describing collective effects in many quantum dots.

We will first calculate the rate for transitions of an additional electron from the left to the right quantum dot using Fermi's Golden Rule. As we are interested in the inelastic current, we assume a positive bias, $\varepsilon > 0$. The coupling to the environment V_p (5.5), however, does not introduce transitions between the basis states $|L\rangle$ and $|R\rangle$ since we assumed a diagonal coupling. In the absence of T_c, $|L\rangle$ and $|R\rangle$ are still eigenstates of the interacting system and no transitions occur. In other words, only the combination of a finite T_c and the coupling to the dissipative environment results in transitions. Thus, we have to calculate the transition rate between the eigenstates of the unperturbed Hamiltonian H_0 of the double dot, including T_c. The solutions of H_0 are the hybridized states,

$$\begin{aligned} |+\rangle &= \frac{1}{\sqrt{2\Delta(\Delta+\varepsilon)}} \begin{pmatrix} \varepsilon+\Delta \\ 2T_c \end{pmatrix} \\ |-\rangle &= \frac{1}{\sqrt{2\Delta(\Delta-\varepsilon)}} \begin{pmatrix} \varepsilon-\Delta \\ 2T_c \end{pmatrix} \end{aligned} \tag{5.35}$$

expressed in the basis of

$$|L\rangle = \begin{pmatrix} 1 \\ 0 \end{pmatrix}, \qquad |R\rangle = \begin{pmatrix} 0 \\ 1 \end{pmatrix}. \tag{5.36}$$

Without loss of generality we set $\varepsilon_L = -\varepsilon_R = \varepsilon/2$ and find for the eigenenergies of the hybridized states $\pm\Delta/2$. From the form of $|+\rangle$ and $|-\rangle$ in (5.35) we see that the hybridized states approach $|L\rangle$ and $|R\rangle$ for $T_c \ll \varepsilon$.

We consider transitions from the initial state $|i\rangle$ with an electron in the upper state $|+\rangle$ to the final state $|f\rangle$ with the electron in the lower state $|-\rangle$ under the emission of a phonon of mode q,

$$|i\rangle = |+\rangle \otimes |0\rangle_{\mathrm{p}}\,, \qquad |f\rangle = |-\rangle \otimes a_q^\dagger\,|0\rangle_{\mathrm{p}}\,, \tag{5.37}$$

where $|0\rangle_{\mathrm{p}}$ denotes any state of the phonon bath. The matrix element with respect to the interaction operator V_{p} (5.5) follows as

$$\langle f|\,V_p\,|i\rangle = -\frac{2T_c\gamma_q}{\Delta}\,. \tag{5.38}$$

Applying Fermi's Golden Rule (see for example [67]) leads to the transition rate

$$\nu_{i\to f} = \frac{8\pi\,T_c^2}{\hbar\,\Delta^2}\;\rho(\Delta), \tag{5.39}$$

where $\rho(\omega=\Delta)$ is the spectral function of the environment as defined in (3.33). Similarly, we find for the transition rates of an electron tunneling from the left lead to the left quantum dot $\Gamma_L/\hbar$ and for tunneling from the right dot to the right lead $\Gamma_R/\hbar$ with $\Gamma_{L/R}$ as defined in (5.17).

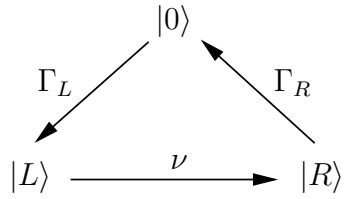

Figure 5.3: Possible transitions in the rate equation (5.40).

These transition rates are used to model the transport of electrons through the double quantum dot in the inelastic regime. If no additional electron is in either of the two dots, an electron can tunnel from the left lead to the left dot with a rate $\Gamma_L/\hbar$. This corresponds to transition from state $|0\rangle$ to state $|L\rangle$ as indicated in Fig. 5.3. Then, the electron tunnels to the right dot with a rate ν as derived in the previous paragraph. Actually, we do not have to distinguish between the states $|L\rangle$ and $|+\rangle$ or between $|R\rangle$ and $|-\rangle$ since these become identical in the limit $T_c \ll \varepsilon$. This distinction was only necessary for the derivation of the rate ν. Finally, the additional electron can leave the right dot to the right lead, $|R\rangle \to |0\rangle$. As a result of this cycle, one electron has been transferred from the left to the right lead and the system returned to the initial state such that the process can start again from the beginning. Let us consider the change in the probabilities p_L, p_R, and p_0 for the three states,

$$\begin{aligned} \dot{p}_0 &= \Gamma\,p_R - \Gamma\,p_0, \\ \dot{p}_L &= \Gamma\,p_0 - \nu\,p_L, \\ \dot{p}_R &= \nu\,p_L - \Gamma\,p_R, \end{aligned} \tag{5.40}$$

where we assumed equal tunnel rates to the left and right leads, $\Gamma = \Gamma_L/\hbar = \Gamma_R/\hbar$. The probability for the state $|L\rangle$, for instance, is increased by transitions to this state weighted with the probability of no additional electrons in the dots, p_0, and decreased by transitions to the right dot, weighted with the probability of an electron in the left dot, p_L. Taking into account the normalization of the total probability, $p_L + p_R + p_0 = 1$, the rate equation can be solved easily in the stationary case,

$$p_L = \frac{1}{2x+1}\,, \qquad p_R = \frac{x}{2x+1}\,, \qquad p_0 = \frac{x}{2x+1}\,, \quad x = \nu/\Gamma\,. \tag{5.41}$$

The inelastic current through the double dot follows directly from these probabilities as the number of electrons tunneling through the system per time. For example, we can count the electrons tunneling from the left to right dot,

$$I_s = e\, p_L\, \nu = \frac{e\,\nu}{2x+1}\,. \tag{5.42}$$

This result for the inelastic current is plotted in Fig. 5.2. Despite the simplicity of the method, it is in reasonable agreement with the result of the Born-Markov approximation for large ε. The rate equation does not give a vanishing inelastic current at zero bias, $\varepsilon = 0$, as one should expect. However, this is not surprising, since in that limit, the state $|+\rangle$ and $|-\rangle$ are even and odd linear combinations of $|L\rangle$ and $|R\rangle$ and transitions between the latter cannot be described by the rate ν. For small couplings to the environment, the tunnel rate ν between the dots becomes much smaller than the rates to or from the leads, Γ, and thus $x \ll 1$. The inelastic current (5.42) is then well approximated by

$$I_s = e\,\nu = \frac{8\pi\, e\, T_c^2}{\hbar\,\Delta^2}\;\rho(\Delta). \tag{5.43}$$

Hence, the inelastic current is proportional to the spectral function for small couplings, in agreement with the similar result deduced from the polaron transformation [33].

5.5 Collective Effects in Two Double Dots

We shall investigate in this section how the indirect interaction between two double quantum dots as mediated by the environment changes the tunnel current. Since the dimension of the density matrix for N double dots grows with 9^N, an analytical solution of the master equation becomes very cumbersome even for $N = 2$. Hence, the linear system of equations to which the master equation (5.23) reduces in the stationary case is solved numerically. This system of equations is given explicitly in the appendix, Eq. (B.1).

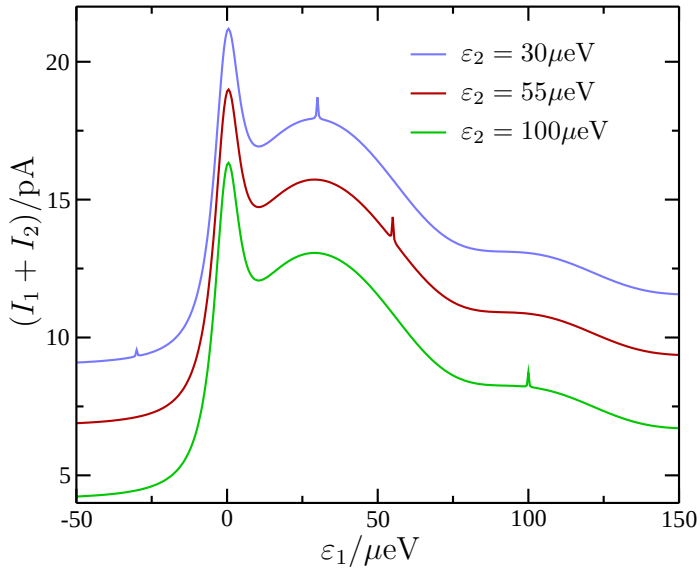

Figure 5.4: Total current through two double quantum dots as a function of the bias ε_1. The parameters are $T_{c,1} = T_{c,2} = 3\mu$eV, $\Gamma_{L,1} = \Gamma_{R,1} = \Gamma_{L,2} = \Gamma_{R,2} = 0.15\mu$eV, and for the spectral function $g = 0.01$, $T = 23$mK, $\omega_d = 10\mu$eV and $\omega_c = 1$meV. These values are used throughout the whole chapter if not stated otherwise.

The current operator for each of the two double dots is the same as for an independent double dot (5.32) as electrons cannot tunnel between the different double dots. Expressed by the density matrix elements, the current through double dot 1 and 2 reads,

$$\begin{aligned} I_1 &= -\frac{2\,T_{c,1}\,e}{\hbar}\ \mathrm{Im}\big\{\rho_{LRLL} + \rho_{RRLR} + \rho_{0RL0}\big\}, \\ I_2 &= -\frac{2\,T_{c,2}\,e}{\hbar}\ \mathrm{Im}\big\{\rho_{RLLL} + \rho_{RRRL} + \rho_{R00L}\big\}, \end{aligned} \tag{5.44}$$

with the notation of the matrix elements defined as

$$\rho_{j\,i\,i'\,j'} = {}_2\langle j| \otimes {}_1\langle i|\ \rho\ |i'\rangle_1 \otimes |j'\rangle_2\,, \qquad i,j \in \{L,R,0\}. \tag{5.45}$$

The total current through both double dots, $I_1 + I_2$, is shown in Fig. 5.4 as a function of the bias in the first double dot, ε_1, while the bias in the second double dot, ε_2, is kept constant. The overall shape of the current is identical to the case of an independent double dot, Fig. 5.2. Again, the elastic peak around $\varepsilon_1 = 0$ and the inelastic current can clearly be identified. The interesting new feature here is the additional peak at the resonance $\varepsilon_1 = \varepsilon_2$ on the background of the inelastic current. This peak is caused by the indirect interaction between the two double dots due

to the coupling to the same phonon environment. What happens exactly at this resonance? To answer this question, we shall employ two different approximations. At first, we will investigate the effects of the indirect interaction in the master equation and find that they introduce a cross coherence between the two double dots, which in turn leads to the new peak in the current. A rate equation allows to connect the additional peak to the Dicke effect by taking into account modified transition rates. This is fully consistent with the emergence of the cross coherence.

5.5.1 Cross Coherences

The effective interaction between the two double quantum dots results from the simultaneous coupling of both double dots to the same phonon environment. It appears in the master equation (5.23) as the mixed terms $i \neq j$ in the summation. In the explicit form of the master equation (B.1), the effective interaction is connected to six matrix elements only (and their complex conjugates). These elements are ρ_{RLLL}, ρ_{LRLL}, ρ_{RRLR}, and ρ_{RRRL}, all of which enter the expression for the current (5.44), and the two *cross coherence* matrix elements

$$\rho_{RLRL} = \langle p_1^\dagger p_2 \rangle, \qquad \rho_{RRLL} = \langle p_1 p_2 \rangle. \tag{5.46}$$

It seems reasonable to suppose that the cross coherences play an important part for the collective effects. This is indeed confirmed in the following.

We approximate the effects of the indirect interaction by assuming that only those six matrix elements mentioned above are affected by the interaction. All other density matrix elements are supposed to stay unchanged. It is shown in appendix B that the change of the current through the first double dot due to collective effects can be approximated by

$$\Delta I_1 = -\frac{2e\,T_{c,1}\,\gamma_2}{\hbar\,\varepsilon_1} \Big(\mathrm{Re}\big\{ \langle p_1^\dagger p_2 \rangle \big\} - \mathrm{Re}\big\{ \langle p_1 p_2 \rangle \big\} \Big). \tag{5.47}$$

Correspondingly, the change ΔI_2 of the current through the second double dot is obtained from ΔI_1 by exchanging the subscripts 1 and 2. Hence, the alteration of the current is proportional to the real parts of the cross coherences $\langle p_1^\dagger p_2 \rangle$ and $\langle p_1 p_2 \rangle$ between the two double dots, which underlines the collective character of the effect. This result is confirmed by plotting the real parts of the cross coherences as a function of ε_1, Fig. 5.5. One recognizes that $\langle p_1^\dagger p_2 \rangle$ is peaked around $\varepsilon_1 = \varepsilon_2$, whereas $\langle p_1 p_2 \rangle$ has a peak at $\varepsilon_1 = -\varepsilon_2$. The increase of the current at $\varepsilon_1 = \varepsilon_2$ is therefore due to the maximum of the first correlation $\langle p_1^\dagger p_2 \rangle$.

If we neglect the changes of all other elements of the density matrix that are caused by the effective interaction between the two double quantum dots, the real

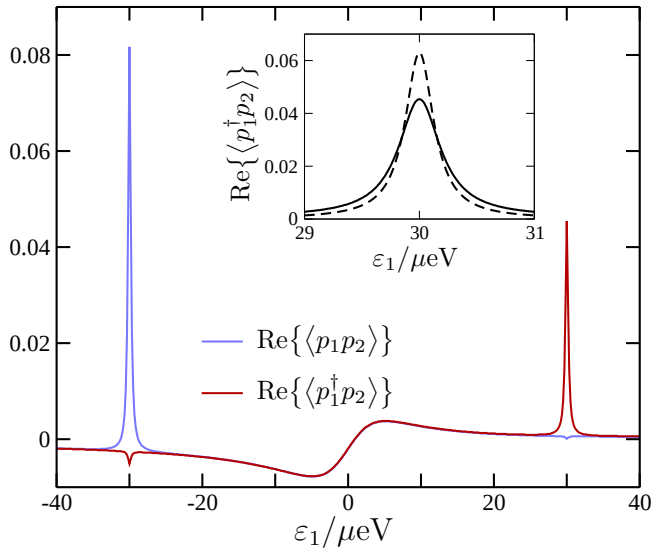

Figure 5.5: Real parts of the cross coherences as functions of the bias in the first double dot ($\varepsilon_2 = 30\mu$eV and the other parameters agree with Fig. 5.4). The inset compares the approximation (5.48) for $\mathrm{Re}\{\langle p_1^\dagger p_2\rangle\}$ (dotted line) with the numerical solution (solid line).

part of the cross coherence $\langle p_1^\dagger p_2\rangle$ can be approximated near the resonance $\varepsilon_1 = \varepsilon_2$ as

$$\mathrm{Re}\{\langle p_1^\dagger p_2\rangle\} = -\frac{\frac{1}{2}(\Gamma_{R,1}+\Gamma_{R,2})\big(\gamma_1\,\mathrm{Re}\{\langle p_2\rangle\}\,\langle n_{L,1}\rangle + \gamma_2\,\mathrm{Re}\{\langle p_1\rangle\}\,\langle n_{L,2}\rangle\big)}{(\varepsilon_1-\varepsilon_2)^2 + \frac{1}{4}(\Gamma_{R,1}+\Gamma_{R,2})^2}, \quad (5.48)$$

as shown in appendix B. Thus, the cross coherence $\langle p_1^\dagger p_2\rangle$ is put down to expectation values of a noninteracting double dot, $\langle p\rangle$ and $\langle n_L\rangle$, which were calculated in the previous section, Eq. (5.29). One recognizes that $\langle p_1^\dagger p_2\rangle$ is Lorentzian shaped as a function of the energy difference $\varepsilon_1 - \varepsilon_2$. The result (5.48) is in good agreement with the numerical solution of the master equation (5.23), as shown in the inset of Fig. 5.5. A similar expression is also derived for the other cross coherence $\langle p_1 p_2\rangle$ in appendix B and will be used in section 5.5.5.

Next, we insert the approximation for the cross coherence in (5.47) and find for the change of the tunnel current due to interaction effects between the two double quantum dots around the resonance $\varepsilon_1 = \varepsilon_2$:

$$\Delta I_1 = \frac{e\,T_{c,1}\,\gamma_2\,(\Gamma_{R,1}+\Gamma_{R,2})}{\hbar\,\varepsilon_1} \cdot \frac{\gamma_1\,\mathrm{Re}\{\langle p_2\rangle\}\,\langle n_{L,1}\rangle + \gamma_2\,\mathrm{Re}\{\langle p_1\rangle\}\,\langle n_{L,2}\rangle}{(\varepsilon_1-\varepsilon_2)^2 + \frac{1}{4}(\Gamma_{R,1}+\Gamma_{R,2})^2}. \quad (5.49)$$

Again, the change in the current through the second double dot, ΔI_2, is obtained by exchanging the subscripts. For the parameters used in Fig. 5.4, this approximation

overestimates the actual change in the current by a factor of roughly 3, but provides a good qualitative description for the effect of the enhanced tunnel current. A comparison between this result and the numerical solution will be given in a later section for different parameters.

5.5.2 Singlet and Triplet States

The cross coherence $p_1^\dagger p_2$ is regarded more closely in this paragraph. We express the four basis states with an additional electron in each of the two double dots by the pseudo-triplet and pseudo-singlet states,

$$\begin{aligned} |T_+\rangle &= |L\rangle_1 |L\rangle_2 , \\ |T_0\rangle &= \frac{1}{\sqrt{2}} \Big(|L\rangle_1 |R\rangle_2 + |R\rangle_1 |L\rangle_2 \Big), \\ |T_-\rangle &= |R\rangle_1 |R\rangle_2 , \\ |S_0\rangle &= \frac{1}{\sqrt{2}} \Big(|L\rangle_1 |R\rangle_2 - |R\rangle_1 |L\rangle_2 \Big). \end{aligned} \tag{5.50}$$

The terms triplet and singlet do not refer to the electron spin but to the charge. It turns out that the cross coherence is closely related to the triplet state $|T_0\rangle$ and singlet state $|S_0\rangle$, as expressed by the operator identity

$$p_1^\dagger p_2 + p_2^\dagger p_1 = \mathrm{P}_{T_0} - \mathrm{P}_{S_0}. \tag{5.51}$$

Here, P_ψ is the projection operator on the state $|\psi\rangle$, $\mathrm{P}_\psi \equiv |\psi\rangle \langle\psi|$. Hence, the increase of the stationary current at the resonance $\varepsilon_1 = \varepsilon_2$ is related to an increased probability of finding the two double dots in a triplet state rather than in a singlet state,

$$\Delta I_1 \propto \mathrm{Re}\big\{\big\langle p_1^\dagger p_2 \big\rangle\big\} = \frac{1}{2} \big(\langle \mathrm{P}_{T_0} \rangle - \langle \mathrm{P}_{S_0} \rangle \big). \tag{5.52}$$

According to this equation, an increased probability for the singlet state would lead to a reduced tunnel current. We will come back to that point below.

5.5.3 Dicke Effect

The fact, that triplet and singlet states are connected to a change of the tunnel current resembles the Dicke effect where the same states lead to a modified emission rate of excited two level atoms. The Dicke effect of an ensemble of N excited two level systems was discussed in Sec. 2.2.2. We will recall the basic features for $N = 2$ in order to relate the Dicke effect to the two double quantum dots. The modified transition rates due to the Dicke effect are then taken into account in a classical

rate equation to model the transport through the two double dots. It turns out that the collective effects found in the previous sections are very well described by this model.

We follow the original work by Dicke [12] who considered the collective decay of two identical two-level systems, for instance two-level atoms, coupled to the same radiation field. For our purpose, this system is best described in the singlet and triplet basis (5.50) where $|L\rangle$ corresponds to the excited state and $|R\rangle$ to the ground state. It can be seen directly from the Hamiltonian (2.6) that the singlet state $|S_0\rangle$ is an eigenstate of the Hamiltonian which consequently does not decay to the ground state $|T_-\rangle$. Nor does any triplet state decay to the singlet state. Hence, the decay of two excited atoms takes place via the triplet states. Moreover, the decay rates $|T_+\rangle \to |T_0\rangle$ and $|T_0\rangle \to |T_-\rangle$ are identical. They are twice as large as the decay rate of one independent atom. This can be understood directly from $|T_+\rangle$ which corresponds to both atoms in the excited state. The rate for the first decay of these atoms is naturally doubled as it does not play any role which of the atoms decays first. Since also the second transition, $|T_0\rangle \to |T_-\rangle$, takes place with double the rate, the total decay of two excited atoms coupled to the same environment is faster than that of two independent atoms. In any real system, the coupling to the radiation field is not perfectly identical as assumed above. Typically the coupling constants differ by a wavelength dependent phase. Then, the decay via the singlet state becomes also possible but it is much slower than the decay via the triplet states. These two decay channels are called *subradiant* and *superradiant*, respectively. The interplay between the two decay channels was demonstrated experimentally by DeVoe and Brewer [54]. They measured the spontaneous emission rate of two Ba^+_{138} ions in a laser trap as a function of the ion-ion distance.

These results can be applied to a system of two identical double quantum dots, that is, at the resonance $\varepsilon_1 = \varepsilon_2$. Accordingly, a singlet superposition in the double dots leads to a reduced transition of electrons from the left to the right dots and thus to a decreased current. On the other hand, a triplet superposition results in an enhanced tunnel current, as observed in the previous section. But then the question arises why the double dots prefer to form a triplet superposition in the first place. We employ a classical rate equation similar to that in section 5.4.3 to answer this question. The collective effects are considered by modified transition rates according to the Dicke effect.

The possible transitions between the nine states of our model are depicted in Fig. 5.6. In contrast to the Dicke effect, a third state exists in each of the double dots such that transitions to and from the singlet state are also possible. Take for instance the state $|0R\rangle$ with an additional electron in the right dot of the second double dot. A further electron can tunnel into the first double dot with a rate $\Gamma_{L,1}$. We assume that the two additional electrons form a singlet $|S_0\rangle$ or the triplet state $|T_0\rangle$ with probability one half each. The rate equation for the probabilities of the

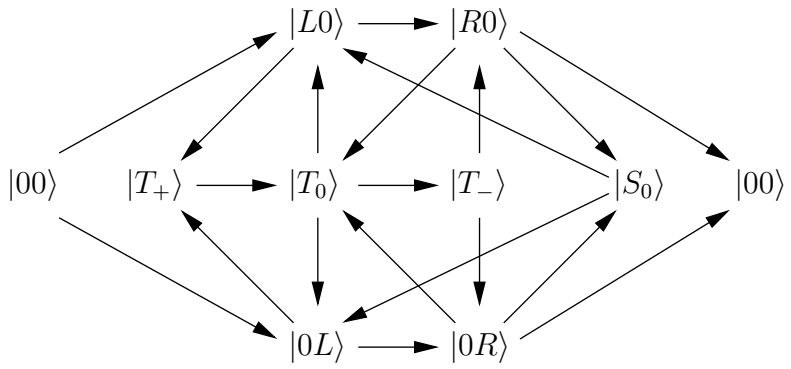

Figure 5.6: Possible transitions in the rate equation (5.53).

nine states is given by

$$\begin{aligned}
\dot{p}_{00} &= \Gamma\, p_{R0} + \Gamma\, p_{0R} - 2\Gamma\, p_{00},\\
\dot{p}_{L0} &= \Gamma\, p_{00} + \frac{1}{2}\,\Gamma\, p_{T_0} + \frac{1}{2}\,\Gamma\, p_{S_0} - (\nu+\Gamma)\, p_{L0},\\
\dot{p}_{0L} &= \Gamma\, p_{00} + \frac{1}{2}\,\Gamma\, p_{T_0} + \frac{1}{2}\,\Gamma\, p_{S_0} - (\nu+\Gamma)\, p_{0L},\\
\dot{p}_{R0} &= \nu\, p_{L0} + \Gamma\, p_{T-} - 2\Gamma\, p_{R0},\\
\dot{p}_{0R} &= \nu\, p_{0L} + \Gamma\, p_{T-} - 2\Gamma\, p_{0R},\\
\dot{p}_{T+} &= \Gamma\, p_{0L} + \Gamma\, p_{L0} - 2\nu\, p_{T+},\\
\dot{p}_{T_0} &= 2\nu\, p_{T+} + \frac{1}{2}\,\Gamma\, p_{0R} + \frac{1}{2}\,\Gamma\, p_{R0} - (2\nu+\Gamma)\, p_{T_0},\\
\dot{p}_{T-} &= 2\nu\, p_{T_0} - 2\Gamma\, p_{T-},\\
\dot{p}_{S_0} &= \frac{1}{2}\,\Gamma\, p_{0R} + \frac{1}{2}\,\Gamma\, p_{R0} - \Gamma\, p_{S_0}.
\end{aligned} \tag{5.53}$$

The probability to find the first double dot in state $|L\rangle$ and the second in state $|0\rangle$ is denoted by p_{L0}. Note the doubled rate 2ν for transitions between the triplet states, in order to take into account the Dicke effect. The rate ν for transitions between the dots was calculated in (5.39) using Fermi's Golden Rule. We assume identical tunnel rates to all four leads $\Gamma_{L,1}=\Gamma_{R,1}=\Gamma_{L,2}=\Gamma_{R,2}=\Gamma$.

In the stationary case, the rate equation (5.53) can be easily solved. For the current through one of the two double dots we obtain

$$I_d \;=\; e\,\Gamma\,(p_{00}+p_{0L}+p_{0R}) \;=\; \frac{e\nu(4x+1)}{9x^2+5x+1}, \qquad x=\nu/\Gamma. \tag{5.54}$$

This can be compared with the tunnel current I_s (5.42) through one independent double dot. The difference $\Delta I = I_d - I_s$ represents the additional current due to the Dicke effect and is shown in Fig. 5.7 as a function of the dimensionless

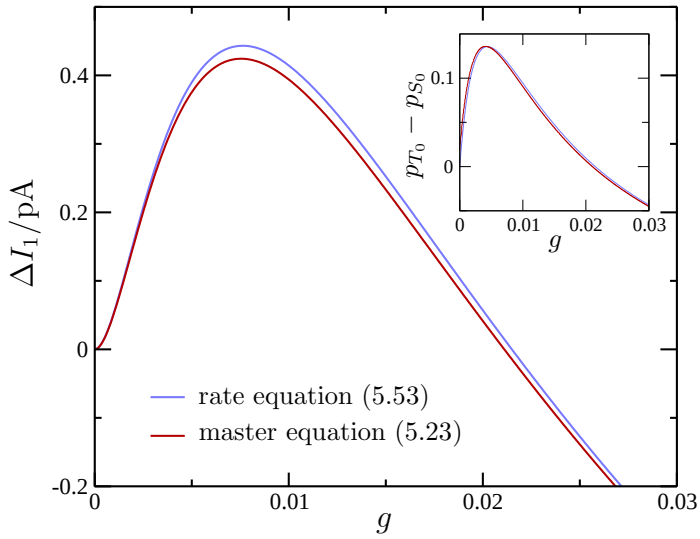

Figure 5.7: Enhancement of the tunnel current ΔI at the resonance $\varepsilon_1 = \varepsilon_2 = 30\mu$eV as a function of the dimensionless electron phonon coupling constant g. The additional current vanishes at $g \approx 0.02$ when the tunnel rates between the dots and to the leads become equal, $\nu = \Gamma$. The inset shows the difference in probabilities for triplet and singlet.

coupling strength g to the bosonic environment, together with ΔI as obtained from the numerical solution of the master equation (5.23). Both results agree very well, indicating that it is indeed the Dicke effect that leads to the increase in the tunnel current. In addition, we show (Fig. 5.7, inset) the difference between triplet and singlet occupation probability that follows from (5.53) as

$$p_{T_0} - p_{S_0} = -\frac{2x(x+2)(x-1)}{9x^3 + 23x^2 + 11x + 2}. \tag{5.55}$$

This is in excellent agreement with the numerical results and underlines that the change in the tunnel current due to collective effects is proportional to $p_{T_0} - p_{S_0}$, as already discussed above. The effect of superradiance amplifies the tunneling of electrons from the left to the right dots resulting in an enhanced current through the two double quantum dots.

5.5.4 Current Subradiance

The close analogy with the Dicke effect suggests the existence of not only current super-, but also current subradiance in the double quantum dots. In the subradiant regime, the two double dots form a singlet state which diminishes the tunneling from the left to the right dots leading to a weaker tunnel current. Subradiance

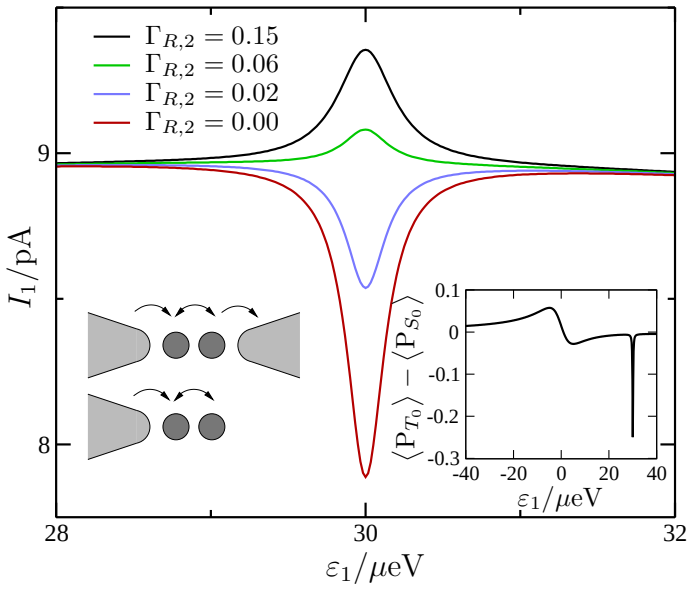

Figure 5.8: Transition from an increased to a decreased current through the first double quantum dot for different tunnel rates $\Gamma_{R,2}$ (in μeV) and $\varepsilon_2 = 30\mu$eV. The left inset shows schematically the set-up for $\Gamma_{R,2} = 0$. The right inset gives the difference of triplet and singlet for that case.

occurs in our system in a slightly modified set-up where electrons in the second double dot are prevented from tunneling into the right lead, $\Gamma_{R,2} = 0$, as indicated in the inset of Fig. 5.8. Then, the additional electron is trapped and no current can flow through the second double dot. Nevertheless, this electron can affect the tunnel current through the first double dot: Instead of a maximum, we now find a minimum at the resonance $\varepsilon_1 = \varepsilon_2$. Figure 5.8 shows how the positive peak in the current I_1 develops into a minimum as the tunneling rate $\Gamma_{R,2}$ is decreased to zero. This minimum is indeed related to an increased probability of finding the two dots in the singlet state $|S_0\rangle$ rather than in the triplet state $|T_0\rangle$, as can be seen from the inset of Fig. 5.8. Thus, in this regime the effect of subradiance dominates, leading to a decreased current.

This behavior is again consistent with the approximation (5.49) for the change of the tunnel current through the first double dot, ΔI_1. Taking into account the different non-interacting matrix elements in the two double dots, $\langle n_{L,1} \rangle \neq \langle n_{L,2} \rangle$ and $\langle p_1 \rangle \neq \langle p_2 \rangle$ due to $\Gamma_{R,1} \neq \Gamma_{R,2}$, we find a negative cross coherence at the resonance from (5.48). This corresponds to an increased probability for the singlet state and according to (5.47) to a reduced tunnel current, in agreement with our numerical solution.

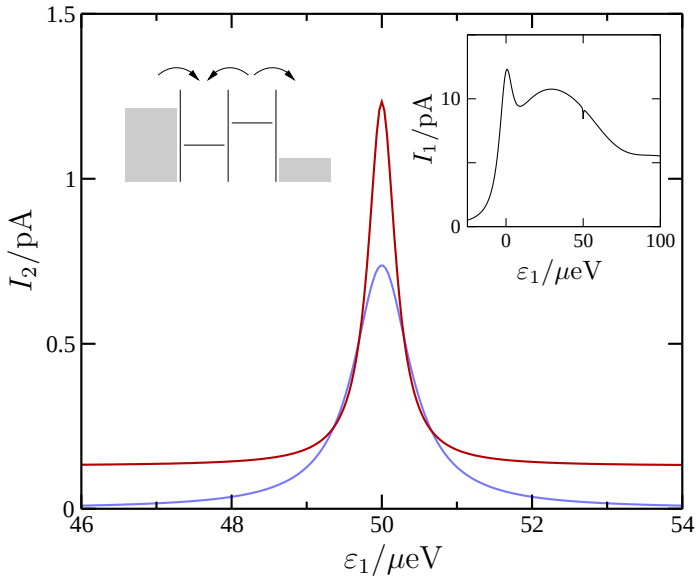

Figure 5.9: Tunnel current through the second double dot which is blocked due to a negative bias, $\varepsilon_2 = -50\mu$eV, as depicted in the left inset ($g = 0.015$). Red: Numerical solution of the master equation (5.23), the finite offset is the tail of the elastic current at $\varepsilon_2 = 0$. Blue: Approximation (5.56) for ΔI_2. The right inset shows the current I_1.

5.5.5 Inelastic Current Switch

Up to now, we have regarded collective effects in the two double quantum dots connected with the cross coherence $\langle p_1^\dagger p_2 \rangle$ around the resonance $\varepsilon_1 = \varepsilon_2$. However, the tunnel current can also be changed by the other cross coherence $\langle p_1 p_2 \rangle$, cf. (5.47). This cross coherence exhibits a resonance if the bias in one dot equals the negative bias in the other dot, $\varepsilon_1 = -\varepsilon_2$ (see Fig. 5.5). The effects of $\langle p_1 p_2 \rangle$ on the current are demonstrated in this section.

We use a fixed negative bias $\varepsilon_2 < 0$ in the second double dot as indicated in the inset of Fig. 5.9. Consequently, electrons cannot tunnel from the left to the right dot such that the second double dot is blocked and no current can flow through it. The presence of the first double dot, though, lifts this blockade and enables a current through the second double dot if the resonance condition $\varepsilon_1 = -\varepsilon_2$ is fulfilled. The current I_2 is shown in Fig. 5.9 as a function of the bias in the first double dot, ε_1. Due to the coupling to the common phonon environment, energy is transferred from the first to the second double dot, allowing electrons to tunnel from the left to the right in the second double dot. At the same time, the current through the first double dot is decreased (see Fig. 5.9, inset).

We can approximate the current through the second double dot around $\varepsilon_1 = -\varepsilon_2$

taking into account only $\langle p_1 p_2 \rangle$ in (5.47). Inserting the approximation (B.15) which is derived in appendix B for the real part of $\langle p_1 p_2 \rangle$ yields for the increase of the current through the second double dot

$$\Delta I_2 \;=\; \frac{T_{c,2}\,\gamma_1\,e}{\varepsilon_2\,\hbar} \;\cdot\; \frac{\left(\Gamma_{R,1}+\Gamma_{R,2}+16\alpha\right)\left(\gamma_1\,\mathrm{Re}\big\{\langle p_2\rangle\big\}\;\langle n_{L,1}\rangle + \gamma_2\,\mathrm{Re}\big\{\langle p_1\rangle\big\}\;\langle n_{L,2}\rangle\,\right)}{(\varepsilon_1+\varepsilon_2)^2 + (\frac{1}{2}\Gamma_{R,1}+\frac{1}{2}\Gamma_{R,2}+8\alpha)^2}\,, \tag{5.56}$$

with $\alpha=\alpha_1=\alpha_2$ evaluated at the resonance, where both systems are identical except for the opposite sign of the bias. This approximation again is in good agreement with the numerical solution of the master equation (5.23), as can be seen from Fig. 5.9.

Our results suggest that the current through one of the double dots can be switched on and off by appropriate manipulation of the other one. We emphasize that this mechanism is mediated by the dissipative phonon environment and not the Coulomb interaction between the charges. As this effect is very sensitive to the energy bias, it allows to detect a certain energy bias in one double dot by observing the current through the other double dot.

5.6 Conclusion

In this chapter, we have investigated collective effects in two double quantum dots and their consequences on the tunnel current. An indirect interaction arises between the double dots due to the coupling to the same phonon environment. We predict the emergence of the Dicke effect in this system as a result of the indirect interaction. Depending on the choice of parameters, the two double dots tend to form a charge-triplet or a charge-singlet superposition leading to an increase or a decrease, respectively, of the tunnel current.

The occurrence of the Dicke effect in the transport through mesoscopic systems has already been pointed out by Shahbazyan and Raikh [98]. In their system, the coupling to the same lead is responsible for collective effects. Usually, the Dicke effect manifests itself in a dynamic process like the spontaneous emission of an ensemble of identical atoms [54, 56]. Transport through double quantum dots, however, allows to study a time independent form of the Dicke effect. Moreover, we have demonstrated that the change of the tunnel current is connected with an entanglement of the different double dots. This opens the possibility to realize and to measure specific entangled states of two double dots. In particular, one can switch from a predominant triplet superposition of the two double dots connected with an increased tunnel current to a predominate singlet state leading to a reduced current.

The results discussed here were derived for the ideal case of an identical electron-phonon coupling in both double quantum dots. Furthermore, the Coulomb interaction between the two double dots has not been considered here. In a real experiment,

these assumption will never be perfectly fulfilled and would lead to deviations from the collective effects presented above. However, we predict that even in presence of inter-dot Coulomb interactions, phonon mediated collective effects should persist as long as a description of the quantum dots in terms of few many-body states is possible. These many-body states (that would depend on the specific geometry of the system) would than replace the many-body basis $\{|0,i\rangle, |L,i\rangle, |R,i\rangle\}$ $(i = 1, 2)$ used in our model here.

We have derived the master equation for the general case of N double dots but only focused on $N = 2$ which is the simplest case where collective effects occur. In general, one of the main characteristics of superradiance is the quadratic increase of the effect with increasing number of coupled systems, as discussed in chapter 2. For the spontaneous collective emission from N excited two-level atoms, this means that the maximum of the intensity of the emitted radiation increases with the square number of systems, N^2, while the time in which the decay takes place decreases inversely to the number of systems, $1/N$. Therefore, we expect that the collective effects as presented here become even more pronounced if more than two double dots are indirectly coupled by the common phonons.

Chapter 6

Conclusion

The subject of this thesis are collective effects in an ensemble of two-state systems caused by the coupling to a dissipative environment. The main part of this work, chapters 3 and 4, is devoted to the investigation of a large spin under the influence of a dissipative environment. This model applies both to an intrinsic spin of arbitrary size and to the collective behavior of an ensemble of independent identical two-state systems. Possible collective effects in such an ensemble are caused by the indirect interaction between the two-state systems resulting from the coupling of all systems to the same dissipative environment. A well-known collective effect of this kind is the superradiance shown by the Dicke model. The model describes an ensemble of initially excited two-level atoms coupled to the radiation field. The indirect interaction between the atoms leads to a collective spontaneous emission – the superradiance. The model of a dissipative large spin studied in this thesis is more general than the Dicke model since it also takes into account tunneling in the two-state systems, a feature not included in the Dicke model. Formally, the model of a dissipative large spin is the generalization of the spin-boson model to spins greater than one half.

We have investigated the model in two regimes of parameters, in the weak and in the strong-coupling limit. The results are derived for an ohmic dissipation, yet some conclusions can be generalized to other forms of the spectral function. The spin is described by a master equation, derived within the Born-Markov approximation. This method is perturbative in the spin-environment interaction. A comparison with the results of the spin-boson model shows that this approach yields reliable results for all temperatures in the weak-coupling limit. As the spin size is increased the large spin shows a superradiance-like decay. For zero bias, beats are observed in the coherent oscillations of the large spin. They are explained by the influence of the nonresonant bosons of the environment. In the opposite limit, the strong-coupling regime, a combination of a polaron transformation and the Born-Markov approximation allows for the perturbative treatment of the tunneling. This method

is not reliable for intermediate couplings at low temperatures. At finite temperatures or strong couplings, we have found a good agreement with the results of the spin-boson model. The behavior of the large spin in the strong-coupling regime differs entirely from the weak-coupling limit. Collective effects do not lead to an accelerated dynamics but instead to a slow relaxation. The large spin approaches one of the polarized states. Which of the two is determined by its initial value. For an ohmic dissipation, the relaxation is approximately logarithmic in time.

In the last chapter of this thesis, chapter 5, we propose a realistic system in which dissipation induced collective effects can be detected. We calculate the tunnel current through two double quantum dots interacting with the same dissipative environment, the phonons. Collective effects become indeed visible in the inelastic tunnel current. We predict that superradiance of the double dots leads to an increased tunnel current while the opposite effect, the subradiance, reduces the tunnel current.

It seems inevitable in the treatment of such a wide subject that many interesting questions remain open. We will mention but two points that in our opinion are worth further considerations. One question mark concerns the thermodynamic limit of an infinite spin with a renormalized interaction strength. The Dicke model with only one bosonic mode instead of a continuum shows a phase transition in that limit [57, 58]. Does a similar phase transition also exist in the model of a dissipative large spin? Furthermore, we have studied the large spin in the two opposite limits of weak and strong coupling to the environment. It is hardly surprising that we have found quite different answers. Yet, this brings up the question of the physics of the large spin in the intermediate regime. Other theoretical methods than those employed in this work are necessary to tackle that regime. A perturbative treatment of either the coupling or the tunneling is not possible since both effects become equally important in the intermediate regime.

Appendix A

Bosonic Expectation Values

In the course of the derivation of the master equation (4.17) for the large spin with strong ohmic dissipation different expectation values of bosonic operators occur, Sec. 4.2. Some of them lead to the correlation function $C(t)$ of the environment (4.13), while others give no contribution to the master equation. It is the purpose of this appendix to show that the expectation values $\langle X_t \rangle$, $\langle X_t^\dagger \rangle$, $\langle X_t X \rangle$, and $\langle X_t^\dagger X^\dagger \rangle$ vanish for an ohmic dissipation.

The Expectation Value $\langle X_t \rangle$

We recall that X_t is the interaction representation of the bosonic operator X (4.8) and that the expectation value refers to the thermal equilibrium of the environment. First, we note that $\langle X_t \rangle$ does actually not depend on the time,

$$\langle X_t \rangle = \mathrm{Tr}_{\mathrm{Res}}\{X_t \bar{R}_0\} = \mathrm{Tr}_{\mathrm{Res}}\{X \bar{R}_0\} = \langle X \rangle \,. \tag{A.1}$$

This follows from the cyclic invariance property of the trace and the fact that $\bar{R}_0$, the density matrix of the reservoir in thermal equilibrium, commutes with the unperturbed Hamiltonian $\bar{H}_0$. The next step is to write the expectation value $\langle X \rangle$ as a product over all bosonic modes,

$$\langle X \rangle = \prod_q \left\langle \, e^{(\gamma_q a_q^\dagger - \gamma_q^* a_q)/\omega_q} \, \right\rangle_q \,, \tag{A.2}$$

since the operator X as well as the equilibrium density matrix $\bar{R}_0$ factorize. The expectation value on the right hand side of this equation only refers to the mode q. It is calculated as a sum over all possible occupation numbers n_q of that mode,

$$\langle A \rangle_q = (1 - e^{-\beta\omega_q}) \sum_{n_q=0}^{\infty} \langle n_q | \, A \, e^{-\beta\omega_q a_q^\dagger a_q} \, | n_q \rangle \,. \tag{A.3}$$

The remaining exponential function can be written as a product with the theorem

$$e^{A+B} = e^{A}\, e^{B}\, e^{-\frac{1}{2}[A,B]}\,, \tag{A.4}$$

which requires that both operators A and B commute with their commutator, $[A,[A,B]]=[B,[A,B]]=0$. Thus, we find for the expectation value

$$\langle X\rangle = \prod_q\; e^{-|\gamma_q|^2/2\omega_q^2}\, \Big\langle\, e^{(\gamma_q/\omega_q)\, a_q^\dagger}\; e^{-(\gamma_q^*/\omega_q)\, a_q}\, \Big\rangle_q\,. \tag{A.5}$$

The expectation value on the right hand side is also referred to as the *quantum characteristic function* [105]. It is shown in the same reference that the expectation value can be expressed by the Bose distribution $n_B(\omega)$ as

$$\Big\langle\, e^{(\gamma_q/\omega_q)\, a_q^\dagger}\; e^{-(\gamma_q^*/\omega_q)\, a_q}\, \Big\rangle_q = e^{-|\gamma_q/\omega_q|^2\, n_B(\omega_q)}\,. \tag{A.6}$$

Then, the expectation value of X reads

$$\langle X\rangle = e^{-\Phi}, \tag{A.7}$$

with Φ defined as

$$\Phi = \sum_q\; \left|\frac{\gamma_q}{\omega_q}\right|^2 \Big(n_B(\omega_q)+\frac{1}{2}\Big) = \frac{1}{2}\sum_q\; \left|\frac{\gamma_q}{\omega_q}\right|^2 \coth\Big(\frac{\beta\omega_q}{2}\Big)\,. \tag{A.8}$$

The right hand side of this equation follows by inserting the Bose distribution $n_B(\omega)$. An identical result can be found in [106]. Finally, we express the exponent Φ by the spectral function $\rho(\omega)$ (3.33) as

$$\Phi = \frac{1}{2}\int_0^\infty d\omega\; \frac{\rho(\omega)}{\omega^2}\; \coth\Big(\frac{\beta\omega}{2}\Big)\,. \tag{A.9}$$

It follows immediately upon applying the power-law model (3.34) of the spectral function that the integral diverges to plus infinity for $s \leq 1$. In that case, the expectation value vanishes,

$$\langle X_t\rangle = 0, \qquad s \leq 1. \tag{A.10}$$

Naturally, also the expectation value of the adjoint operator vanishes in that case, $\langle X_t^\dagger\rangle = 0$. We conclude that for spectral functions with exponents $s \leq 1$, the expectation values of single bosonic operators X_t result to zero, in agreement with [86].

The Expectation Value $\langle X_t X \rangle$

There are four possibilities to combine two bosonic operators from $X^\dagger$ and X. The mixed pairs $\langle X_t^\dagger X \rangle$ and $\langle X_t X^\dagger \rangle$ form the correlation function $C(t)$ (4.13) that was calculated in section 4.3. We will show in this section that pairs consisting of identical operators lead to a zero expectation value for ohmic and sub-ohmic spectral functions of the environment. The mixed pairs can be written as an exponential function (4.19), the derivation of which is given in [85]. The same calculation yields for the identical pairs a quite similar result,

$$\langle X_t^\dagger X^\dagger \rangle = \langle X_t X \rangle = e^{-\tilde{\Phi}(t)}\,, \tag{A.11}$$

with the new function $\tilde{\Phi}(t)$ defined as

$$\tilde{\Phi}(t) = \int_0^\infty d\omega\, \frac{\rho(\omega)}{\omega^2} \Big[\big(1 + \cos(\omega t)\big)\, \coth\Big(\frac{\beta\omega}{2}\Big) - i \sin(\omega t) \Big]. \tag{A.12}$$

The expression for $\tilde{\Phi}(t)$ is almost identical to the result of $\Phi(t)$ for the mixed operator combinations (4.20). The only difference is the opposite sign of the cosine and the sine function. This, however, has an important consequence. We will show that the function $\tilde{\Phi}(t)$ diverges for ohmic dissipation. It is therefore sufficient to study the real part of that function. With $\rho(\omega)$ in the form of (3.34) the real part reads

$$\begin{aligned} \mathrm{Re}\big\{\tilde{\Phi}(t)\big\} &= g \int_0^\infty d\omega\, \omega^{s-2}\, e^{-\omega/\omega_c} \big(1 + \cos(\omega t)\big) \coth\Big(\frac{\beta\omega}{2}\Big) \\ &> g \int_0^\infty d\omega\, \omega^{s-2}\, e^{-\omega/\omega_c} \big(1 + \cos(\omega t)\big) \\ &= +\infty, \qquad s \leq 1. \end{aligned} \tag{A.13}$$

Hence, the expectation values in (A.11) vanish for ohmic and sub-ohmic dissipation,

$$\langle X_t^\dagger X^\dagger \rangle = \langle X_t X \rangle = 0, \qquad s \leq 1, \tag{A.14}$$

as claimed in equation (4.12) of chapter 4.

Appendix B

Master Equation for Two Double Quantum Dots

Some parts of the calculations of chapter 5 are given in detail in this appendix. At first, the master equation (5.23) is presented explicitely for two double quantum dots. We show in the second part, how the approximations for the change of the current, ΔI, and for the cross coherences, $\langle p_1^\dagger p_2 \rangle$ and $\langle p_1 p_2 \rangle$, follow from this master equation.

Master Equation for Two Double Dots

With the three basis states $|L\rangle$, $|R\rangle$, and $|0\rangle$ for each double quantum dot, the Hilbert space for N double dots is of the dimension of 3^N. Consequently, the density matrix ρ has 9^N entries. For two double dots, $N=2$, the master equation (5.23) thus corresponds to 81 coupled differential equations (not all of them independent, though). It is, however, not necessary to solve all 81 equations since we study the current which requires the knowledge of six matrix elements only, cf. (5.44). It turns out that the smallest closed subset of equations, containing the equations for the desired six elements, consists of 25 equations. The equations for the matrix elements $\dot{\rho}_{ji i' j'}$ with either i or i' equal to zero (but not both) need not to be considered. The same applies to j and j'. We use the notation (5.45) for the matrix elements.

The mixed terms in the master equation (5.23), $i \neq j$, describing the indirect interaction between the two DQDs due to the coupling to the same phonons, are marked in the following with an additional prefactor q. Setting $q=0$ results in the master equation for two completely independent double dots coupled to independent phonons. The interacting case corresponds to $q=1$. Finally, the subset of the 25

equations follows from the master equation (5.23) as

$$
\begin{aligned}
\dot\rho_{LLLL} &= iT_{c,1}(\rho_{LLRL}-\rho_{LRLL}) + iT_{c,2}(\rho_{LLLR}-\rho_{RLLL}) + \Gamma_{L,1}\,\rho_{L00L} + \Gamma_{L,2}\,\rho_{0LL0},\\
\dot\rho_{LLLR} &= iT_{c,1}(\rho_{LLRR}-\rho_{LRLR}) + iT_{c,2}(\rho_{LLLL}-\rho_{RLLR}) + \Gamma_{L,1}\,\rho_{L00R}\\
&\quad + \gamma_2^*\,\rho_{LLLL} - \beta_2\,\rho_{RLLR} - \big(i\varepsilon_2 + \frac{1}{2}\Gamma_{R,2} + \alpha_2 + \alpha_2^*\big)\,\rho_{LLLR}\\
&\quad + q\,\big((\alpha_1^*-\alpha_1)\,\rho_{LLLR} + \beta_1^*\,\rho_{LLRR} - \beta_1\,\rho_{LRLR}\big),\\
\dot\rho_{LLRL} &= iT_{c,1}(\rho_{LLLL}-\rho_{LRRL}) + iT_{c,2}(\rho_{LLRR}-\rho_{RLRL}) + \Gamma_{L,2}\,\rho_{0LR0}\\
&\quad + \gamma_1^*\,\rho_{LLLL} - \beta_1\,\rho_{LRRL} - \big(i\varepsilon_1 + \frac{1}{2}\Gamma_{R,1} + \alpha_1 + \alpha_1^*\big)\,\rho_{LLRL}\\
&\quad + q\,\big((\alpha_2^*-\alpha_2)\,\rho_{LLRL} + \beta_2^*\,\rho_{LLRR} - \beta_2\,\rho_{RLRL}\big),\\
\dot\rho_{LLRR} &= iT_{c,1}(\rho_{LLLR}-\rho_{LRRR}) + iT_{c,2}(\rho_{LLRL}-\rho_{RLRR})\\
&\quad + \gamma_1^*\,\rho_{LLLR} - \beta_1\,\rho_{LRRR} + \gamma_2^*\,\rho_{LLRL} - \beta_2\,\rho_{RLRR}\\
&\quad - \big(i\varepsilon_1 + i\varepsilon_2 + \frac{1}{2}\Gamma_{R,1} + \frac{1}{2}\Gamma_{R,2} + \alpha_1 + \alpha_1^* + \alpha_2 + \alpha_2^*\big)\,\rho_{LLRR}\\
&\quad - q\,\big((\alpha_1+\alpha_1^*+\alpha_2+\alpha_2^*)\rho_{LLRR} + \beta_2\,\rho_{RLRR} + \beta_1\,\rho_{LRRR} - \gamma_2^*\,\rho_{LLRL} - \gamma_1^*\,\rho_{LLLR}\big),\\
\dot\rho_{RLLR} &= iT_{c,1}(\rho_{RLRR}-\rho_{RRLR}) + iT_{c,2}(\rho_{RLLL}-\rho_{LLLR}) + \Gamma_{L,1}\,\rho_{R00R} - \Gamma_{R,2}\,\rho_{RLLR},\\
\dot\rho_{RLRL} &= iT_{c,1}(\rho_{RLLL}-\rho_{RRRL}) + iT_{c,2}(\rho_{RLRR}-\rho_{LLRL})\\
&\quad + \gamma_1^*\,\rho_{RLLL} - \beta_1\,\rho_{RRRL} + \gamma_2\,\rho_{LLRL} - \beta_2^*\,\rho_{RLRR}\\
&\quad - \big(i\varepsilon_1 - i\varepsilon_2 + \frac{1}{2}\Gamma_{R,1} + \frac{1}{2}\Gamma_{R,2} + \alpha_1 + \alpha_1^* + \alpha_2 + \alpha_2^*\big)\,\rho_{RLRL}\\
&\quad + q\,\big((\alpha_1+\alpha_1^*+\alpha_2+\alpha_2^*)\rho_{RLRL} - \gamma_2\,\rho_{LLRL} + \beta_1\,\rho_{RRRL} + \beta_2^*\,\rho_{RLRR} - \gamma_1^*\,\rho_{RLLL}\big),\\
\dot\rho_{RLRR} &= iT_{c,1}(\rho_{RLLR}-\rho_{RRRR}) + iT_{c,2}(\rho_{RLRL}-\rho_{LLRR})\\
&\quad + \gamma_1^*\,\rho_{RLLR} - \beta_1\,\rho_{RRRR} - \big(i\varepsilon_1 + \frac{1}{2}\Gamma_{R,1} + \Gamma_{R,2} + \alpha_1 + \alpha_1^*\big)\,\rho_{RLRR}\\
&\quad + q\,\big((\alpha_2-\alpha_2^*)\,\rho_{RLRR} - \gamma_2\,\rho_{LLRR} + \gamma_2^*\,\rho_{RLRL}\big),\\
\dot\rho_{0LL0} &= iT_{c,1}(\rho_{0LR0}-\rho_{0RL0}) + \Gamma_{L,1}\,\rho_{0000} + \Gamma_{R,2}\,\rho_{RLLR} - \Gamma_{L,2}\,\rho_{0LL0},\\
\dot\rho_{0LR0} &= iT_{c,1}(\rho_{0LL0}-\rho_{0RR0}) + \Gamma_{R,2}\,\rho_{RLRR}\\
&\quad + \gamma_1^*\,\rho_{0LL0} - \beta_1\,\rho_{0RR0} - \big(i\varepsilon_1 + \frac{1}{2}\Gamma_{R,1} + \Gamma_{L,2} + \alpha_1 + \alpha_1^*\big)\,\rho_{0LR0},\\
\dot\rho_{LRRL} &= iT_{c,1}(\rho_{LRLL}-\rho_{LLRL}) + iT_{c,2}(\rho_{LRRR}-\rho_{RRRL}) + \Gamma_{L,2}\,\rho_{0RR0} - \Gamma_{R,1}\,\rho_{LRRL},\\
\dot\rho_{LRRR} &= iT_{c,1}(\rho_{LRLR}-\rho_{LLRR}) + iT_{c,2}(\rho_{LRRL}-\rho_{RRRR}) + \gamma_2^*\,\rho_{LRRL} - \beta_2\,\rho_{RRRR}\\
&\quad - \big(i\varepsilon_2 + \Gamma_{R,1} + \frac{1}{2}\Gamma_{R,2} + \alpha_2 + \alpha_2^*\big)\,\rho_{LRRR}\\
&\quad + q\,\big((\alpha_1-\alpha_1^*)\,\rho_{LRRR} - \gamma_1\,\rho_{LLRR} + \gamma_1^*\,\rho_{LRLR}\big),\\
\dot\rho_{RRRR} &= iT_{c,1}(\rho_{RRLR}-\rho_{RLRR}) + iT_{c,2}(\rho_{RRRL}-\rho_{LRRR}) - \big(\Gamma_{R,1}+\Gamma_{R,2}\big)\,\rho_{RRRR},\\
\dot\rho_{0RR0} &= iT_{c,1}(\rho_{0RL0}-\rho_{0LR0}) + \Gamma_{R,2}\,\rho_{RRRR} - \big(\Gamma_{R,1}+\Gamma_{L,2}\big)\,\rho_{0RR0},
\end{aligned}
$$

$$
\begin{aligned}
\dot\rho_{L00L} &= iT_{c,2}(\rho_{L00R}-\rho_{R00L}) + \Gamma_{R,1}\,\rho_{LRRL} + \Gamma_{L,2}\,\rho_{0000} - \Gamma_{L,1}\,\rho_{L00L},\\
\dot\rho_{L00R} &= iT_{c,2}(\rho_{L00L}-\rho_{R00R}) + \Gamma_{R,1}\,\rho_{LRRR} + \gamma_2^*\,\rho_{L00L} - \beta_2\,\rho_{R00R}\\
&\quad - \big(i\varepsilon_2 + \Gamma_{L,1} + \frac{1}{2}\Gamma_{R,2} + \alpha_2 + \alpha_2^*\big)\,\rho_{L00R},\\
\dot\rho_{R00R} &= iT_{c,2}(\rho_{R00L}-\rho_{L00R}) + \Gamma_{R,1}\,\rho_{RRRR} - (\Gamma_{L,1}+\Gamma_{R,2})\,\rho_{R00R},\\
\dot\rho_{0000} &= \Gamma_{R,1}\,\rho_{0RR0} + \Gamma_{R,2}\,\rho_{R00R} - \big(\Gamma_{L,1}+\Gamma_{L,2}\big)\,\rho_{0000}.
\end{aligned}
\tag{B.1}
$$

The remaining 8 equations follow immediately since ρ is a hermitian operator,

$$
\rho_{j\,i\,i'\,j'} = \rho^*_{j'\,i'\,i\,j}\,. \tag{B.2}
$$

Approximation for the Tunnel Current

This system of equations serves as the point of departure for the derivation of an approximation for the change of the stationary current due to collective effects in the two double dots. The calculations below are valid for real parameters α_j, β_j, and γ_j, as used throughout chapter 5, but can easily be generalized to complex parameters if desired. Without any interactions between the two double quantum dots, $q=0$, the density matrix ρ for the combined system is simply the tensor product of two density matrices for independent double dots. The solution of the density matrix for one independent double dot is given in (5.29). How does the indirect interaction, i.e. the terms with the prefactor q in the master equation (B.1), change this solution? First, we notice that only six matrix elements (and their complex conjugates) occur in connection with the factor q. These elements are ρ_{RLLL}, ρ_{LRLL}, ρ_{RRLR} and ρ_{RRRL}, all of which enter the expression (5.44) for the current, and the two 'cross coherence' matrix elements

$$
\rho_{RLRL} = \big\langle p_1^\dagger p_2 \big\rangle, \qquad \rho_{RRLL} = \big\langle p_1 p_2 \big\rangle. \tag{B.3}
$$

We assume that only those six elements are affected by the interaction and that all other elements are identical to the non-interacting case. According to equation (5.44), the change in the stationary current due to the interaction is then

$$
\begin{aligned}
\Delta I_1 &= -\,\frac{2\,T_{c,1}\,e}{\hbar}\;\mathrm{Im}\big\{\Delta\rho_{LRLL} + \Delta\rho_{RRLR}\big\},\\
\Delta I_2 &= -\,\frac{2\,T_{c,2}\,e}{\hbar}\;\mathrm{Im}\big\{\Delta\rho_{RLLL} + \Delta\rho_{RRRL}\big\},
\end{aligned}
\tag{B.4}
$$

where Δ denotes the difference between the interacting case, $q=1$, and the non-interacting case, $q=0$.

We will consider the equations for these matrix elements in detail, starting with the equation for $\dot\rho_{LRLL}$, the complex conjugate of $\dot\rho_{LLRL}$. In the stationary case, the terms of the right hand side add up to zero. We neglect the matrix elements

ρ_{RLRL} and ρ_{RRLL} for non-interacting double dots, $q = 0$. This is justified as the cross coherences are then simply the product of the corresponding matrix elements of independent double dots,

$$\langle p_1^\dagger p_2 \rangle = \langle p_1^\dagger \rangle \langle p_2 \rangle , \qquad \langle p_1 p_2 \rangle = \langle p_1 \rangle \langle p_2 \rangle . \tag{B.5}$$

These tend to zero in the inelastic regime, $T_c \ll \varepsilon$, as can be seen from the solution (5.29) for $\langle p \rangle$. Thus, the equation for ρ_{LRLL} reduces for $q=0$ to

$$(iT_{c,1} - \beta_1)\, \rho_{LRRL} - (iT_{c,1} - \gamma_1)\, \rho_{LLLL} + \Gamma_{L,2}\, \rho_{0RL0} + \big(i\varepsilon_1 - \frac{1}{2}\Gamma_{R,1} - 2\alpha_1\big)\, \rho_{LRLL} = 0 \tag{B.6}$$

The new term which appears for interacting double dots, $q=1$, must be compensated by a change of the matrix elements ρ_{LRLL}, ρ_{RLRL}, and ρ_{RRLL} since the other elements are assumed not to be affected by the interaction,

$$(iT_{c,2} - \beta_2)\, \Delta\rho^*_{RLRL} - (iT_{c,2} - \beta_2)\, \Delta\rho_{RRLL} + \big(i\varepsilon_1 - \frac{1}{2}\Gamma_{R,1} - 2\alpha_1\big)\, \Delta\rho_{LRLL} = 0 \tag{B.7}$$

Taking into account only the real parts of $\Delta\rho_{RLRL}$ and $\Delta\rho_{RRLL}$ and using $(\Gamma_R/2 + 2\alpha_2)^2 \ll \varepsilon_2^2$, the imaginary part of $\Delta\rho_{LRLL}$ becomes

$$\mathrm{Im}\big\{\Delta\rho_{LRLL}\big\} = \frac{T_{c,2}\,(\frac{1}{2}\Gamma_{R,1} + 2\alpha_1) - \varepsilon_1\beta_2}{\varepsilon_1^2} \Big(\mathrm{Re}\big\{\Delta\rho_{RLRL}\big\} - \mathrm{Re}\big\{\Delta\rho_{RRLL}\big\}\Big). \tag{B.8}$$

A similar approximation is applied to derive the change of the matrix element ρ_{RRLR} that also enters the expression (B.4) for the current ΔI_1,

$$\mathrm{Im}\big\{\Delta\rho_{RRLR}\big\} = -\frac{T_{c,2}\,(\frac{1}{2}\Gamma_{R,1} + \Gamma_{R,2} + 2\alpha_1) - \varepsilon_1\gamma_2}{\varepsilon_1^2} \Big(\mathrm{Re}\big\{\Delta\rho_{RLRL}\big\} - \mathrm{Re}\big\{\Delta\rho_{RRLL}\big\}\Big). \tag{B.9}$$

Hence, the change of the stationary current due to the indirect interaction is expressed by the two cross coherence matrix elements as

$$\Delta I_1 = -\frac{2eT_{c,1}\big(\varepsilon_1(\gamma_2 - \beta_2) - T_{c,2}\Gamma_{R,2}\big)}{\hbar\,\varepsilon_1^2} \Big(\mathrm{Re}\big\{\Delta\rho_{RLRL}\big\} - \mathrm{Re}\big\{\Delta\rho_{RRLL}\big\}\Big). \tag{B.10}$$

At low temperatures $kT < \varepsilon$ and in the inelastic regime $T_c \ll \varepsilon$, the parameter β_j is much smaller than γ_j, as can be seen from (5.26). Moreover, also the term proportional to $T_{c,2}$ is neglected. Then, we find for ΔI the expression (5.47) given in chapter 5 since ρ_{RLRL} and ρ_{RRLL} are assumed to vanish in the non-interacting case,

$$\Delta I_1 = -\frac{2e\,T_{c1}\gamma_2}{\hbar\,\varepsilon_1} \Big(\mathrm{Re}\big\{\rho_{RLRL}\big\} - \mathrm{Re}\big\{\rho_{RRLL}\big\}\Big). \tag{B.11}$$

Performing the same analysis for ΔI_2 leads to the same expression, with exchanged subscripts 1 and 2.

In a second step, we approximate the cross coherences $\rho_{RLRL} = \langle p_1^\dagger p_2 \rangle$ and $\rho_{RRLL} = \langle p_1 p_2 \rangle$ by a combination of non-interacting matrix elements. In the equations for ρ_{RLRL} and ρ_{RRLL}, we assume that all other matrix elements are identical for $q=0$ and $q=1$. Then, the additional term in these equations appearing for $q=1$ must be compensated by a finite ρ_{RLRL} or ρ_{RRLL}, respectively,

$$\big(\beta_1\,\rho_{RRRL} - \gamma_1\,\rho_{RLLL} + \beta_2\,\rho_{RLRR} - \gamma_2\,\rho_{LLRL}\big) - \big(i(\varepsilon_1 - \varepsilon_2) + \frac{1}{2}\Gamma_{R,1} + \frac{1}{2}\Gamma_{R,2}\big)\,\rho_{RLRL} = 0. \tag{B.12}$$

Again, we use $\beta_j \ll \gamma_j$ and neglect the matrix elements connected with β_j. For the remaining two elements, ρ_{RLLL} and ρ_{LLRL}, we insert the non-interacting expressions,

$$\rho_{RLLL} = \langle n_{L,1} \rangle \, \langle p_2 \rangle \,, \qquad \rho_{LLRL} = \langle p_1^\dagger \rangle \, \langle n_{L,2} \rangle \,. \tag{B.13}$$

The solutions for $\langle n_L \rangle$ and $\langle p \rangle$ are given in (5.29). Neglecting the imaginary part of $\langle p \rangle$, we find the approximation (5.48) for real part of the cross coherence

$$\mathrm{Re}\big\{\rho_{RLRL}\big\} = -\frac{\frac{1}{2}\,(\Gamma_{R,1} + \Gamma_{R,2})\big(\gamma_1\,\mathrm{Re}\big\{\langle p_2 \rangle\big\}\,\langle n_{L,1} \rangle + \gamma_2\,\mathrm{Re}\big\{\langle p_1 \rangle\big\}\,\langle n_{L,2} \rangle\big)}{(\varepsilon_1 - \varepsilon_2)^2 + \frac{1}{4}(\Gamma_{R,1} + \Gamma_{R,2})^2} \,. \tag{B.14}$$

A similar calculation leads to the approximation for the other cross coherence ρ_{RRLL} employed in (5.56),

$$\mathrm{Re}\big\{\rho_{RRLL}\big\} = \frac{\frac{1}{2}\big(\Gamma_{R,1} + \Gamma_{R,2} + 8(\alpha_1 + \alpha_2)\big)\big(\gamma_1\,\mathrm{Re}\big\{\langle p_2 \rangle\big\}\,\langle n_{L,1} \rangle + \gamma_2\,\mathrm{Re}\big\{\langle p_1 \rangle\big\}\,\langle n_{L,2} \rangle\big)}{(\varepsilon_1 + \varepsilon_2)^2 + \big(\frac{1}{2}\Gamma_{R,1} + \frac{1}{2}\Gamma_{R,2} + 4(\alpha_1 + \alpha_2)\big)^2} \,. \tag{B.15}$$

The main difference between these cross coherences is seen immediately. The real part of ρ_{RLRL} exhibits a resonance if the bias in both double dots becomes equal, $\varepsilon_1 = \varepsilon_2$, while ρ_{RRLL} is resonant for an exactly opposite bias in the dots, $\varepsilon_1 = -\varepsilon_2$. This property can clearly be identified in Fig. 5.5.

Bibliography

[1] F. Hund, Z. Phys. **43**, 805 (1927).

[2] E. F. Barker, Phys. Rev. **33**, 684 (1929).

[3] N. C. van der Vaart, S. F. Godijn, Y. V. Nazarov, C. J. Harmans, J. E. Mooij, L. W. Molenkamp, and C. T. Foxon, Phys. Rev. Lett. **74**, 4702 (1995).

[4] R. H. Blick, R. J. Haug, J. Weiss, D. Pfannkuche, K. v. Klitzing, and K. Eberl, Phys. Rev. B **53**, 7899 (1996).

[5] T. H. Oosterkamp, T. Fujisawa, W. G. van der Wiel, K. Ishibashi, R. V. Hijman, S. Tarucha, and L. P. Kouwenhoven, Nature **395**, 873 (1998).

[6] T. Hayashi, T. Fujisawa, H. D. Cheong, Y. H. Jeong, and Y. Hirayama, cond-mat/0308362 (2003).

[7] B. d'Espagnat, *Veiled Reality* (Addison-Wesley Publishing, Reading, 1995).

[8] D. Giulini, E. Joos, C. Kiefer, J. Kupsch, I.-O. Stamatescu, and H. D. Zeh, *Decoherence and the Appearance of a Classical World in Quantum Theory* (Springer-Verlag, Berlin, 1996).

[9] A. J. Leggett, S. Chakravarty, A. T. Dorsey, M. P. A. Fisher, A. Garg, and W. Zwerger, Rev. Mod. Phys. **59**, 1 (1987).

[10] U. Weiss, *Quantum Dissipative Systems* (World Scientific, Singapore, 1999).

[11] N. H. March and M. Parrinello, *Collective Effects in Solids and Liquids* (Adam Hilger Ltd, Bristol, 1982).

[12] R. H. Dicke, Phys. Rev. **93**, 99 (1954).

[13] M. G. Benedict, A. M. Ermolaev, V. A. Malyshev, I. V. Sokolov, and E. D. Trifonov, *Super-radiance* (Institute of Physics Publishing, Bristol, 1996).

[14] A. V. Andreev, V. I. Emel'yanov, and Y. A. Il'inskiĭ, *Cooperative Effects in Optics* (Institute of Physics Publishing, Bristol, 1993).

[15] K.-H. Ahn and P. Mohanty, Phys. Rev. Lett. **90**, 085504 (2003).

[16] T. Fujisawa, T. H. Oosterkamp, W. G. van der Wiel, B. W. Broer, R. Aguado, S. Tarucha, and L. P. Kouwenhoven, Science **282**, 932 (1998).

[17] R. Sessoli, D. Gatteschi, A. Caneschi, and M. A. Novak, Nature **365**, 141 (1993).

[18] W. Wernsdorfer and R. Sessoli, Science **284**, 133 (1999).

[19] H. Carmichael, *An Open Systems Approach to Quantum Optics* (Springer-Verlag, Berlin, 1993).

[20] L. Jacak, P. Hawrylak, and A. Wójs, *Quantum Dots* (Springer-Verlag, Berlin, 1998).

[21] M. A. Kastner, Physics Today **46**, 24 (1993).

[22] R. C. Ashoori, Nature **379**, 413 (1996).

[23] D. Goldhaber-Gordon, H. Shtrikman, D. Mahalu, D. Abusch-Magder, U. Meirav, and M. A. Kastner, Nature **391**, 156 (1998).

[24] S. Sasaki, S. De Franceschi, J. M. Elzerman, W. G. van der Wiel, M. Eto, S. Tarucha, and L. P. Kouwenhoven, Nature **405**, 764 (2000).

[25] D. Loss and D. P. DiVincenzo, Phys. Rev. A **57**, 120 (1998).

[26] H. Grabert and M. H. Devoret, eds., *Single Charge Tunneling* (Plenum Press, New York, 1992).

[27] F. R. Waugh, M. J. Berry, D. J. Mar, R. M. Westervelt, K. L. Campman, and A. C. Gossard, Phys. Rev. Lett. **75**, 705 (1995).

[28] C. Cohen-Tannoudji, B. Diu, and F. Laloë, *Quantenmechanik* (de Gruyter, Berlin, 1997).

[29] L. P. Kouwenhoven, S. Jauhar, K. McCormick, D. Dixon, P. L. McEuen, Y. V. Nazarov, N. C. van der Vaart, and C. T. Foxon, Phys. Rev. B **50**, 2019 (1994).

[30] L. P. Kouwenhoven, S. Jauhar, J. Orenstein, P. L. McEuen, Y. Nagamune, J. Motohisa, and H. Sakaki, Phys. Rev. Lett. **73**, 3443 (1994).

[31] S. Fafard, K. Hinzer, S. Raymond, M. Dion, J. McCaffrey, Y. Feng, and S. Charbonneau, Science **274**, 1350 (1996).

[32] T. Fujisawa, W. G. van der Wiel, and L. P. Kouwenhoven, Physica E **7**, 413 (2000).

[33] T. Brandes and B. Kramer, Phys. Rev. Lett. **83**, 3021 (1999).

[34] S. Debald, T. Brandes, and B. Kramer, Phys. Rev. B **66**, 041301(R) (2002).

[35] E. M. Höhberger, R. H. Blick, T. Brandes, J. Kirschbaum, W. Wegscheider, M. Bichler, and J. P. Kotthaus, cond-mat/0304136 (2003).

[36] A. Würger, *From Coherent Tunneling to Relaxation* (Springer-Verlag, Berlin, 1997).

[37] P. Esquinazi, ed., *Tunneling Systems in Amorphous and Crystalline Solids* (Springer-Verlag, Berlin, 1998).

[38] W. A. Phillips, J. Low Temp. Phys. **7**, 351 (1972).

[39] P. W. Anderson, B. I. Halperin, and C. M. Varma, Philos. Mag. **25**, 1 (1972).

[40] L. Thomas, F. Lionti, R. Ballou, D. Gatteschi, R. Sessoli, and B. Barbara, Nature **383**, 145 (1996).

[41] W. Wernsdorfer, R. Sessoli, A. Caneschi, D. Gatteschi, and A. Cornia, Europhys. Lett. **50**, 552 (2000).

[42] T. Lis, Acta Cryst. B **36**, 2042 (1980).

[43] M. N. Leuenberger and D. Loss, Nature **410**, 789 (2001).

[44] M. N. Leuenberger, F. Meier, and D. Loss, Monatshefte für Chem. **134**, 217 (2003).

[45] E. M. Chudnovsky and D. A. Garanin, Phys. Rev. Lett. **89**, 157201 (2002).

[46] W. W. Paudler, *Nuclear Magnetic Resonance* (John Wiley & Sons, New York, 1987).

[47] F. Bloch, Phys. Rev. **70**, 460 (1946).

[48] R. K. Wangsness and F. Bloch, Phys. Rev. **89**, 728 (1953).

[49] F. Bloch, Phys. Rev. **105**, 1206 (1957).

[50] A. G. Redfield, IBM Journal **1**, 19 (1957).

[51] C. Cohen-Tannoudji, J. Dupont-Roc, and G. Grynberg, *Atom-Photon Interactions* (John Wiley & Sons, New York, 1998).

[52] W. Apel and Y. A. Bychkov, Phys. Rev. B **63**, 224405 (2001).

[53] G. S. Agarwal, *Quantum Statistical Theories of Spontaneous Emission and their Relation to Other Approaches* (Springer-Verlag, Berlin, 1974).

[54] R. G. DeVoe and R. G. Brewer, Phys. Rev. Lett. **76**, 2049 (1996).

[55] M. Gross and S. Haroche, Phys. Reports **93**, 301 (1982).

[56] C. Greiner, B. Boggs, and T. W. Mossberg, Phys. Rev. Lett. **85**, 3793 (2000).

[57] K. Hepp and E. H. Lieb, Ann. Phys. (NY) **76**, 360 (1973).

[58] Y. K. Wang and F. T. Hioe, Phys. Rev. A **7**, 831 (1973).

[59] C. H. Lewenkopf, M. C. Nemes, V. Marvulle, M. P. Pato, and W. F. Wreszinski, Phys. Lett. A **155**, 113 (1991).

[60] C. Emary and T. Brandes, Phys. Rev. Lett. **90**, 044101 (2003).

[61] A. J. Leggett, in *Percolation, Localization, and Superconductivity*, edited by A. M. Goldman and S. A. Wolf (Plenum Press, New York, 1984), NATO ASI Series, p. 1.

[62] M. Grifoni and P. Hänggi, Phys. Reports **304**, 229 (1998).

[63] A. Schmid, Phys. Rev. Lett. **51**, 1506 (1983).

[64] F. Guinea, V. Hakim, and A. Muramatsu, Phys. Rev. Lett. **54**, 263 (1985).

[65] M. P. A. Fisher and W. Zwerger, Phys. Rev. B **32**, 6190 (1985).

[66] M. Thorwart, M. Grifoni, and P. Hänggi, Phys. Rev. Lett. **85**, 860 (2000).

[67] F. Schwabl, *Quantenmechanik* (Springer-Verlag, Berlin, 1988).

[68] W. Greiner, L. Neise, and H. Stöcker, *Thermodynamik und Statistische Mechanik* (Verlag Harri Deutsch, Thun, 1993).

[69] M. Keil and H. Schoeller, Phys. Rev. B **66**, 155314 (2002).

[70] U. Weiss and M. Wollensak, Phys. Rev. B **37**, 2729 (1988).

[71] C. H. Mak and R. Egger, Phys. Rev. E **49**, 1997 (1994).

[72] D. F. Walls and G. J. Milburn, *Quantum Optics* (Springer-Verlag, Berlin, 1995).

[73] M. Grifoni, M. Winterstetter, and U. Weiss, Phys. Rev. E **56**, 334 (1997).

[74] W. H. Press, S. A. Teukolsky, W. T. Vetterling, and B. P. Flannery, *Numerical Recipes in C* (Cambridge University Press, 1994).

[75] T. Dittrich, P. Hänggi, G.-L. Ingold, B. Kramer, G. Schön, and W. Zwerger, *Quantum Transport and Dissipation* (Wiley-VCH, Weinheim, 1998).

[76] I. S. Gradshteyn and I. M. Ryzhik, *Table of Integrals, Series, and Products* (Academic Press, New York, 1980).

[77] W. Magnus, F. Oberhettinger, and R. P. Soni, *Formulas and Theorems for the Special Functions of Mathematical Physics* (Springer-Verlag, Berlin, 1966).

[78] T. Brandes and T. Vorrath, Phys. Rev. B **66**, 075341 (2002).

[79] A. Erdélyi, W. Magnus, F. Oberhettinger, and F. G. Tricomi, *Higher Transcendental Functions* (McGraw Hill Book Company, New York, 1953).

[80] M. Abramowitz and I. A. Stegun, *Handbook of Mathematical Functions* (Dover Publications, New York, 1972).

[81] L. Hartmann, I. Goychuk, M. Grifoni, and P. Hänggi, Phys. Rev. E **61**, R4687 (2000).

[82] L. D. Landau and E. M. Lifschitz, *Lehrbuch der Theoretischen Physik*, vol. III (Akademie-Verlag, Berlin, 1965).

[83] A. A. Abrikosov, *Fundamentals of the Theory of Metals* (North-Holland, Amsterdam, 1988).

[84] N. W. Ashcroft and N. D. Mermin, *Solid State Physics* (Saunders College Publishing, Fort Worth, 1976).

[85] G. D. Mahan, *Many-Particle Physics* (Plenum Press, New York, 1990).

[86] C. Aslangul, N. Pottier, and D. Saint-James, J. Physique **47**, 1657 (1986).

[87] T. Brandes, Ph.D. thesis, University of Hamburg (1994).

[88] S. Chakravarty, Phys. Rev. Lett. **49**, 681 (1982).

[89] A. J. Bray and M. A. Moore, Phys. Rev. Lett. **49**, 1545 (1982).

[90] V. Hakim, A. Muramatsu, and F. Guinea, Phys. Rev. B **30**, 464 (1984).

[91] M. P. A. Fisher and A. T. Dorsey, Phys. Rev. Lett. **54**, 1609 (1985).

[92] H. Grabert and U. Weiss, Phys. Rev. Lett. **54**, 1605 (1985).

[93] M. Sassetti and U. Weiss, Phys. Rev. A **41**, 5383 (1990).

[94] R. H. Blick, D. Pfannkuche, R. J. Haug, K. v. Klitzing, and K. Eberl, Phys. Rev. Lett. **80**, 4032 (1998).

[95] R. H. Blick, D. W. van der Weide, R. J. Haug, and K. Eberl, Phys. Rev. Lett. **81**, 689 (1998).

[96] T. Fujisawa, D. G. Austing, Y. Tokura, Y. Hirayama, and S. Tarucha, Nature **419**, 278 (2002).

[97] T. Vorrath, S. Debald, T. Brandes, and B. Kramer, in *Proc. 26th Int. Conf. Phys. Semicond.*, edited by A. R. Long and J. H. Davies (Edinburgh, 2002), p. D197.

[98] T. V. Shahbazyan and M. E. Raikh, Phys. Rev. B **49**, 17123 (1994).

[99] T. Brandes, J. Inoue, and A. Shimizu, Phys. Rev. Lett. **80**, 3952 (1998).

[100] T. Brandes, in *Interacting Electrons in Nanostructures*, edited by R. Haug and H. Schoeller (Springer, Heidelberg, 2001), vol. 579 of *Lecture Notes in Physics*.

[101] J. H. Reina, L. Quiroga, and N. F. Johnson, Phys. Rev. A **65**, 032326 (2002).

[102] T. Brandes and T. Vorrath, in *Recent Progress in Many-Body Theories*, edited by R. F. Bishop, T. Brandes, K. A. Gernoth, N. R. Walet, and Y. Xiang (World Scientific, Singapore, 2002), p. 471.

[103] T. H. Stoof and Y. V. Nazarov, Phys. Rev. B **53**, 1050 (1996).

[104] S. A. Gurvitz and Y. S. Prager, Phys. Rev. B **53**, 15932 (1996).

[105] C. W. Gardiner, *Quantum Noise* (Springer-Verlag, Berlin, 1991).

[106] G. M. Palma, K.-A. Suominen, and A. K. Ekert, Proc. Roy. Soc. Lond. A **452**, 567 (1996).

Acknowledgments

It is a pleasure to express my gratitude to all the people who contributed to the progress of this thesis. First of all I would like to thank Prof. Dr. B. Kramer who gave me the opportunity to join his group and to write my thesis under excellent conditions. I very much appreciate that he enabled me to attend numerous conferences and workshops where I could present and discuss parts of this work.

I am grateful to Dr. Tobias Brandes for supervising this thesis. I enjoyed many discussions in a friendly atmosphere. His patience and his constant encouragement are particularly appreciated.

Stefan Debald I thank for accompanying me on the daily excursion to the coffee-machine and many entertaining discussions. His immediate help with all computer problems was invaluable. I would also like to thank Dr. Stefan Kettemann for his helpfulness. Tobias Kleimann was a true companion on all conferences we attended during the last few years.

I learned a great deal from the members and the guests of the 1st institute for theoretical physics. In particular, I enjoyed discussions with Thorsten Dröse, Virgílio Carvalho dos Anjos, and Michael Tews.

Finally, I would like to express my appreciation for the collaboration with Prof. Dr. J. Appel who died at the end of last year. His catching enthusiasm and his expertise made our meetings an unforgettable experience.